Synthesis, characterization and anticancer effects of Quantum dots in neuroblastoma and glioblastoma cell lines

Sashca Yosima Lasher

A mini-thesis submitted in partial fulfilment of the requirements for the degree Magister of Scientiae in Nanoscience, in the Department of Medical Biosciences, University of the Western Cape

Supervisor: Dr. Okobi Ekpo

November 2018

ABSTRACT

Introduction: Nanoparticles (NPs) are gaining increased popularity for cancer treatment, especially the multifunctional nanoparticles like Quantum dots (QDs) which have a wide range of applications in nanotheranostics, cell imaging and targeted drug delivery to cancerous tissue. QDs comprise of very tiny crystals of a semiconductor material (diameter: 2-10 nm) capable of producing bright, intensive and size-tuneable near-infrared fluorescence emissions. In particular, 3-mercaptopropionic acid -capped Cadmium Telluride Quantum Dots with a zinc sulphide shell (MPA-capped CdTe/ZnS QDs), are known to be very stable, highly photoluminescent, less toxic with long-lasting "fluorophore" effects, thus making them the preferred QDs for this study.

Aims: To synthesize and characterize biocompatible MPA-capped CdTe/ZnS QDs to determine size range, polydispersity index (PdI), zeta (**ζ**) potential, photoluminescence (PL) spectra, stability in various milieus as well as to evaluate the effects of the synthesized QDs on the viability and morphology of neuroblastoma (NB) and glioblastoma (GB) cell lines using the WST-1 cell viability assay, imaging and cell cycle analysis.

Materials and methods: MPA-capped CdTe/ZnS QDs were synthesized and analysed with the Zetasizer to determine **ζ**-potential, hydrodynamic (h_d) size and PdI, while high resolution-transmission electron microscopy (HR-TEM) was used to validate the h_d size and elemental composition using energy dispersive X-ray (EDX) spectra. Pl absorption and emission spectra were obtained with a fluorometer and stability studies were done using UV-Vis spectroscopy, permitting further biological evaluation. A concentration range of 5-20µg/ml QDs was exposed to U87 and SH-SY5Y cancer cell lines to determine biological effects at different time points, using the WST-1 assay. Confocal fluorescence microscopy was used to establish uptake and cellular localization of the QDs, cell morphology was visualized with an inverted microscope while cell cycle distribution analysis was done using the C6 flow cytometer.

Results: Highly luminescent and uniformly monodispersed, anionic red-emitting MPA-capped CdTe/ZnS QDs of high stability, were successfully synthesized at h_d diameter (HD) size range of 3.66nm - 5.91nm. Exposure to cancer cells resulted in morphological changes that were time, concentration and cell line dependent. U87 cells which had significantly lower cell viability compared to SH-SY5Y cells were also more rounded in shaped with grape-like clusters. Uptake and localization studies showed that the MPA-capped CdTe/ZnS QDs were detectable in the nuclei

of both cell lines and there were slightly more SH-SY5Y cells at the G_2/M phase which corresponds with the increase cell viability recorded for these cells.

Conclusion and Future recommendation: Taken together, our results showed that the effects of QDs on cell viability and morphology were highly variant and dependent on cancer cell type. Since rounding of cells was evident in both cell lines used in this study, a non-casual relationship between cell viability and cell morphology is suggested, thus requiring future ameboid migration studies. Furthermore, highly-optimized surface-functionalization of QDs for targeted uptake and delivery is recommended in future studies in addition to extensive *in vitro* and *in vivo* toxicity studies to determine the absorption, distribution, metabolism and excretion (ADME) of MPA-capped CdTe/ZnS QDs.

KEYWORDS:

Formulation

Functionalization

Glioblastoma (GB)

Nanoparticles (NPs)

Neuroblastoma (NB)

Photoluminescence (Pl)

Quantum dots (QDs)

Stability

Viability

DECLARATION

I, Sashca Yosima Lasher, declare that '***Synthesis, characterization and anticancer effects of Quantum dots in neuroblastoma and glioblastoma cell lines***' is my own work, that it has not been submitted before for any degree or assessment in any other university, and that all the sources I have used or quoted in this work have been indicated and acknowledged by means of complete references.

Full name: **Sashca Yosima Lasher**

Date: **November 2018**

Signed 

TABLE OF CONTENTS

LIST OF FIGURES

LIST OF TABLES

LIST OF ABBREVIATIONS

DEDICATION

For my Parents…

God, I declare that no human wisdom, understanding, or counsel can prevail against you. Deliverance and victory come from You alone.

Adapted from Proverbs 21: 30,31

ACKNOWLEDGEMENTS

Firstly, I would like to give all praise to the most high, Jesus Christ my saviour, deliverer and rock, for I am nothing without Christ. The Lord has given me the strength and discipline required day to day and to complete this degree, while seeking his Godly wisdom, knowledge and understanding.

I will like to give my special thanks and appreciation to my supervisor Dr. Okobi Ekpo, you have been such a great mentor and supervisor who has helped me to grow on this journey and motivated me to always give my best and never give up. Thank you to the support of our Laboratory research group, especially to Taahirah Boltman, not only are you such an amazing friend, with a positive and caring heart, but always motivating me and reminding me never to doubt myself, you have assisted me in the laboratory every step of the way and I am very grateful for it. To PhD student Edwina Uzunuigbe, thank you for supervising me with the QD synthesis it was pleasure working with you. To every person who has contributed to this journey, I appreciate you very much. Mrs Valencia Jamalie, you know my journey and I can't thank you enough for being my second mother, at the University, with unending support, motivation and care.

Additional thanks go to Professor Martin Onani (Chemistry department), and Prof. Mervin Meyer (Biotechnology department), for allowing access to your laboratories and equipment. The National Nanoscience Teaching and Training Platform, Department of Science and Technology and NIC for funding my studies and this research.

To my best friend, you made me see the sun where there once were clouds, your encouragement, diligence, humility and emanating love, sets you apart. Lastly, many thanks to my family; an amazing sister who encourages and motivates me every step of the way, always lifting my spirit and enduring my crazy work mode behaviour. My wonderful parents, thank you for your endless love and support. You always push me to be the best I can be; I would never achieve anything or be where I am in this life if it wasn't for you, your loving support and guidance.

It's never too late, to finish what you started…

It is never too late to start either…

But always remember, to finish what you start.

CHAPTER 1

INTRODUCTION

Cancers are heterogenous entities triggered by epigenetic or genetic mutations/damage that are hereditary or sporadic in mutation, furthermore, leading to a disruption in homeostasis and the consequent onset of neoplasms (Balani *et al*., 2017; Tomasetti *et al*., 2017). Tumours of the central nervous system (CNS) are among the most typical paediatric neoplasms accounting for approximately 20-23% of childhood cancers, while gliomas are responsible for 70% brain tumours (glioblastomas (GBs) being highly malignant and recurrent, further constituting 16% of primary brain and CNS neoplasms), in addition, metastatic cancers account for roughly 90% of cancer-related fatalities, (Oghaki, 2009; Penn, 2013; Heine *et al*., 2015; Davis, 2017). Conventional treatment modalities such as radiation therapy, chemotherapy and surgical resection are currently available, however, early detection and imaging techniques are not yet fully satisfactory. Low tolerance toward cancer therapy especially in adults may occur in the form of non-specific cell death (concurrently killing healthy cells), tumour recurrence and drug resistance all of which are associated with some of the current treatment modalities (Singh and Nehru, 2008; Han *et al*., 2016; Oh *et al*., 2017). To circumvent the limitations and challenges in detecting cancers at the cellular level, improvement in technologies and treatments are needed with much better specificity and sensitivity. From a therapeutic standpoint, it is vital to elucidate the pathophysiology of the cells responsible for tumour formation, progression and recurrence (Galli *et al*., 2004).

Nanotechnology, the "engineering and manufacturing of materials using atomic and molecular components" at the nano-meter (nm) sized scale, is finding relevance and application in medicine generally and oncology in particular (Alexis *et al*., 2008). Quantum dots (QDs) are a semiconductor nanocrystal, with lesser physical dimensions than exciton Bohr radius (Noh *et al*., 2010). In this study, the synthesis, characterization and biological application of QDs are investigated. Various types of QDs can be synthesized and this requires high temperatures and non-aqueous medium, as the constituent materials possess low efficiency. However, these incongruities can be corrected with the synthesis of Cadmium Telluride (CdTe) QDs which possess high fluorescence efficiency and good stability (Kim *et al*., 2015). Owing to their quantum confinement effects, QDs possess inimitable optical and electronic properties, which surpass those of traditional organic dyes (Wang and Chen, 2011). QDs have broad absorption excitation spectra's while emitting a narrow emission spectrum and also allow for multiplexing since several QDs can be

emitted via a single excitation light source. In addition, varying QD sizes allow for size-tuneable emissions across the electromagnetic spectrum acting as a multicolour probe for imaging and tracking purposes in biological applications. In addition, due to their high quantum yield and large molar distinction coefficients, QDs possess increased photoluminescence (PL) less prone to photobleaching (Chan *et al*., 2002; Rzigalinski and Strobl, 2009; Wang and Chen, 2011; Onoshima *et al*., 2015).

The aberrant or compromised vasculature observed in most tumours, typified by hyperpermeability with large fenestrations and a leaky vasculature, often serves as a window for nanoparticle (NP) uptake into the tumour interstitium with an enhanced permeability retention (EPR) effect (Haley and Frenkel, 2008; Mattoussi *et al*., 2011). The small size of QDs (1-20nm radius) enables them to enter tumour tissue and along with their manipulative surface and size properties, these particles show promise in imaging and detection modalities, serving as an ideal fluorophore for ultrasensitive and multiplexing applications, leading to the development of multiplexed molecular diagnostic tools for *in vivo* imaging, facilitated drug delivery and bioanalytic applications (Chan *et al*., 2002; Smith *et al*., 2008; Mattoussi *et al*., 2011; Wang and Chen, 2011). Thus, the introduction of NPs in cancer research, for improved diagnostics, targeting and drug delivery is invaluable (Choi *et al*., 2007).

1.1 Justification of Current Research

Current options for early detection and treatment of neuroblastoma (NB) and glioblastoma GB cancers are poorly effective, with many attendant side effects. There is therefore the need for improved and targeted treatment modalities with higher stability and specificity in order to circumvent the current limitations. Nanomedicine involves the application of the nanotechnology concepts, principles and methods to produce biocompatible NPs which function to improve diagnosis and treatment of cancer and other diseases (Wang *et al*., 2011; Aliosmanoglu and Basaran, 2012).

Highly luminescent QDs are favourable in bioanalytical applications, imaging and detection modalities. QD labelling has been reported to facilitate drug delivery within live cells and small animals, thus, eliciting the development of fluorescent nanoprobes for cancer detection and treatment (Wang *et al*., 2011; Liu *et al*., 2015). Thus, drugs can be labeled with molecules/ nanocarriers, making QD-based therapeutics very invaluable alternatives to conventional cancer treatments (Wang *et al*., 2011).

1.2 Aim

The aim of this study was to synthesize monodispersed and highly luminescent non-functionalized MPA-capped CdTe/ZnS (3-Mercaptopropionic acid capped with Cadmium Telluride and a zinc sulphide shell) QDs, known to be water-soluble, biocompatible and have relatively low toxicity within the CdTe spectra range; and to evaluate their physical and optical properties as well as their long-lasting biological effects on two cancerous neuronal cell lines namely, GB U87 cells and NB SH-SY5Y cells.

1.3 Objectives

To synthesize mono-dispersed and highly luminescent non-functionalized MPA-capped CdTe/ ZnS QDs and evaluate:

1.3.1 The physical characteristics

1.3.2 Biological activity thereof in two cancerous neuronal cell lines

1.4 Hypothesis

We hypothesize, that the MPA-capped CdTe/ZnS QDs will be water soluble, biocompatible for biological application and selectively cytotoxic to U87 and NB SH-SY5Y cells.

CHAPTER 2

LITERATURE REVIEW

2.1 Tumorigenesis and Vasculature

Tumourigenesis is defined as a "multistep process" involved in the formation of cell masses or a tumours which need not be cancerous but could be malignant or benign. It is driven by dedifferentiation, increased cell proliferation, metabolic dysregulation, epigenetics, apoptotic evasion and immunosurveillance (Ashkenazi *et al*., 2008; Califano and Alvarez, 2017; Cao, 2017). The observed mutations are therefore subsequent to and accountable for a disruption in homeostasis, driven by the above-mentioned cancer malignant properties, to reiterate fast cell proliferation, dedifferentiation and extracellular matrix (ECM) metabolism, which creates a growth favourable environment, restricted death rate and ECM stability (Ashkenazi *et al*., 2008; Cao, 2017).

Cancers are heterogenous entities made up of multiple cell lineages, which require the slightest genetic mutation for the onset of neoplastic development, thus suggesting genetic instability thereof (Ashkenazi *et al*., 2008). Cancer progression is also characteristic of "dominant gain-of-function and recessive loss-of-function alterations in gatekeeper genes", viz the mutation of oncogenes and tumour suppressor genes, which allow somatic gene mutations to alter their expression activities/levels and are further believed to be accountable at the root of neoplasia initiation (Tlsty and Coussens, 2006; Cao, 2017). Sequential changes in tumour cell genomes and epigenomes denote the modeling of human tumour formation, by means of clonal expansions, which ultimately creates aggressive cell populations with marked neoplastic phenotypes, presenting as the primary or metastatic tumour (Chaffer and Weinberg, 2015). Consequentially there is much variability in the pathways of tumour initiation and progression, such as the varying oncogenic mechanisms including the multistep processes involved in chromosomal rearrangements for various oncogene activation, oncogene mutation, inactivation of tumour suppressor genes and the possible chromosomal translocations, among others (Pierotti *et al*., 2003).

An increase in cell proliferation is concomitant with the influx in oxygen and nutrient demands at cell sizes > 2-4mm^3 and thus the high metabolic activity expressed in tumourigenic masses are met by means of new blood vasculature, a process known as angiogenesis wherein nascent vessels

form from pre-existing vascular beds (Tlsty and Coussens, 2006). Endothelial cells are both proliferative and migrative shifting toward assisted perivascular support to ensure stabilization of pro- and anti-angiogenic molecules and lymphatic drainage of waste products under homeostasis. However, in incipient neoplasia, tumour vessels may lack the protective effects of perivascular cells triggering proangiogenic molecular and cellular programmes, via signals such as genetic mutations, metabolic and mechanical stress and immune/inflammatory response, subsequent to tortuous tumour-associated angiogenesis (Carmeliet and Jain, 2000; Tlsty and Coussens, 2006; Siemann, 2011).

Tumour vasculature is convoluted and unstable, with its vessels being structurally and functionally abnormal, typified by hyperpermeability due to various openings such as endothelial fenestrae, arteriolar-venous shunts and discontinuous/absent basement membranes with uneven diameters. Moreover, the clumped like growth of endothelial cells projecting into the lumen in addition to dilated, leaky lymphatic vessels, creates a fluid engorged vessel, all characteristic of a leaky vasculature in tumours (Carmeliet and Jain, 2000; Siemann, 2011). Being structurally disparate with impaired blood flow stems abnormal micro-environmental conditions which deter traditional therapeutic anti-cancer therapies (Siemann, 2011). Figure 2.1 further elaborates on the mechanisms of tumour vessels formation.

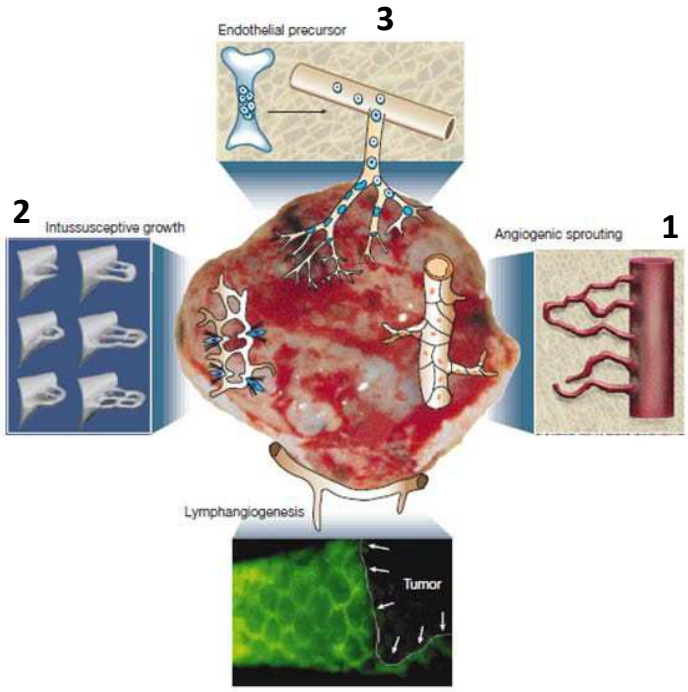

Figure: 2.1 Tumour Vessel Formations. Cellular mechanisms of tumour (lymph) angiogenesis. Tumour vessels grow by various mechanisms: (1) the host vascular network expands by budding of endothelial sprouts or formation of bridges (angiogenesis); (2) tumour vessels remodel and expand by the insertion of interstitial tissue columns into the lumen of pre-existing vessels (intussusception); and (3) endothelial cells precursors (angioblasts) home from bone marrow or peripheral blood into tumours and contribute to the endothelial lining of tumour vessels (vasculogenesis). Lymphatic vessels around tumours drain the interstitial fluid and provide a gateway for metastasizing tumour cells (Carmeliet and Jain, 2000).

2.2 The Nervous System

The nervous system includes all neural tissue and is comprised of two major anatomical divisions namely; the CNS, which includes the brain and spinal cord mainly involved in integration, processing and coordination of sensory and motor commands, as well as the peripheral nervous system (PNS), which includes all the outer lying neural tissue retrospect of the CNS, comprised of a network of spinal and cranial nerves, in addition to receptors which assist in detecting environmental changes and delivering such information to the CNS (Martini, 2006). Thus the PNS has afferent and efferent divisions; the efferent division branches into two components; the somatic nervous system (SNS), constituting voluntary and controlled skeletal muscle contractions and the autonomic nervous system (ANS) also known as the visceral/involuntary system, which functions in maintenance of homeostasis, regulating blood pressure, thermoregulation, nutritional responses of the gastrointestinal (GIT), contraction of the urinary bladder, convergence and focusing of the

eyes, among other functions (McCorry, 2007).

Neurons are specialized cells forming the building units of the nervous system and are further supported and protected by neuroglia cells. The neuron doctrine defines nerve cells as polarized structures owing to the law of polarization wherein the nerve cell body and dendrites serve as a receptor platform for incoming messages in contrast to the axonal body's output of communication, which moreover, form the structural, functional, developmental and trophically individualistic components of the nervous system (Guillery, 2005). Functionally, neurons may be categorized as sensory (afferent) neurons which deliver information to the CNS arising from sensory receptors, or motor (efferent) neurons which are effective in the transmission of signals from the CNS to peripheral effector cells within the peripheral tissues and organs.

In addition, interneurons (associated neurons) relay sensory information and coordinate motor activity, with an involvement in higher functions such as learning, memory and planning (Martini, 2006). Whereas the nervous system is said to regulate stem and precursor cell function thereby modulating development, homeostasis and plasticity, cancers reciprocally modulate the activity thereof via excitation of brain neurons and encourage ingrowth of new neuronal branches (Venkatesh and Monje, 2017).

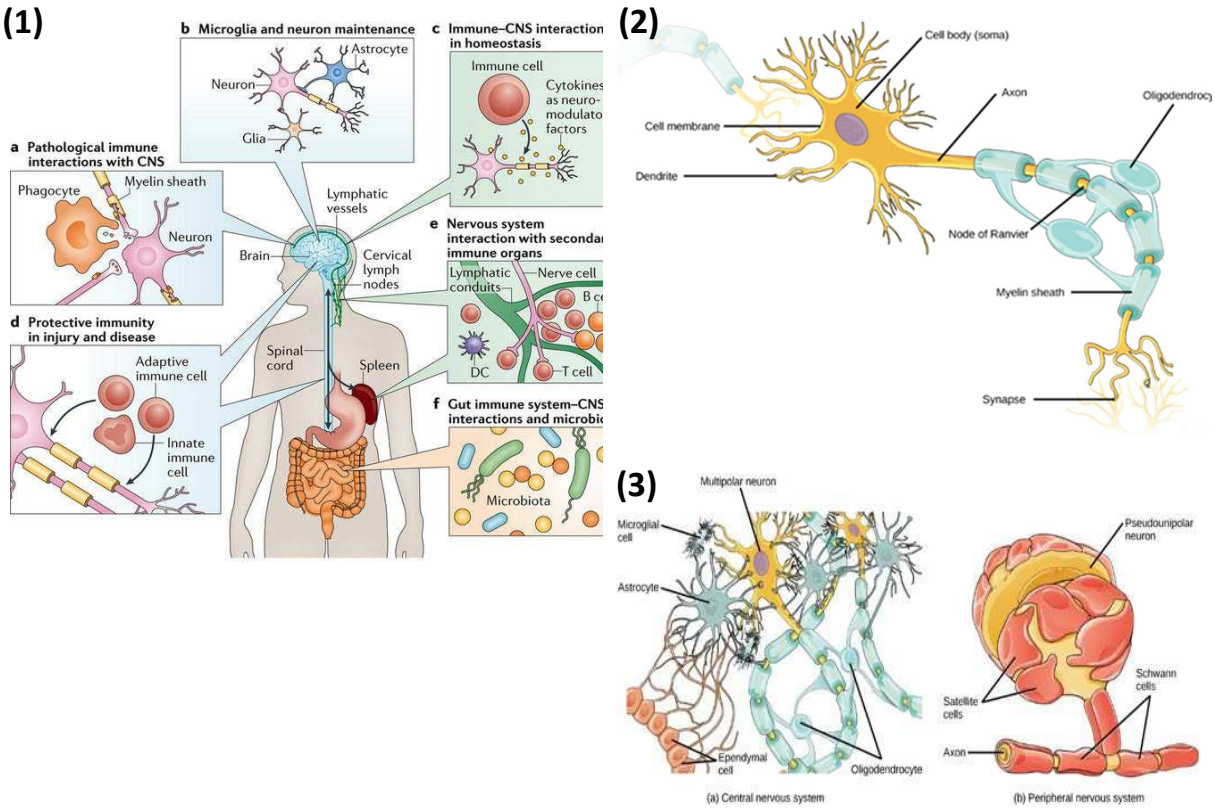

Figure: 2.2 The CNS and Structural Classification of Neurons. (1) Human Nervous system (2) Neurons contain organelles common to many other cells, such as nucleus and mitochondria. They also have more specialized structures, including dendrites and axons. (3) (Glial cells support neurons and maintain their environment. Glial cells of the (a) CNS, include oligodendrocytes, astrocytes, ependymal cells, and microglial cells. Oligodendrocytes form the myelin sheath around axons. Astrocytes provide nutrients to neurons, maintain their extracellular environment, and provide structural support. Microglia scavenge pathogens and dead cells. Ependymal cells produce cerebrospinal fluid that cushions the neurons. Glial cells of the (b) PNS, include Schwann cells, which form the myelin sheath, and satellite cells, which provide nutrients and structural support to neurons. (OpenStax, 2015; Kipnis and Filiano, 2018).

2.2.1 Barriers of the Central Nervous System (CNS)

The blood brain barrier (BBB) and blood-cerebrospinal fluid barrier (BCB) are an intricate vasculature network which implements the cellular barrier between systemic circulation and the CNS, thus providing protection and maintenance of a healthy microenvironment of the CNS (Alvarez *et al*., 2011).

2.2.1.1 The Blood Brain Barrier (BBB)

The BBB serves as a vital regulator in maintaining the constancy of the core environment of the

brain, such as the provision of essential nutrients, drugs and hormones, elimination of metabolites from the brain and protecting it from the external bloodstream environment (Faria *et al*., 2013; He *et al*., 2018). A complex network of microvessels constitutes the BBB, characteristic of tight circumferential junctions (zona-occludens) which offer a regulatory role, thus lowering the permeation of ions and hydrophilic solutes by aqueous intra-paracellular pathways, lowered densities of pinocytic vesicles and efflux carriers, amongst other transporters (Youdim *et al*., 2004; Alvarez *et al*., 2011; He *et al*., 2018). Anatomical and physiological protection is thus provided for the CNS, which ensures selective restriction of the passage of substances, such as small polar molecules and macromolecules from the cerebrovascular circulation into the nervous tissue of the brain, regulation over transendothelial molecular flow and brain extracellular fluid composition (Pachter *et al*., 2003; Youdim *et al*., 2004; Hanson and Frey, 2008). In this way, the BBB restricts anticancer therapeutic agents from reaching the CNS thus serving as a regulatory interface, dependent on the drug size and charge (Pachter *et al*., 2003; Youdim *et al*., 2004). The high permeability and fenestrated capillaries of circumventricular organs (CVOs), permits hormonal exit of the brain without engaging the BBB and similarly allow substances to trigger changes in the brain without crossing the BBB (Ganong, 2000). However, the comparative surface area of CVOs and BBB capillaries is 1:5000 and thus does not serve as a realistic means of anti-cancer therapeutics entering the brain (Begley, 1996).

2.2.1.2 The Blood Cerebrospinal Fluid Barrier (BCB)

The anatomical foundation of the BCB lies in the epithelial cells constituting the choroid plexus (CP), with contact-mediated mechanisms and/or soluble factors being accountable for barrier function (Alvarez *et al*., 2011). Although CP capillaries are fenestrated and leaky, and do not possess BBB properties, the tight junctions of their epithelial-like ependymal cells, account for the barrier formation (Cipolla, 2009). Primarily, the CP functions as a secretor of cerebrospinal fluid (CSF), which is vital for the mechanical safeguard of the brain (via provision of cushioning effect), implements normalization of intracranial volumes, delivery of neuroendocrine factors and buffering of extracellular fluids, among other solutes (Alvarez *et al*., 2011). Thus, the CP serves as a barrier between choroid epithelial cells which separate blood and the CSF.

2.3 Apoptosis in Cancer

Cancers are quite relative in their characterization, typified by defects of apoptosis resulting in immortal replicas of cell types, in addition to various alternate malignancies which flaw the regulatory pathways of apoptosis (Ghobrial *et al*., 2005). Comparative examples thereof include B-cell chronic lymphocytic leukaemia, follicular lymphoma and tumours affected by human T-cell leukaemia/lymphoma virus-1, in contrast to regulatory defects such as p53 and the nuclear factor kappa B (NF_B) (Ghobrial *et al*., 2005). Apoptosis is a well-studied form of programmed cell death (PCD), operating in chemotherapeutic cell death and in the event of not sensing chemotherapeutic agent-induced damage for subsequent apoptotic initiation, may possibly result in multidrug resistance (Yu and Hung, 2009; Tan and Yu, 2013; Tait *et al*., 2014). Similarly, epidermal growth factor receptor type 2 (ErbB2) (which is overexpressed in roughly 30% human breast cancers) rendered these cells resistant to the intended chemotherapeutic drug, paclitaxel (Yu and Hung, 2009; Tan and Yu, 2013). Given the understanding of apoptosis, it has therefore enabled novel targeted routes for the culmination of cell death in cancerous cells or the sensitization thereof, thereby establishing cytotoxic agents and radiation therapy (Ghobrial *et al*., 2005).

2.3.1 Apoptosis vs Non-apoptotic cell death

Regulated cell death (RCD) is essential for homeostasis and is partitioned into apoptotic PCD1, followed by necrosis and regulated non-apoptotic cell death mechanisms, which include autophagy, necroptosis, pyroptosis and caspase-independent cell death (CICD), built on respective morphological changes, enzymatic activity, the amount of adenosine triphosphate (ATP) and adjacent cellular effects (Carlson *et al*., 2000; Hongmei and Ntuli, 2012; Tait *et al*., 2014).

2.3.1.1 Non-apoptotic cell death

Non-apoptotic cell death mechanisms can be initiated independent of apoptosis or in the event of apoptosis failing to follow through (Tait *et al*., 2014). Necrosis is a passive form of inadvertent cell death arising from environmental trepidations such as toxic or physical injury which may succumb to damage of the plasma membrane accompanied by uncontrolled inflammatory release of cellular contents (Tsujimoto, 1997; Fink and Cookson, 2005). The causation thereof is rooted in the inability of cells to maintain homeostasis, leading to an influx of water and extracellular ions which inevitably results in lysis of intracellular organelles, and discharging cellular contents into the extracellular fluid (Wyllie *et al*., 2003). Necrosis is therefore a non-apoptotic process, marked

by random deoxyribonucleic acid (DNA) cleavage due to consequent cellular degeneration, as presented on electrophoretic smears, and more pronounced inflammatory responses due to plasma membrane rupture culminating in the death of cells (Tsujimoto, 1997; Carlson *et al*., 2000).

Necrosis can further be distinguished by its regulated PCD forms, namely, necroptosis, pyroptosis, ferroptosis and parthanatos, forming a subset of non-apoptotic cell death mechanisms and are suggested to be important for pathological and physiological processes (Kim, 2017). Although morphologically similar to necrosis, necroptosis is initiated by various stimuli as an active form of RCD, initiated by death receptor ligands such as tumour necrosis factor (TNF) and FAS, highly dependent on mixed lineage kinase domain-like (MLKL) protein, RIPK1 and RIPK3 kinases components for signaling, honing its ultimate morphological feature in the swelling and rupturing of the cell membrane, releasing damage-associated molecular patterns (DAMPs) (Tait *et al*., 2014; Kim, 2017; Galuzzi and Vitale, 2018). Parthanatos is initiated by PARP1 hyperactivation, due to the overreaction of DNA damage-responsive nuclear PARP enzymes, subsequent to the depletion of ATP and AIF dependent DNA degradation (Kim, 2017; Galuzzi and Vitale, 2018). Thirdly, another form of necrotic PCD, is ferroptosis, a process characterized by lipid peroxidation which perturbs the intracellular microenvironment due to the accumulation of lethal ROS, thus, culminating in cell death and is furthermore, associated in degenerative diseases (Kim, 2017; Galuzzi and Vitale, 2018). Biochemically and morphologically different from apoptosis, pyroptosis is another caspase-dependent PCD initiated by the pro-inflammatory caspase-1 or caspase-5 in humans, which is highly dependent on plasma membrane pore formations by gasdermin protein family, further denoted by inflammation, in particular swelling of cells, marked lyses of the plasma membrane and exhibits a distinct form of chromatin condensation, void of mitochondrial permeabilisation (Tait *et al*., 2014; Galuzzi and Vitale, 2018). Contrarily, CICD is induced by the pro-apoptotic triggers which cause mitochondrial outer membrane permeabilisation (MOMP), void of caspase activation, although it has shared features of apoptosis, it is distinctly different at many levels viz morphologically, biochemically and kinetically (Tait *et al*., 2014).

Microautophagy, macroautophagy and chaperone-mediated autophagy each reflect autophagy, however, the more established macroautophagy will majorly depict the term autophagy (Mizushima, 2007). Autophagy is carried out by ATG proteins, denoted by a lysosomal process, whereby cytosolic contents are engulfed by an isolated membrane creating an autophagosome and

further lysed by the fusion of lysosomes conferred with autophagic/ type II cell death, which in its entirety serves as an "intracellular degradation system" (Mizushima, 2007; Tait *et al*., 2014). Autophagy is thus not only a sequential process, but a multifunctional one, which surpasses its expected physiological and pathophysiological role, in that it can be employed as a pro-survival stress response in nutrient starvation adaption, intracellular protein, organelle and microorganism clearance, anti-aging, development, tumour suppression and of course cell death. (Mizushima, 2007; Tait *et al*., 2014). In minor context, the process can be divided into "induced autophagy", such as the pro-survival stress response, resulting in concomitant amino acid production and increased phagosomal assembly, in order to digest the intracellular constituents and thus provide nutrition for the cell, contrarily, "basal autophagy", embodies the cytosolic component turnover (Mizushima, 2007; Castro-Obregon, 2010).

The various aspects highlighting programmed versus non-programmed cell death mechanisms are further tabulated in table 2.1 below.

Table 2.1 Overview of the various cell death pathways

Variables	Programmed						Non-programmed
	Apoptosis	Autophagy	Programmed necrosis				Necrosis
			Necroptosis	Parthanatos	Pyroptosis	Ferroptosis	
Trigger	Death receptor	Starvation	Death receptor activation and inhibition of caspase-8	Genotoxic stress	Inflammasomes	Experimental compounds	Infection
	Intrinsic	Rapamycin		Excitotoxicity		Clinical drugs	Toxins
							Trauma
Inflammatory response	No	Yes	Yes	Yes	Yes	Yes	Yes
Aspects	Chromatin condensation	Membrane blebbing	Mitochondrial swelling	Chromatin condensation	Cell swelling	Increased Membrane density	Mitochondrial swelling
	Nuclear fragmentation	Autophagic vacuoles	Cell swelling	Nuclear fragmentation	Membrane rupture	Small mitochondria	Cell swelling
	Apoptotic body	Increased lyssomal activity	Membrane rupture		Maintained Mitochondrial integrity		Membrane rupture
	Membrane blebbing						
Key regulators	Cytochrome c Caspases	Atg proteins Beclin-1	RIP 1/3 MLKL	PARPs AIF	Caspase-1/4/5/11 Gasdermin D	GPX4	-

(Kim, 2017)

2.3.1.2 Apoptosis

Apoptosis PCD1, is a control mechanism which requires the activation of caspase proteases to eliminate unwanted/irrelevant cells, culminating in cell death with distinct biological and

morphological traits, and thus plays a key role in various biological events, such as, morphogenesis, tissue sculpting during embryogenesis, homeostatic maintenance of tissues and the removal of harmful/damaged cells, development of the immune/nervous system and endocrine-dependent tissue atrophy (Tsuijimoto, 1997; Wyllie *et al*., 2003; Tait *et al*., 2014). Apoptosis is morphologically typified by cytoplasmic and nuclear condensation, chromatin cleavage, cellular fragmentation and assemblage into membrane-bound particles (apoptotic bodies). These structures are phagocytosed by other cells in the body and do not therefore elicit inflammation, however, *in vitro* these apoptotic bodies swell and eventually lyse, termed as "secondary necrosis" (Wyllie *et al*., 2003; Fink and Cookson, 2005). Additionally, apoptosis is characterized by DNA fragments of 180-200 base pairs, formed by the cleavage of genomic DNA between nucleosomes, potentially resolved as DNA ladders, succeeding electrophoresis (Carlson *et al*., 2000; Fink and Cookson, 2005). Multi-signal pathways account for the onset of apoptosis, induced by various stimuli including depletion of growth factors and hormones, heat shock, gamma-irradiation and crosslinking of the Fas antigen, and the regulation thereof is due to a variety of complex extrinsic and intrinsic ligands (Tsujimoto, 1997; Hongmei and Ntuli, 2012).

Apoptosis can also be described as a cysteine aspartic acid-specific protease (caspase)-mediated cell death, based on the proteolytic activity thereof, which can be divided among primarily apoptotic associated caspases (caspase 2, 3, 6, 7, 8, 9 and 10), as well as those which are central to cytokine processing in the event of inflammatory responses (caspase 1, 4, 5, 11, 12, 13 and 14) (Fink and Cookson, 2005). The proteolytic activity of additional substrates orchestrates cell death and packaging for cell clearance, and thus accounts for the morphological traits of apoptosis, which include plasma membrane blebbing (resulting from caspase-mediated activation of the actin depolymerizing enzyme, gelsolin), loss of cell shape due to cleavage of cytoskeleton proteins, foldrin in particular, in addition to the cleavage of PAK2 (a p21 activated kinase family) producing apoptotic bodies (Green, 1998; Fink and Cookson, 2005).

The interplay between autophagy and apoptosis, along with the cross talk between various modes of cell death, are illustrated in figure 2.3 below.

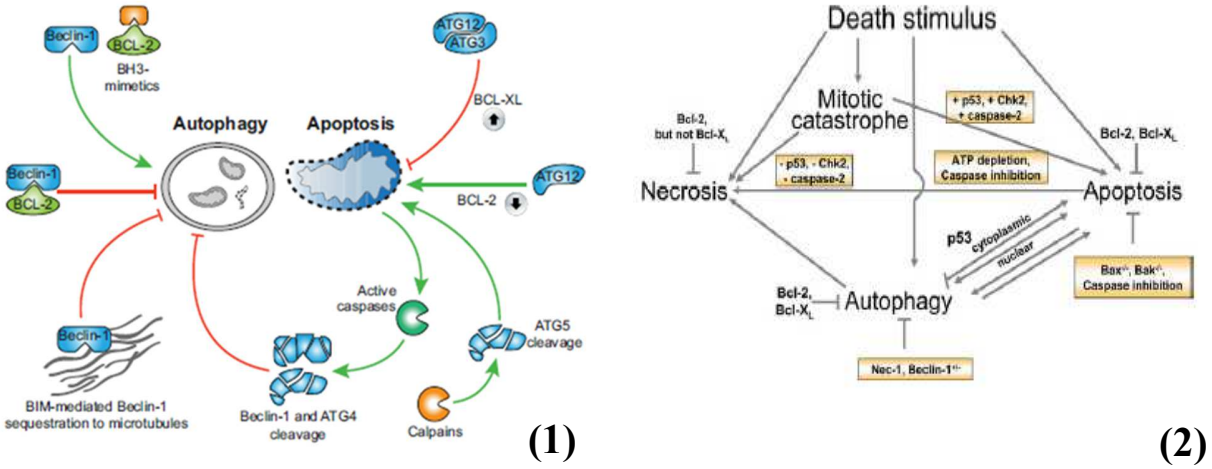

Figure: 2.3 Apoptosis and non-apoptotic cell death. **(1)** Interplay between autophagy and apoptosis. BCL-2 sequesters Beclin-1, thereby inhibiting autophagy that can be reversed by BH3 mimetics. Furthermore, Bim can sequester Beclin-1 onto microtubules, which also inhibits autophagy (shown on the left). In contrast, ATG12 conjugation to ATG3 enhances BCL-XL expression, thereby inhibiting apoptosis. Unconjugated ATG12 can act in a manner like BH3-only proteins and induce mitochondrial-dependent apoptosis. Calpain-mediated cleavage of ATG5 results in the liberation of a proapoptotic fragment of ATG5 that leads to mitochondrial outer membrane permeabilisation and cell death. In addition, caspase-mediated cleavage of autophagy proteins inhibits autophagy (shown on the right). **(2)** Cross talk between different modes of cell death. Toxicants might trigger different modes of cell death depending on which pathways can be activated. Inhibition of one particular pathway might lead to cell death by a different mechanism. However, some inhibitors (Bcl-2) can block several cell death modalities. The p53 status of the cell is also important for the mode of cell death that is induced (Tait *et al*., 2014).

2.3.2 Apoptotic Pathways

Apoptosis subsumes two pathways, the extrinsic (cytosplasmic) pathway initiated by the Fas death receptor, a member of the TNF receptor family, closely followed by intitation of the Intrinsic (mitochondrial) pathway, which releases cytochrome-c and activation of the death receptor, upon stimulation (Ghobrial *et al*., 2005). These pathways converge at the cleavage of caspases, into one shared pathway, wherein the mitochondria serve as the "cross talk organelle", connecting the two pathways, resulting in cell death (Hongmei and Ntuli, 2012). Given their relatively simplistic distinction, overexpression of B-cell lymphoma 2 (Bcl-2) in the intrinsic pathway may inhibit the extrinsic pathway, while TNF alpha (TNFα) might increase the expression of nuclear factor kappa-light- chain enhancer of Bcells (NFkB), thus stimulating antiapoptotic members of the Bcl-2 family proteins (Ghobrial *et al*., 2005).

2.3.2.1 Extrinsic Pathway

Several multisignal pathways and proteins conduct the onset of extrinsic mediated apoptosis, with its initiator lying in the ligation of multicomplicated death receptors at the cell surface (Hongmei and Ntuli, 2012). Membrane bound Fas ligand (FasL), is triggered by a death stimulus which subsequently forms the death-inducing signalling complex (DISC) containing the Fas associated death domain proteins, which in turn activate caspases 8/10 propagating the death signals in a downstream of effector caspase events leading to cell death (Fink and Cookson, 2005; Ghobrial *et al*., 2005). However, Caspase 8 may also interact with the intrinsic pathway, by cleaving BID and releasing cytochrome-c, wherein the mitochondria serves as the "cross talk organelle" as previously mentioned (Ghobrial *et al*., 2005; Hongmei and Ntuli, 2012).

2.3.2.2 Intrinsic Pathway

The Bcl-2 family of proteins are key conductors of the intrinsic pathway, which comprises proapoptotic (e.g. Bcl-2 associated X protein (Bax)) and antiapoptotic (e.g.: Bcl-2) members which are repressors that block the release of cytochrome-c. Death signals trigger the proapoptotic protein to undergo posttranslational modifications and thus migrate to the mitochondria, furthermore the mitochondrial membrane potential is compromised and becomes permeable, releasing cytochrome-c into the cytosol, which activates caspase-9, -3 leading to inevitable apoptotic cell death (Wyllie *et al*., 2003; Ghobrial *et al*., 2005; Hongmei and Ntuli, 2012). Lamin proteins which are cleaved by effector caspases, result in nuclear shrinkage and fragmentation through caspase 3 (Fink and Cookson, 2005), while apoptosis-inducing factor (AIF), one of the predominant "caspase independent" proapoptotic members, is released from the mitochondria into the cytoplasm, causing a cleavage of DNA due to its proteolytic effects (Hongmei and Ntuli, 2012). Thus, apoptosis occurs if the DNA impairment is not restored (Wyllie *et al*., 2003; Hongmei and Ntuli, 2012). Given the overexpression of Bcl-2 in many malignancies, a resistance of chemotherapeutic drug and radiation therapy may occur, in addition to cell accumulation in the G_0 phase of the cell cycle attributing to chemoresistance. On the contrary, reduced Bcl-2 expression may have a positive response to chemotherapeutic drugs (Ghobrial *et al*., 2005). Figure 2.3 illustrates the two apoptotic cell death pathways.

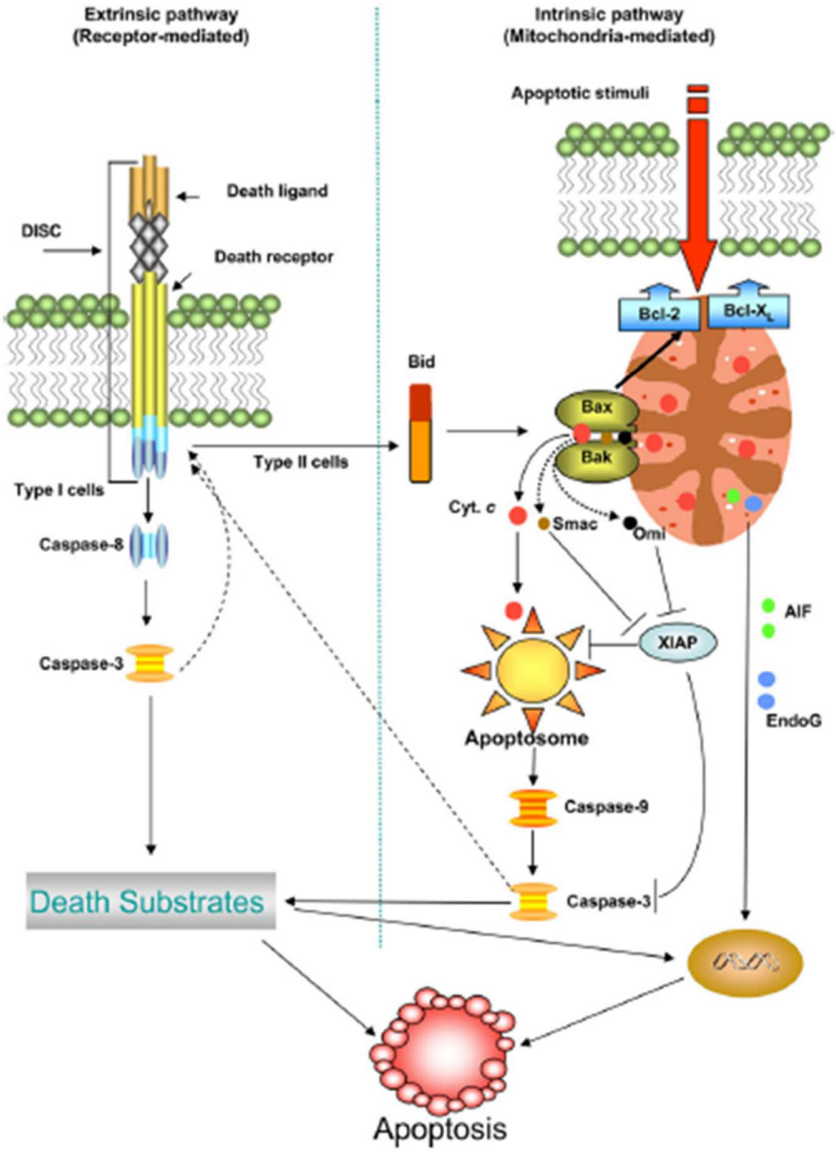

Figure: 2.4 Schematic illustration of apoptotic cell death pathways. The extrinsic pathway is triggered by ligands binding to receptors on the cell surface (TNFR1, CD95, TRAIL), resulting in their oligomerization, formation of DISC, and caspase-8 activation. In Type I cells, caspase-8 activates caspase-3, which results in the cleavage of a host of target proteins and apoptosis. In Type II cells, caspase-8 cleaves Bid, resulting in the engagement of the mitochondrial pathway. The latter involves the release of proapoptotic proteins (cytochrome c, Smac, Omi, AIF, and EndoG) from the mitochondrial intermembrane space into the cytosol via Bax/Bak-mediated pores in the outer membrane. Here, cytochrome c, Smac, and Omi participate in the activation of the caspase cascade, whereas AIF and EndoG are further translocated to the nucleus, where they participate in chromatin condensation and large-scale DNA fragmentation. X-Inhibitor of Apoptosis Protein is a cytosolic IAP, whose activity is blocked by Smac and Omi (Orrenius *et al.,* 2011).

2.4 Cancers: Neuroblastoma (NB) and Glioblastoma (GB)

Tumours of the CNS are among the most common paediatric neoplasms accounting for

approximately 20-23% of childhood cancers (Ahmed *et al*., 2007; Penn, 2013). Moreover, CNS tumours are associated with a range of symptoms and complications, such as oedema, seizures, endocrinopathy, fatigue, psychiatric disorders, and venous thromboembolism, which may pose extreme impacts on quality of life (Brem *et al*., 2000).

Primary and metastatic brain tumours are heterogenous neoplasms wherein the primary ranges from non-invasive, surgically curable pilocytic astrocytomas, to highly invasive and incurable GB multiforme. The metastatic forms on the other hand, may or may not be associated with systemic disease (Brem *et al*., 2000). Primary spinal cord tumours make up 2-4% of primary CNS tumours, with extramedullary lesions accounting for 70-80% of the spinal tumours and the most common intramedullary spinal tumours comprising astrocytomas (predominant in children) and ependymomas (predominant in adults) (Brem *et al*., 2000). Metastatic cancers account for roughly 90% of cancer-related fatalities and require specific physical changes such as acquiring migratory phenotypes in onset to invade adjacent tissues via chemotaxis into lymphatic/blood vessels in distant organs and tissues (Heine *et al*., 2015).

2.4.1 Neuroblastoma (NB) Cancer

NB is the most typical extra-cranial solid tumour in childhood, usually presenting as an abdominal mass and accounting for 7% of childhood cancers (1 case per 100 000 children/year opposed to 1 case per 10 million adults/year) (Conter *et al*., 2014; Dumba *et al*., 2014). NB arises from sympathetic neuroepithelial cells during early development and can be situated in the adrenal medulla, abdomen, paraspinal sympathetic ganglia of the neck, chest, or pelvis (Choi *et al*., 2007; Conter *et al*., 2014). Presentation of symptoms is dependent on the location of the tumour and the extent of disease, with the localized form being asymptomatic in contrast to the metastatic form which presents with fever and bone pain, manifesting ecchymoses and spinal cord compression observed in those with the paraspinal tumour (Weinstein *et al*., 2003).

The human neuroblast-like NB cell line, SH-SY5Y is derived from a metastatic bone marrow biopsy, subcloned from the parental cell line SK-N-SH, and resembles catecholaminergic neurons, because it expresses tyrosine hydroxylase activity and mechanistic catecholamine uptake (Gomez-Santos *et al*., 2003; Kovalevich and Langford, 2013; Shipley *et al*., 2017). The cells are arrested in an immature neuronal stage marked by a low level of neuronal markers, but when exposed to

the appropriate environmental growth factors, these cells undergo differentiation into mature, neuronal (noradrenergic and cholinergic) phenotypes, with marked sensitivity to oxidative stress, associated with dopamine synthesis (Gillany *et al*., 2008). Factors which influence overall NB survival (OS) include "stage, age, histology, tumour grade, MYCN oncogene status (associated with the metastatic form and 20% of primary NBs), chromosome 11q status and DNA ploidy" which constitutes part of the international NB risk assessment system, with a five-year survival rate in 85% of infants (Weinstein *et al*., 2003; Conter *et al*., 2014). The tumours may undergo spontaneous regression or differentiate into a ganglioneuroma (Weinstein *et al*., 2003). Traditional chemical and surgical treatments are insufficient in preventing the progression, metastasis and recurrence of the tumour, predominantly in adults with poorer tolerance and thus remaining a therapeutic challenge, with poor prognosis. Existing imaging techniques are yet to provide fully satisfactory diagnostic images for early and accurate diagnosis (Choi *et al*., 2007). Dose intense cytotoxic chemotherapy, high-dose chemotherapy together with autologous stem cell rescue (HDCSR) and external beam radiation, are a few of the alternate treatments with greater response to survival (Conter *et al*., 2014).

2.4.2 Glioblastoma (GB) Cancer

Astrocytic tumours are the most common primary brain tumours, with GBs, a fatal neoplasm possessing the highest malignancy and resembling behaviour of cancerous neuronal cells (Hirose *et al*., 2001; Galli *et al*., 2004; Heine *et al*., 2015; Oh *et al*., 2017). It constitutes 16% of primary CNS neoplasms, which occur predominantly in the brain, but may also be present in the brainstem, cerebellum and spinal cord (Davis, 2017). GB multiforme, is a highly aggressive cancer, characterized by marked invasiveness and extensive intra- and inter-tumour heterogeneity, caused by the epi/genetic alterations. GB have the most unfavourable prognosis and complete resection of these tumours is not only challenging due to the difficulty and near impossibility of eradicating the whole cancerous area, but also because recurrence is very high, usually within one year post-radiation and chemotherapy (Hirose *et al*., 2001; Yukawa *et al*., 2013; Heine *et al*., 2015; Xie *et al*., 2015; Jiang *et al*., 2017). The most conclusive prognostic factors include the extent of tumour resection, age of diagnosis and the Karnofsky performance status (Ostrom *et al*., 2014). The survival rate is 1-year at roughly 36.5%, with 70% patients experiencing progression within the first year and less than 5% surviving five years after diagnosis. Moreover, its resistance to therapy

may be attributed to glioma stem cells (GSCs) (Xie *et al*., 2015; Davis, 2017). Symptomatically, patients may present increased intracranial pressure, headaches, focal or progressive neurological deficits and seizures (in about 25% patients) which may also present at a later stage in about 50% of GB patients (Davis, 2017).

From a therapeutic standpoint, it is vital to elucidate the pathophysiology of the cells which form GB as well as its, progression and recurrence (Galli *et al*., 2004). Drug resistance is one of the crucial problems faced in cancer treatment especially in chemotherapy as most chemotherapeutic agents are limited and short lived in action (Han *et al*., 2016). Traditional diagnostic imaging techniques are limited to detect brain cancers at the cellular level, but emerging advances in fluorescence imaging (FI) technology, can achieve this but are yet to be applied in the clinical setting (Yukawa *et al*., 2013). Furthermore, significant advances have created opportunities for new treatments such as tumour treating fields (TTFs), receptor targeted drug delivery and immunotherapy (Davis, 2016).

Treatment of cancers has mainly been achieved by aggressive means, such as nonspecific chemotherapy, which adversely affects non-cancerous tissues and surrounding organs. Short-term chemotherapy has been shown to in/directly affect brain functions to cause acute injury in progenitor cells in addition to delayed damage to myelin (Meyers, 2008).

2.5 Nanotechnology and Cancer

Conventional detection techniques, for diagnosis as well as treatment therapies are currently being implemented to eradicate cancer and ameliorate the damaging mutations/alterations in genes or stop the blood supply to cancerous cells (Singh and Nehru, 2008). Although various detection and treatment modalities such as magnetic resonance imaging (MRI), radiation therapy, chemotherapy or invasive surgical resection may be applied, further complications of late detection, low tolerances, nonspecific cell death (concurrently killing healthy cells), tumour recurrence and drug resistance, are some of the identified limitations (Singh and Nehru, 2008; Han *et al*., 2016; Oh *et al*., 2017).

To circumvent the challenges and limitations of conventional cancer treatment, nanotechnology applications have been explored since NPs are very small (nm sized) and possess increased surface-to-volume ratios, which enable them to exhibit distinct functional and structural properties,

which do not exist at the bulk level of the material (Singh and Nehru, 2008). NPs at a scale of 1-100 nm, can be compared to a small molecule (1nm), a virus (100nm) and a bacterium (1000nm) (Alexis *et al*., 2008), and are used in nanotechnology for improved diagnosis, aimed at developing novel imaging and therapeutic techniques, efficient drug delivery and molecular targeting therapies, such as photothermal and radiotherapy techniques (Alexis *et al*., 2008; Aliosmanoglu and Basaran, 2012).

Optical NPs allow for detection of the molecular changes sequestered in disease pathogenesis; better imaging and diagnosis. In addition, as tumour microvessels are more permeable, possessing large fenestrations with a leaky vasculature, the small scaled NPs are able to passively enter the tumour interstitium with extended retention times due to its deficient lymphatic network and in doing so confer the EPR effect, with enhanced specificity and sensitivity (Alexis *et al*., 2008; Haley and Frenkel, 2008; Aliosmanoglu and Basaran, 2012).

Nanotherapeutics may either be passively or actively targeted. Initially, passive targeting takes place by diffusion-mediated transport which is purely disease-dependent besides NP size, shape and surface chemistry which play vital roles in the cellular uptake mechanism and longevity taking advantage of the tumorigenic vasculature to manipulate the EPR effect. It has been reported that the EPR effect increases the drug load by 10-100-fold at the tumour site compared to the administration of free drugs that are not conjugated/encapsulated to a nano drug delivery system (Torchillin, 2010; Wakaskar, 2017). To circumvent non-specific delivery and potential toxicities, active targeting can be achieved through ligation strategies and target specific receptors/moieties (overly expressed on cancer cells with a higher binding affinity) in order to achieve receptor-mediated endocytosis with marked specificity (Torchillin, 2010; Wakaskar, 2017).

Highly luminescent QDs are favourable in imaging and detection modalities as a powerful fluorescent probe and have facilitated drug delivery within live cells and small animals, thus presenting NPs as alternative improvements to diagnostic targeting and drug delivery strategies (Choi *et al*., 2007; Wang and Chen, 2011).

2.6 Quantum Dots (QDs)

A QD is a well-defined semiconductor nanocrystal, which possesses a crystalline metalloid structure, ranging between the sizes of 2-100 nm (Rzigalinski and Strobl, 2009; Smith and Nie,

2010; Mattoussi *et al*., 2011). The name itself, reflects the underlying quantum mechanics thereof and thus its' optical properties, deducing the nanocrystal term "quantum dot" (Juzenas *et al*., 2008; Rosenthal *et al*., 2010). The atomic arrangement which exists at the bulk material and the nm scale is alike, however, the latter possesses a high surface-area-to-volume ratio, thus a marked increase of surface atoms, due to its three-dimensional (3D) truncation. (Rosenthal *et al*., 2010; Vasudevan *et al*., 2015). A semiconductor in its bulk form, constitutes a "composition- dependent band gap energy" in that the energy bandgap existing between the valence and conductance bands, forms a concrete determining factor dependent on the material make up thereof, in contrast to a size-dependent band energy elicited by QDs based on NP size (Smith *et al*., 2008; Smith and Nie, 2010). When one scales the bulk material down to less than the Bohr radius at the nanoscale level, the resultant quantum confinement effect is implemented (Juzenas *et al*., 2008; Mattoussi *et al*., 2011). Ultimately, the absorption of a photon by the semiconductor, promotes an electron to the conduction "energy" band, which would generate a positively charged hole in the "ground state" valence band, and thus scale down to not only the nm scale but below the Bohr exciton radius (around 1-5 nm), squeezing the electron and hole pair, resultant in confinement energy and thus the quantum confinement effect (Juzenas *et al*., 2008; Rosenthal *et al*., 2010; Smith and Nie, 2010; Mattoussi *et al*., 2011). To further elaborate on the quantum mechanics, the smaller the "squeeze" of a QD, the higher the energy level thereof quite like the "particle-in-a- box" model. Furthermore, the respective increase or decrease of a QD size relative to the energy band gap, illustrates the change in the absorption spectra, which will display an emission wavelength in the blue (small QDs) or red (large QDs) spectrum respectively (Juzenas *et al*., 2008; Rosenthal *et al*., 2010; Mattoussi *et al*., 2011; Vasudevan *et al*., 2015).

2.6.1 Distinct properties of QDs

QDs possess attractive yet distinctive properties, which give rise to their unique competences. Firstly, beginning with their favourable small size, ranging between 2-100 nm, with radii roughly between 1-20 nm (Smith and Nie, 2010; Mattoussi *et al*., 2011). As aforementioned, the quantum confinement effect yields a bandgap energy which is concomitant with particle size in that the energy increases with a decrease in particle size, thus being able to tune the optical properties thereof namely, the excitation, emission and fluorescence (Rzigalinski and Strobl, 2009; Rosenthal *et al*., 2010; Vasudevan 2015). The absorbance window is broad, spanning from ultraviolet (UV)

to near infrared (NIR) at the band edge, additionally emitting a narrow, size-tuneable emission spectrum, which can be excited at a single wavelength, thus enabling multiplexing (Chan *et al*., 2002; Rosenthal *et al*., 2010; Wang *et al*., 2011). Moreover, it is robust in that it exudes exceptional photostability and is less prone to photobleaching, due to their high quantum yield (QY) and large molar distinction coefficients (almost 10-50 times larger than organic dyes) thus rendering QDs highly photoluminescent and advantageous over the common fluorophores used, which will be further elaborated on (Resch-Genger *et al*., 2008; Rosenthal *et al*., 2010; Wang *et al*., 2011; Onoshima *et al*., 2015). Lastly, colloidal QDs exhibit a striking phenomenon called "blinking", which is not evident in their self-assembled counterparts, a phenomenon defined by a fluorescence emission of the individual QD under a continuous wave irradiation. The phenomenon is in actual fact not continuous but rather intermittent, which accounts for the blinking and is further said to be derived from repetitive ionization due to an auger process, or the entrapment of a charge carrier in close proximity of the QD surface (Smith and Nie, 2010; Mattoussi *et al*., 2011).

2.7 Chromophores: QDs versus Organic dyes

Following the conventional approach of organic fluorophores which pose as the standard in fluorescence tagging, QDs inclusive of their exceptional properties, show promise in imaging and bioanalytic applications (Mattoussi *et al*., 2011). QDs are therefore rendered as a powerful fluorescent probe, for the ultrasensitive, multicolour and multiplexing applications in molecular biotechnology and bioengineering (Chan *et al*., 2002; Wang *et al*., 2011). The physicochemical properties of a chromophore play a big role in its potential applications. Furthermore, extrapolating on the fluorescence methods "excitation and emission wavelengths, the fluorescence lifetime and the intensity thereof, in addition to emission anisotropy", constituting key parameters which in all needs to perform at the nanoscale and be of a hopeful promise at the singular molecular level for heightened sensitivity (Resch-Genger *et al*., 2008).

Literature suggests pre-requisites for a suitable fluorescence imaging agent for biological applications, in that it possess the desired properties of independent excitation of the fluorescent tag without simultaneously exciting the biological matrix, a highly photoluminescent tag capable of rendering its solubility and stability in various milieu, the allocation of site-specific uptake and the need to exist as a reproducible product. Latter considerations include steric and size related effects, desired targeted delivery and uptake, the potential toxicity associated with the tag and

lastly whether it allows for multiplexing (Resch-Genger *et al*., 2008; Wang *et al*., 2011). To further elaborate on the distinctive and functional properties of QDs as a powerful fluorescent moiety, Table 2.2 (below), highlights the comparative properties of organic dyes and QDs, indicating the advantages and limitations of both.

Table 2.2 - Properties of organic dyes compared to QDs

Property	Organic Dye	QDs
Absorption spectra	Discrete bands, FWHM[b] 35 nm[c] to 80-100 nm[d]	Steady increase toward UV wavelengths starting from absorption onset; enables free selection of excitation wavelength
Emission Spectra	Asymmetric, often tailing to long-wavelength side: FWHM, 35 nm[c] to 70-100 nm[d]	Symmetric, Gaussian profile; FWHM, 30-90 nm
Stokes shift	Normally < 50 nm[c] up to >150 nm[d]	Typically, < 50 nm for visible wavelength-emitting QDs
Quantum yield (QY)	0.5- 1.0 (visible[e]), 0.5- 0.25 (NIR[e])	0.1- 0.8 (visible) 0.2- 0.7 (NIR)
Fluorescence lifetimes	1-10 ns, mono-exponential decay	10-100 ns, typically multi-exponential decay
Solubility or dispersibility	Control by substitution pattern	Control via surface chemistry (ligads)
Binding to biomolecules	Via functional groups following established protocols. Often several dyes bind to s single biomolecule. Labelling-induced effects on spectroscopic properties of reporter, studied for many common dyes.	Via ligand chemistry, few protocols available. Several biomolecules bind to a single QD. Very little information available on labeling-induced effects.
Size	0.5 nm; molecules	6-60 nm HD; colloid
Thermal stability	Dependent on dye class; can be critical for NIR- wavelength dyes	High; depends on shell or ligands
Photochemical stability	Sufficient for many applications (visible wavelength), but can be insufficient for high-light influx application; often problematic for NIR- wavelength dyes	High (visible and NIR wavelengths); orders of magnitude higher than that of organic dyes; can reveal photo brightening
Toxicity	From very low to high; dependent on dye	Little known yet (heavy metal leakage must be prevented, potential nanotoxicity)
Reproducibility of labels (optical, chemical properties)	Good, owing to defined molecular structure and established methods of characterization; available from commercial sources	Limited by complex structure and surface chemistry; limited data available; few commercial systems available
Applicability to single molecule analysis	Moderate; limited by photobleaching	Good; limited by blinking
FRET	Well described FRET pairs; mostly single-donor single-acceptor configurations; enables optimization of reporter properties	Few examples; single-donor-multiple acceptor configurations possible, limitation of FRET efficiency dye to nm size of QD coating
Spectral multiplexing	Possible, 3 colours (MegaStokesDyes), 4 colours (energy-transfer cassettes)	Ideal for multi-colour experiments; up to 5 colours demonstrated
Lifetime multiplexing	Possible	Lifetime discrimination between QDs not yet shown; possible between QDs and organic dyes
Signal amplification	Established techniques	Unsuitable for many enzyme-based techniques, other techniques remain to be adapted and/or established

Properties of organic dyes are dependent on dye class and are tuneable via substitution pattern. Properties of QDs are dependent on material, size, size distribution and surface chemistry. A) Emission wavelength regions for QD materials (approximate): CdSe, 470–660 nm; CdTe, 520–750 nm; InP, 620–720 nm; PbS, >900 nm; and PbSe, >1,000 nm. B) FWHM, full width at half height of the maximum. C) Dyes with resonant emission such as fluoresceins, rhodamines and cyanines. D) CT dyes. E) Definition of spectral regions used here: visible, 400–700 nm; and NIR, > 700 nm. Unless stated otherwise, all values were determined in water for organic dyes and in organic solvents for QDs and refer to the free dye or QD (Adapted with modifications from Resch-Genger *et al*., 2008).

2.7.1 Optical properties of QDs versus Organic dyes

Given the summarized comparison above, albeit quantum mechanics conferring novel properties of QDs, the optical properties are governed by the material makeup thereof, with the surface chemistry being a crucial attributing factor in the optical behaviour as dangling bonds favour nonradiative deactivation and determine the fluorescence QY and decay kinetics and stability, alongside size and size distribution factors (Chan *et al*., 2002; Resch-Genger *et al*., 2008; Onoshima *et al*., 2015). The most commonly synthesized QDs for biological applications are cadmium selenide (CdSe) and CdTe from group II/VI elements, in addition to less toxic potential alternatives namely, indium phosphide (InP) and indium gallium phosphide (InGaP) from the III/V group (Chan *et al*., 2002; Resch-Genger *et al*., 2008). One of the optical advantages of QDs is its large molar extinction coefficient of 10-50-fold over organic dyes, essentially 10-20 times brighter. This is derived from the quantum confinement process, in which multiple electronic states exist at higher energy levels allowing for excitation at shorter wavelengths to which molar extinction coefficients increase, accounting for multiplexing via a single excitation light source of biological relevance (Chan *et al*., 2002; Wang and Chen, 2011). Given the initial quantum confinement peak, the latter sharp, emission peak known as the excitonic fluorescence, can be tuned according to QD size and composition, from ultraviolet-visible (UV-Vis) to the NIR band edge of the electromagnetic spectrum, deducing that the particle synthesis and its surface chemistry, are a major attribute depicting the optical properties of the QD. Figure 2.4 (a and b) displays the excitation and emission wavelengths of CdSe-QDs and Rhodamine 6G organic dye, in addition to (c), giving the visual display of ten distinguishable QD emission profiles and their respective spectral colour.

Given the constituent QD formulations which are accountable for their optical behaviour, electronic transitions on the contrary, account for the optical properties of organic dyes and the emission thereof is categorized by those arising from an optical transition delocalized over the

whole chromophore (termed as a resonant dye), opposed to those derived from intramolecular charge transfer transition (termed CT dyes), with resonant dyes constituting the most common fluorophores. However, CT dyes display broad and structureless absorption and emission bands in polar solvents, have larger and yet insensitive stoke shifts, possess small molar extinction coefficients in contrast to the resonant dyes, and furthermore pose limitations in the NIR range due to low photoluminescent quantum yields (PLQYs) (Resch-Genger *et al*., 2008).

In summary, the large absorption window of QDs would mainly account for their high PL boasting a 10-20 fold in brightness over the conventional fluorophore dye, in addition to being a 100-1000 times more photostable eliciting superiority in photobleaching resistance and applications with enhanced detection sensitivity and longer exposure in fluorescence microscopy, additionally, displays a much narrower and symmetric emission spectra further enabling multiplexing capabilities, via excitation of a single light source spanning from UV through to the NIR range controlled by the particle size and composition, in contrast to organic dyes which are limited in the NIR range (Smith *et al*., 2008; Wang and Chen, 2011).

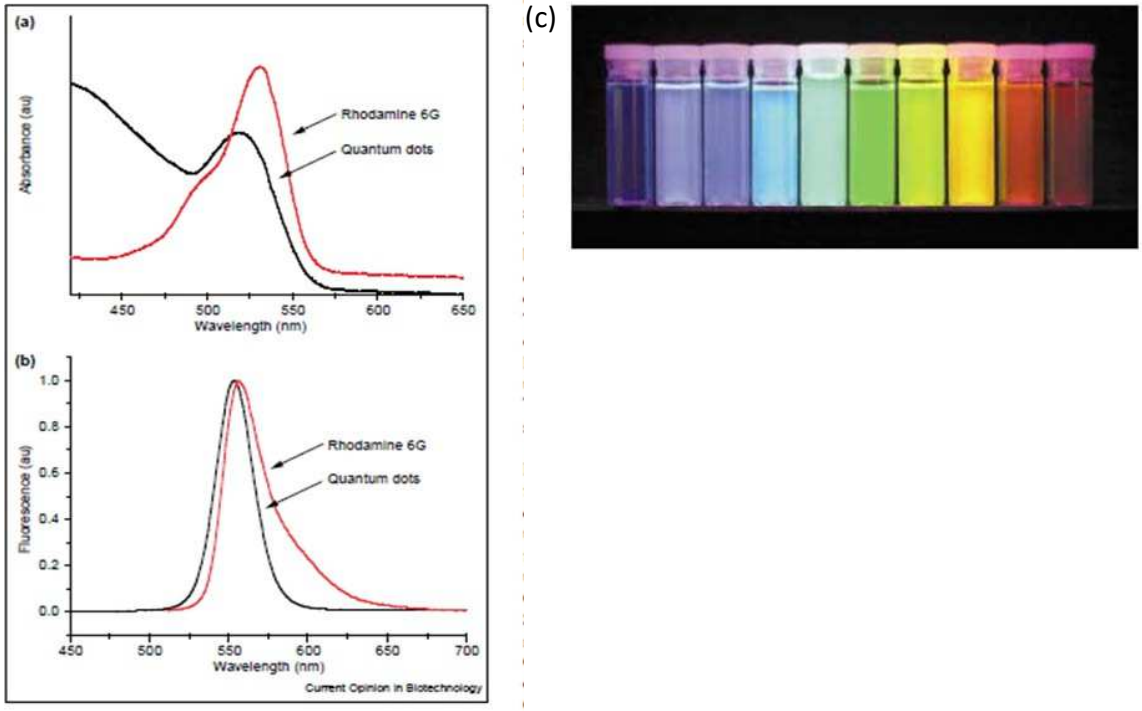

Figure: 2.5 Comparison of **(a)** the excitation and **(b)** the emission profiles between rhodamine 6G (red) and CdSe QDs (black). The QD emission spectrum is nearly symmetric and much narrower in peak width. Its excitation profile is broad and continuous. The QDs can be efficiently excited at any wavelength shorter than ~530nm. By contrast, the organic dye rhodamine 6G has broad and asymmetric emission peak and is excited only in a narrow wavelength range, arbitrary units (AU) (Chan et al., 2002). Image **(c)** displays ten distinguishable emission colours of ZnS capped CdSe QDs excited with a near-UV lamp. From left to right (blue to red), the emission maxima are located at 443, 473, 481, 500, 518, 543, 565, 587, 610 and 655nm (Chan *et al*., 2002).

2.8 Structure and Synthesis

Nanocrystal semiconductors most often used for labelling in bioanalytics or medical diagnostics, are derived from the groups II/VI and III/V (Chan *et al*., 2002; Resch-Genger *et al*., 2008). The crystalline-like structure is colloidal in nature and comprises various shapes such as spherical, tetrapodlike, rodlike and cubic. and constitutes a composition of 200-10 000 atoms with a hydrodynamic (h_d) diameter (HD) ranging between 2-10nm (Smith *et al*., 2008; Mattoussi *et al*., 2011). The first QD synthesis dates back to 1984 by the works of Brus, however, a noticeable interest in QDs really began when Murray and co-workers, synthesized high-quality near monodispersed II/VI QDs (CdS, CdSe, CdTe), yielding consistent crystalline structures, surface derivatization (cap) and sharp absorption and emission profiles via a single step hot injection technique (Murray *et al*., 1993; Rosenthal *et al*., 2013).

Colloidal QDs utilize the bottom-up synthesis method, which allows for the self-assembly of atoms within a solution, followed by the chemical reduction thereof. Smith *et al*, (2008) provides the typical synthesis of a CdSe QDs wherein; the Cd and Se precursor formation is grown upon the nanocrystal nuclei to its desired size and correlating emission wavelength, followed by the ligation process to render colloidal stability and controlled growth. Additionally, the growth of a shell upon the core is subsequent to the coating of aliphatic coordinating ligands, in that the shell consists of a non-alike semiconductor, containing a wider bandgap than the core surface material, thus providing electronic insulation (Smith *et al*., 2008; Rosenthal *et al*., 2013). The precise usage of a ZnS shell specifically, is evident in the majority of QDs, validating it as a highly advantageous entity in that it passivates the surface and enhances PL by counteracting the quenching effect of traps/defects at the surface of the core. Moreover, it reduces toxicity and is less prone to oxidation compared to CdSe and thereby rendering chemical stability for the QD whilst concurrently decreasing oxidative photostability (Smith *et al*., 2008; Rzigalinski and Strobl, 2009; Smith and Nie., 2010; Liu *et al*., 2013; Peng *et al*., 2013). Hence, currently synthesized QDs are a culmination of molecular engineering advances over time, thus yielding highly luminescent, photostable and size-tuneable QDs, which allow for enhanced stability and QYs (Smith *et al*., 2006).

2.9 Surface chemistry and modifications

The surfaces of QDs are not smooth but multifaceted with several planes and edges (Chan *et al.*, 2002). Particle composition and surface chemistry are major attributes depicting the optical properties of QDs. QDs exhibit an atomic composition of 200-1000 atoms, with a large surface-area-to-volume ratio, creating a manipulative platform which permits attachment of various diagnostic and therapeutic agents (Smith *et al*., 2006: Smith *et al*., 2008). Despite the presence of incomplete dangling orbitals which aid fluorescence quenching, ameliorated adsorption of organic surfactants thus, passivate the surface (Smith *et al*., 2006: Smith *et al*., 2008). In the instance of an electron or hole being immobilized by this dangling orbital (also referred to as a trap/defect), it would lose energy with the unlikely recombination to emit light, thus accounting for fluorescence quenching. However, passivation via a core-shell synthesis, ultimately forces the electron hole pair to recombine thus eliminating the defects and emitting light with marked PL (Rosenthal *et al*., 2011). Ultimately, forming part of a surface functionalization process, which elicits significant impact on the PL and QY.

Given the very first semiconductor nanocrystals, which constituted a standalone core structure, with low QY, the deposition of a surface capping layer thus allowed for optimization of the fluorescent QY by 4 to 5-fold (Chan *et al*., 2002; Smith *et al*., 2008). The bandgap would account for this underlying property, in that the capping layer such as ZnS shell, would possess a wider bandgap over the core, essentially allowing epitaxial growth of the core (Chan *et al*., 2002; Smith *et al*., 2008). The surface is further capped with organic ligands, which are bifunctional, characteristic of a polar head which would ultimately bind with the QD surface itself along with passivating the optoelectronic properties; in addition to an aliphatic tail end, which would amalgamate within the environmental milieu (Mattoussi *et al*., 2011). The latter interface between the stabilization of the molecule and QD surface, in addition to pH and temperature parameters of the environmental milieu, affects such colloidal properties as, surface charge, h_d size and the intermolecular interactions, as illustrated in figure 2.5 (Smith *et al*., 2006), indicating correlation between two independent interfaces which thus affect QDs properties.

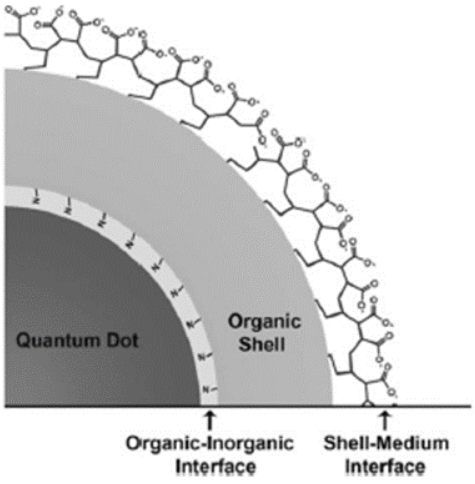

Figure: 2.6 Schematic illustration of QDs dispersed in aqueous medium. The QD surface is directly bonded to organic coordinating molecules. These ligands, and any surrounding polymeric coating, dictate the thickness of the organic shell, which provides a protective barrier from aqueous solutes. The outward facing organic molecules influence the colloidal properties of the QD, such as surface charge and hydrodynamic diameter (Smith *et al.,* 2006).

2.9.1 Water soluble QDs

Organic ligands are mostly nonpolar, thus requiring an additional modification step to make it biologically compatible and soluble in the buffer. Two strategies have been implemented to produce water soluble QDs, that being a complete cap exchange or native surface modification, through a direct adsorption/transfer of native surface ligands with bifunctional hydrophilic ligands or the encapsulation of an amphiphilic polymer as illustrated in figure 2.6 (Chan *et al*., 2002; Clapp *et al*., 2006; Medintz *et al*., 2008; Smith et al., 2008; Mattoussi *et al*., 2012). In this way, the loss of fluorescence in an aqueous milieu would be retained, as well to overcome the hydrophobicity of the surface. Regardless of the method used, purification needs to be implemented for biological application, to remove residual ligands and any extra amphiphiles. Given the additional modifications to render water solubility, the biological and physical properties may be compromised due to the changes applied at the surface coating or the overall physical dimension. Thereby, contributing to the thickness of the coating which affects the h_d size of the NP, possibly aggregating or precipitating in the biological milieu, or potentially reducing the fluorescence intensities (Smith *et al*., 2008). Thus, the overall synthesis of QDs would entail the synthesis, surface capping for passivation and surface modification step by means of ligation, achieved non-

covalently (biotin-avidin binding), electrostatically or covalently via cross linking for targeted delivery, to render it biologically feasible (Clapp *et al*., 2006; Xing *et al*., 2007). Three primary means exist, to deliver a biocompatible QD: antibodies, peptides or small molecules (Bentzen *et al*., 2005; Smith *et al*., 2008; Rosenthal *et al*., 2011).

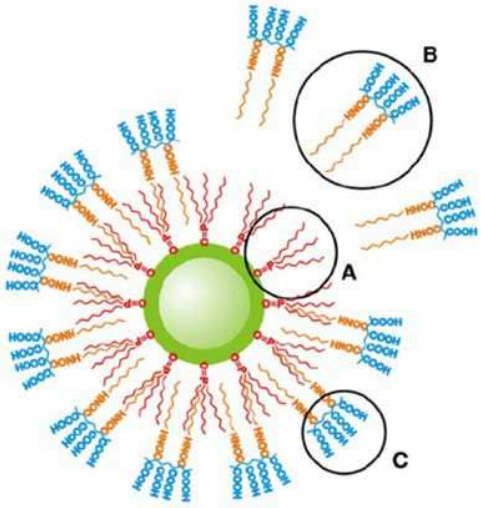

Figure: 2.7 Amphiphilic Polymer Encapsulation Strategy. The original nonpolar ligands on the surface of a quantum dot are left intact (A), and an amphiphilic polymer is used to encapsulate the dot in a water-soluble plastic bag (B). Nonpolar side chains of the polymer intercalate with the nonpolar ligands capping the nanocrystal, and the outer polar, chemically reactive groups of the polymer are used for further conjugation (C) (Rosenthal *et al*., 2010).

2.9.2 Bioconjugation and Modification

Several strategies exist to conjugate a biological targeting moiety to the QD, and such strategies include electrostatic binding, covalent or non-covalent self-assembly and cross-linking ligation surface modifications, all primarily achieved via antibody, peptide or small targeting molecules (Bentzen *et al*., 2005; Clapp *et al*., 2006; Xing *et al*., 2007; Smith *et al*., 2008; Rosenthal *et al*., 2011). To specify the functional terminal group of both the QD and biologically active molecules, along with the proposed chemical reagent for linkage, the proposed chemical reagent [1-ethyl-3-[3-dimethylaminopropyl] carbodiimide hydrochloride (EDAC)], would link the QDs carboxylic ends to amine containing biological moieties (Clapp *et al*., 2006; Rosenthal *et al*., 2011).

Additionally, cross-linking reagents would serve as the linkage for thiols to amino containing QD surfaces and similarly so, in the case of peptides using SIA and Traut's reagents (Clapp *et al*., 2006; Rosenthal *et al*., 2011).

The easiest means of QD labelling occurs in antibodies whether streptavidin coated/directly conjugated. QDs being bound to biotinylated molecules with a high affinity allowing cross linkage through its amine terminals, bound to the carboxylic ends on the QD which yields specificity for a variety of antigens. On the contrary obtainability of antibodies, selectivity and affinity, and the substantial bulk addition increasing the HD, would be a few of the disadvantages (Smith *et al*., 2008; Rosenthal *et al*., 2011; Wang and Chen, 2011). Second to the antibody, would be the usage of peptides, which come in at a lower expense as well as a reduction in the nanoconjugate size. As aforementioned, specific crosslinking agents assist in the covalent linkage of peptides to QDs, additionally proposing the possibilities of multiple peptide conjugation to thus increase the binding affinity thereof via multivalent interactions (Smith *et al*., 2008; Rosenthal *et al*., 2011).

Lastly, the approach of small molecules for targeting are implemented through ligation, rendering high selectivity and affinity, which permits direct binding to the protein of interest and thus allows for the monitoring of processes such as, receptor-mediated endocytosis, protein expression, multiplexed fluorescent assays and allosteric modulation (Smith *et al*., 2008; Rosenthal., *et al* 2011). QDs which contain polyethylene glycol (PEG), eliminate non- specific binding, decrease the surface charge and increase colloidal stability (Bentzen *et al*., 2005; Smith *et al*., 2008). Figure 2.7 illustrates a summary of the conjugation methods, while figure 2.8, shows an attractive visual in both nonfunctionalized and bioconjugated QD probes for imaging and sensing.

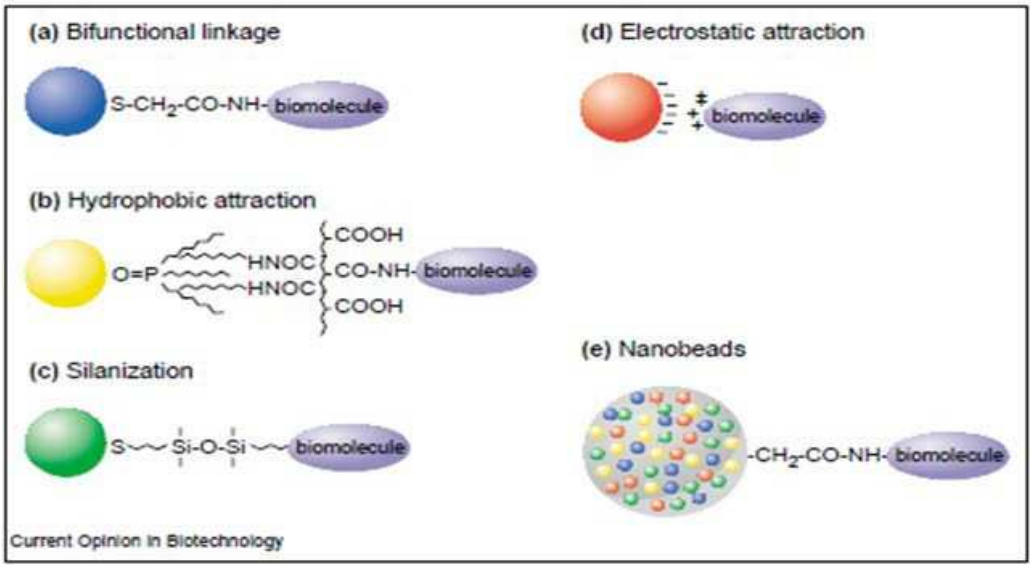

Figure: 2.8 Schematic illustration of bioconjugation methods. **(a)** Use of a bifunctional ligand such as mercaptoacetic acid for linking QDs to biomolecules [8••]. **(b)** TOPO-capped QDs bound to a modified acrylic acid polymer by hydrophobic forces. **(c)** QD solubilization and bioconjugation using a mercaptosilane compound [7••]. **(d)** Positively charged biomolecules are linked to negatively charged QDs by electrostatic attraction [9]. **(e)** Incorporation of QDs in microbeads and nanobeads (Chan *et al*., 2002).

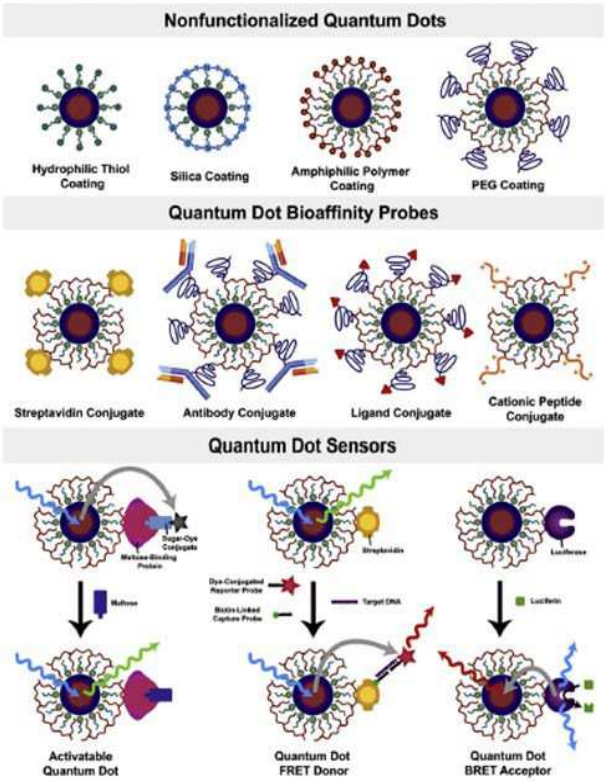

Figure: 2.9 Schematic diagrams of nonfunctionalized and bioconjugated QD probes for imaging and sensing applications (Smith *et al*., 2008).

2.10 Biological and Anti-Cancer Applications of QDs

QDs have become biomedically attractive, with the manipulatable surface chemistry allowing multiple bioconjugation modifications. Its rather unique optical properties have rendered highly luminescent QDs as a powerful fluorescent probe, favourable in bioanalytical applications, imaging and detection modalities, and labelling thereof has facilitated drug delivery within live cells and small animals (Wang *et al*., 2011; Liu *et al*., 2015). QDs display high PLQY, a large absorption spectrum with narrow size-tuneable emission, multiplexing and resistance to photobleaching, rendering it photostable (Chan *et al*., 2002; Rosenthal *et al*., 2010; Yukawa *et al*., 2013; Onoshima *et al*., 2015). Furthermore, QDs are being adopted in Enzyme-Linked ImmunoSorbent Assays (ELISA) for detection and fluorescent immunostaining, cancer diagnostics, nucleic acid detection, biological diagnosis, biosensing, fluorescence resonance

energy transfer (FRET) sensing, biological imaging *in vitro* and *in vivo* and biomodal magnetic-luminescent imaging (Medintz *et al*., 2008; Peng *et al*., 2013; Onoshima *et al*., 2014; Liu *et al*., 2015).

Literature suggests two main aspects of QD application in nanomedicine; viz, the development of fluorescent nanoprobes for cancer detection and therapeutics, by eliciting marked efficiency in targeting and delivery with higher binding affinities, in addition to its great PL and resistance to photobleaching, due to the large surface-area-to-volume ratio and ability for numerous ligations (Smith *et al*., 2008; Wang *et al*., 2011). In addition, being able to capture tumour biomarkers and target vasculature with higher sensitivity and specificity (Smith *et al*., 2008; Wang *et al*., 2011). In doing so, QDs are required to serve as a highly luminescent probes with marked stealth and stability in the aqueous milieu over various pH and ionic strengths (Medintz *et al*., 2008). In the study of Yukawa *et al*, (2013), they report effective high affinity targeting in the human GB U87 cell line, using transferrin (Tf) conjugated QDs (QD-Tf), in this way it would target the overly expressed Tf receptors, found on tumour cell surfaces, in contrast to the very low detection seen on non-cancerous cells. The study exhibited high affinity with a 99.8% labelling efficiency of the QD-Tf, opposed to non-functionalized QD efficiency of 8.4%, and fluorescence emission was both evident and stable for a 2-day period (Yukawa *et al*., 2013).

An earlier study by Yukawa and co-workers, successfully reported the *in vivo* imaging of transplanted Adipose Tissue-Derived Stem Cells (ASCs) labelled with modified QDs, to observe cell behaviour and quantify the proportional uptake of migratory cells in major organs (Yukawa *et al*., 2012). The second main aspect constitutes QD labelling with drug molecules or nanocarriers, which could potentially gain information of real-time dispersion, transportation, drug dispersal and pharmacodynamic mechanisms of nanomedicine in biospecimens (Wang *et al*., 2011).

2.11 Nanomedicine and Toxicology

Nanomedicine initially derives from medicine, further extracting the foundation and knowledge of nanotechnology applicable to the prevention and treatment of diseases (Moghimi *et al*., 2005; Wang *et al*., 2011). Furthermore, it encompasses the usage of materials at the nanoscale such as biocompatible NPs, for diagnosis, treatment, distribution, monitoring and regulation of the biological systems at a singular molecular level (Moghimi *et al*., 2005; Wang *et al*., 2011). NPs

exhibit novel and inimitable properties at the nanoscale in contrast to their bulk material, and when compared to conventional drugs, display unalike reactions to light, electronic and radiation irritations, thus concomitantly altering their physicochemical properties (Kirchner *et al*., 2005; Singh and Nehru, 2008; Wang *et al*., 2011). Nanotechnology assists with improved diagnosis, aimed at developing novel imaging and therapeutic techniques, efficient drug delivery and therapies targeted at molecular level such as, photothermal and radiotherapy techniques (Alexis *et al*., 2008; Aliosmanoglu and Basaran, 2012). Nanomedicine is therefore advantageous to circumvent the limitations of conventional drug delivery methods and therapeutics, with the potential to revolutionize medical treatment, offering protection against drug degradation, heightened stability, prolonged drug circulation, and improved distribution, by means of ligation or nanocarriers to name a few (Wang *et al*., 2011).

Several factors such as toxicity, solubility and stability are often considered in nanomedicine besides the pharmacological parameters of absorption, distribution, metabolism and excretion (ADME), often considered for translational clinical application in humans (Rzigalinski and Strobl, 2009). The biological milieu, intracellular environment and enzymatic conditions, could negatively affect the function, composition and structure of QDs (Kirchner *et al*. 2005). An originally stable synthesized QD, has uncertain biological and chemical fates, in a biological system. The U.S. Food and Drug Administration (FDA), requires injected substances to be completely eliminated from the body within a reasonable time frame (Choi *et al*., 2007b), but for NPs which do not biodegrade into a benign end product this could be a huge safety and toxicity concern as NPs are known to enter and accrue in the reticuloendothelial system (RES) (Choi *et al*., 2007b). The renal filtration threshold and urinary excretion of globular proteins poses a HD of 5-6 nm as the efficient capability of rapid clearance from the body using this as a standard. Choi and co-workers, investigated the biodistribution and elimination of cysteamine coated QDs, covalently linked with a chelated form of gamma ray- emitting isotype ^{99m}TC, to fully track the distribution and clearance, correlating the relationship between "HD, renal clearance and total body retention", and this yielded a turned relationship clearing 50% of the total body at 4 hours and a HD of 5.5 nm (Choi *et al*, 2007b).

One contributory factor to NP toxicity is their inherently small size due to their high surface-to-volume-ratio, the smaller the particle suggesting higher chemical and biological reactivity, which leads to reactive oxygen species (ROS) and free radical production (Singh and Nehru, 2008). ROS

is considered as one of the primary mechanisms in nanotoxicity which may resort to oxidative stress, inflammation and DNA- and membrane damage (Singh and Nehru, 2008). Cd toxicity specifically, may add to liver and kidney injury, osteomalacia, osteoporosis and neurological deficits which would affect the genomic stability and inhibit DNA repair, with the ability to enter through the BBB and accrue in adipose tissue, activate oxidative stress, apoptosis, mitochondrial damage and disruption of intracellular calcium signalling (Medintz *et al*., 2008; Rzigalinski and Strobl, 2009). However, with a ZnS shell grown over the Cd core, toxicity is reduced, oxidative stress and photobleaching minimized, PL and chemical stability enhanced, all to counteract the Cd-associated toxicity (Rzigalinski and Strobl, 2009; Peng *et al*., 2013; Liu *et al*., 2015; Kiplagat *et al*., 2016). A study undertaken by Peng and co-workers, reported subtle toxicity exhibited by CdSe/ZnS QDs opposed to the noticeable toxicity exhibited by exposure of cells to free Cd, suggestive of the protective effects of the ZnS shell and PEG coating (Peng *et al*., 2013). Furthermore, factors such as shape, HD, atomic composition, stability, dosage parameters, surface coating (charge and structure), aggregation and solubility are often considered in pharmacological and toxicity studies of QDs and NPs in general (Choi *et al*., 2007a; Singh and Nehru, 2008; Rzigalinski and Strobl, 2009; Peng *et al*., 2013; Liu *et al*., 2015).

When a NP enters the body, various effects occur; toxic ions are released due to particle degradation upon interaction with elements of the biological milieu, then they get absorbed by cellular membranes thus exerting negative effects and lastly, their irregular shapes could cause physical damage to body cells (Kirchner *et al*., 2005). In the study of Choi and co-workers, they investigated the mechanisms underlying QD-induced cell death in the NB SH-SY5Y cell line, treated with both an unmodified and anti-oxidant N-acetylecysteine (NAC), modified QDs. In particular of oxidative-induced cell death, the FAS (CD95) receptor (also known as the prototypical death receptor), forms part of the tumour necrosis family, which when activated, culminates in caspase activation and cell death (Choi *et al*., 2007a). Thus, the cytotoxicity resultant from high uptake by the unmodified QD, led to FAS upregulation on the surface, increased expression of Fas, lipid membrane peroxidation as well as impaired mitochondrial function consequent to apoptotic and necrotic cell death.

Therefore, the NAC-QD, showed less cytotoxicity and reduced uptake, possibly implying that the CdTe-QD-induced cytotoxicity may be accounted for by multifactorial impairment of cell functions and not from Cd ion (cd2+) concentrations alone (Choi *et al.,* 2007a), and this was recently corroborated by Liu et al., (2015). Additionally, Lovric *et al*., (2005), showed higher uptake and marked toxicity displayed by smaller green-emitting QDs localized in cell nuclei, in contrast to larger red-emitting QDs yielding much less toxicity. For tumour cells, targeted photoactivation toxicity is biomedically advantageous (Rzigalinski and Strobl, 2009), but surrounding normal cells may be affected by NP toxicity. Thus, the need for both short- and long-term cytotoxicity evaluation of NPs, still requires thorough investigation.

CHAPTER 3

MATERIALS AND METHODS

The materials and reagents used for the different experiments in this study are presented in the respective sections below.

3.1 Synthesis of MPA-capped CdTe/ZnS QDs

The materials and reagents used for the synthesis of MPA-capped CdTe/ZnS QDs are listed in Table 3.1 below and the modified method used was adapted from Chomoucka *et al*., (2013) and Yan *et al*., (2010), carried out in the laboratory of Professor M. Onani, Chemistry Department, University of the Western Cape, South Africa.

Table 3.1 - Materials and Reagents for QD Synthesis

Item	Supplier
Acetone	Sigma-Aldrich
Cadmium chloride ($CdCl_2$)	Sigma-Aldrich
Ethanol	Kimix
3-Mercaptopropionic acid (MPA)	Sigma-Aldrich
Sodium Borohydride ($NaBH_4$)	Sigma-Aldrich
Tellurium (Te)	Sigma- Aldrich
Thiourea	Sigma-Aldrich
Zinc Acetate	Sigma-Aldrich

The experiment was carried out under inert gas in a fume hood, as the nitrogen would allow for a sterile environment, thus ensuring limited interference of outside gases with the experiment. The experimental setup included, two down pipes leading down from the Schlenk line wherein three-necked flasks were further connected. Initial preparation was carried out by washing the glassware, rinsing with acetone, followed by deionized water and placing the glassware in an oven to dry at 50°C. The MPA-capped CdTe/ZnS synthesis involved the preparation of three solutions. For Solution A, 0.0378g of $NaBH_4$ (1 mmol) and 0.051g Te (0.04 mmol) were dissolved in 10ml

of deionized water and placed in the three-necked flask. This is the NaHTe complex. Solution A was then heated for 30 minutes at 80°C with continuous stirring using a stirrer block set at speed 1 and this resulted in a colour conversion from clear to greyish/purple. With the contents filled in the three-necked flask, a stopper was placed on the left-hand side (LHS) neck and a temperature prong/cathode, inserted in the right-hand side (RHS) neck.

Solution B was prepared by dissolving 0.162g of $CdCl_2$ (0.4 mmol) and 104µI MPA (0.6 mmol) in 30ml of deionized water in a beaker and the pH raised from 2.48 to pH 11.7, resulting in the formation of the Cd/MPA precursor. The solution was then transferred to the three-necked flask and heated to 100°C. However, prior to reaching the final temperature, 5 ml of solution-A's NaHTe complex, was injected at 80°C. Once the final temperature of 100°C was reached, the reaction was further maintained for 2 hours, thus allowing the growth of CdTe nanocrystals. Solution C, a zinc and sulphur precursor, was prepared by dissolving (0.0918g) zinc acetate (0.1M) and (0.03806) thiourea (0.1 M), in 5ml of deionized water, for later use. The precursor solution was to be prepared fresh on the day for direct usage, not prepared a few hours in advance either. Once the initial two hour reaction had lapsed, solution-B with injected NaHTe complex was rapidly cooled down on ice, yielding the CdTe nanocrystals. Thereafter, 2ml of zinc and sulphur precursor solution was then added to CdTe solution and the pH was raised to 11.5.

The final mixture of the solutions was degassed and subsequently heated to 90°C for 1 hour, which permitted the growth of MPA-capped CdTe/ZnS QDs. The solution eventually resulted in a colour conversion from greyish/purple to greenish yellow. Lastly, impurities were removed by pipetting aliquots of the MPA-capped CdTe/ZnS QDs, into 2ml Eppendorf's and centrifuged for 3 minutes at 14500 rpm, for usage in further characterization and biological applications. The QDs were diluted with deionized water where needed, as they have been made up in double distilled water (ddH20) rendering it water-soluble. The MPA-capped CdTe/ZnS QDs were stored at 4°C wrapped in foil for later use.

3.2 Physical Characterization of MPA-capped CdTe/ZnS QDs

Physical characterization took place in the Biotechnology, Chemistry and Medical Bioscience departments, of University of the Western Cape.

3.2.1 Zeta Size measurement- Dynamic Light Scattering and Polydispersity Index

The Zetasizer NanoZs (Malvern, UK), was utilized to perform size and polydispersity index (PdI) measurements, via Dynamic light scattering (DLS) also known as Photon Correlation Spectroscopy (PCS) (Gaumet *et al*., 2007). A technique which illuminates particles with a laser whereby the intensity fluctuations are analysed in the scattering light, to obtain the h_d size distribution (Saharan and Pal, 2016). The measurement thereof is based on Brownian motion, a ubiquitous phenomenon better defined as the movement of particles due to random collision of molecules in a liquid in thermal equilibrium (Donado *et al*., 2017; Tarafdar and Adhikari, 2015). Ultimately, larger molecules would move at a slower rate in contrast to small, fast moving molecules illustrated by rapid intensity fluctuations, which in turn correlates to a faster rate of decay demonstrated by smaller molecules opposed to the slower decay rate of larger molecules. A translational diffusion coefficient dictates the speed of Brownian motion, which can then be converted to particle size by the Stokes-Einstein equation (Saharan and Pal, 2016).

PdI is a dimensionless measurement spanning size distribution, determined by the cumulants analysis and considers the "particle mean size, refractive index of solvent, measurement angle and the variance of distribution" (Gaumet *et al*., 2007). It is categorized between 0-1, wherein any value smaller than 0.1 represents homogeneity, in contrast to a value greater than 1, being indicative of polydispersity and unsuitable for DLS (Gaumet *et al*., 2007; Saharan and Pal, 2016).

For this study, 1ml of the synthesized MPA-capped CdTe/ZnS QD solution, was placed into the polystyrene cuvette for zeta (**ζ**) size and PdI analysis, wherein the intensity-weighted mean was recorded at eleven runs over three independent analysis on the Zetasizer NanoZs (Malvern, UK).

Both unfiltered and filtrated samples were analyzed, however, it is noteworthy that only the unfiltered MPA-capped CdTe/ZnS QD solution was utilized throughout this study, due to filtration negatively affecting characterization techniques that were carried out.

3.2.2 Zeta (ζ)-Potential – Laser Doppler Velocimetry

ζ-potential allows for the determination of the surface charge of NPs, indicative of the potential colloidal stability, subsequent to a combination of "electrophoretic mobility and having applied the Henry equation" (Clogston and Patri, 2011; Tarafdar and Adhikari, 2015).). The electrical double layer surrounding each particle is resultant from a build-up of counter ions at the surface, wherein ions are strongly bound at the inner stern layer in contrast to the outer lying ions which

are less firmly held together in the diffuse layer. It is in this layer where the surface of the h_d shear exists, also referred to as the slipping lane, wherein the ζ-potential exists, as illustrated in figure 3.1 (Tarafdar and Adhikari, 2015). ζ- potential not only deliberates on the particles itself, but the environmental factors thereof namely; "pH, ionic strength and even so the types of ions present in solution" (Xu, 2008). A large ζ- potential, be it positive or negative, has a high degree of stability with the tendency to repel each other and thus not flocculate. However, the contrary low ζ-potential does not have the forces to keep the molecules apart and therefore, results in flocculation due to interparticle Van der Waals' attractions (Clogston and Patri, 2011; Tarafdar and Adhikari, 2015). A ζ- potential at +30Mv or -30Mv, is considered, stable (Clogston and Patri, 2011; Tarafdar and Adhikari, 2015).

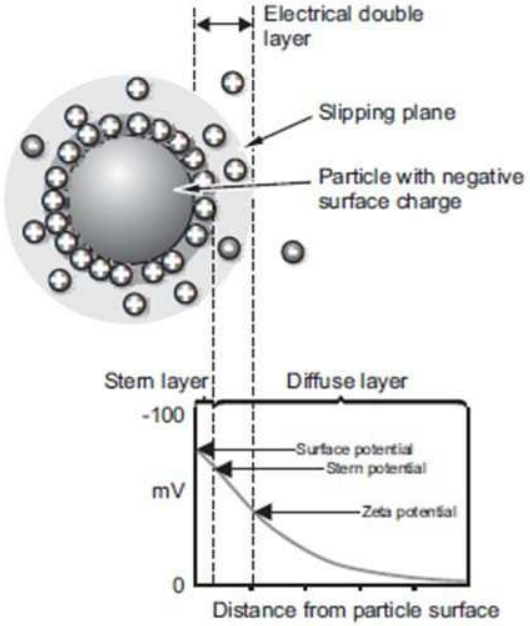

Figure: 3.1 ζ- potential of a particle with negative surface charge (Tarafdar and Adhikari, 2015).

A volume of 1ml of the synthesized MPA-capped CdTe/ZnS QD solution, was placed in the folded capillary ζ cell for ζ- potential analysis and was recorded at eleven runs as the intensity-weighted mean over three independent sample readings, on the Zetasizer NanoZs (Malvern, UK).

Once again, unfiltered and filtrated samples were analyzed, however, only the unfiltered MPA-capped CdTe/ZnS QD solution was utilized throughout this study, due to filtration negatively affecting characterization techniques, that were carried out.

3.2.3 Photoluminescence (PL) Spectroscopy

PL fluorescence intensity was measured using the NanologTM Spectro fluorometer (Horiba Jobin Yvon, Japan). As per the Nanolog accuracy test, a preliminary run was done using ddH20, where the R1 filter was selected for excitation followed by the emission selection S2 filter, which read at 200nm- 850nm, Gravity 1200/500. Hereafter, 1ml MPA-capped CdTe/ZnS QD solution, was placed into the quartz cuvette for PL analysis, recorded over three independent analyses on the Nanolog^{TM} Spectro fluorometer (Horiba Jobin Yvon, Japan).

Photoexcitation is the direction of light upon a sample, therein absorbing and imparting excess energy into the compound/material, one means of dissipation being through the luminescent photon emission of light (a radiative process), rather known as PL (Heiman, 2004; Barron, 2013). PL energy thus relates to the variance in energy levels presented in the transition from excited to equilibrium states, whilst PL quantity is relative to the influence

3.2.4 UV- Vis Spectroscopy

The MPA-capped CdTe/ZnS QD solution, was diluted with ddH_20, to six concentrations ranging between 5µg/ml - 75µg/ml for an appropriate graph reading. Then, 100 µl of each concentration was pipetted into a 96 well plate, for UV-Vis analysis using the POLARstar Omega plate reader (BMG Labtech, Germany), at an absorbance wavelength ranging from 250nm-1000nm. Whilst PL is affiliated with the conversion from an excited to ground state, UV-Vis spectroscopy obtains the absorbance spectra, "by observing the absorbance of light energy/ electromagnetic radiation, which excites electrons from the ground state to first singlet excited state of the compound, owing to its underlying principle of the Beer-Lambert Law" (Barron, 2013).

3.2.5 HR-TEM: Micrographs and EDX Spectroscopy

3.2.5.1 HR-TEM: Micrographs

In preparation for high resolution-transmission electron microscopy (HR-TEM) analysis, the MPA-capped CdTe/ZnS QD solution was drop coated onto a carbon coated copper grid. The grids were dried under a xenon lamp for 10 minutes, followed by HR-TEM analysis. HR-TEM is an indispensable characterization technique for nanocrystals which provides atomic-resolution lattice images in addition to the chemical composition thereof and does so at a resolution "a few thousand times higher than that of the highest resolution present in visible light microscopes (VLMs), by

transmitting through and interacting with the provided specimen via a beam of electrons" (Wang, 2000; Barron et al., 2013). The absorption of these electrons dependent of the specimen's composition would account for the magnification in the TEM image.

The micrographs were obtained using a Tecnai G2 20 field-emission gun (FEG) TEM (FEI, USA), operated in bright field mode, at an accelerating voltage of 200 Kv. These micrographs also allowed for the size measurement of QDs, measured via the built-in software of the TEM, allowing for size analysis. QD samples were submitted in triplicate, over three independent analysis, n=3.

3.2.5.2 HR-TEM: EDX Spectroscopy

Following preparation of HR-TEM analysis, energy dispersive x-ray (EDX) spectra were attained with an EDAX liquid nitrogen cooled, Lithium doped Silicon detector. Excitation via beam electrons or high-energy radiation of the core electrons to elevated energy states, is resultant in lowered energy occupancies of the atom, which is consequential to a deluge of electrons from higher energy levels in order restore a minimum-energy state and whilst transitioning to lower energy states, the electrons emit X-rays, due to energy conservation (Barron *et al*., 2013). The X-ray emission from the sample, strikes the lithium doped silicon plate, which promotes electrons to the conduction band and ultimately results in a voltage between 1 and 10 keV, whilst the liquid nitrogen is in place to cool the detector plate thus inhibiting "electronic noise from thermal excitations" (Wollman *et al*., 1997; Barron *et al*., 2013). These X-ray emissions are then measured both quantitatively and qualitatively based on the energies and intensity of the spectrum peak formations in X-ray spectroscopy, to thus obtain a localized chemical analysis. As per HR-TEM analysis, QD samples were submitted in triplicate, over three independent analysis, n=3.

3.2.6 Stability Assay

The stability assay was carried out using the following media: un-supplemented Dulbecco's modified eagles medium (DMEM), supplemented DMEM with 10% Fetal bovine serum (FBS) and 1% Penicillin streptomycin (pen-strep), Phosphate buffer solution (PBS), 10% FBS and0,5% Bovine serum albumin (BSA). In preparation thereof, glass vials were washed and autoclaved. A volume of 1ml of MPA-capped CdTe/ZnS QD solution was added per glass vial, with the addition of 1ml of the corresponding media. Each of the above were incubated at 25°C and 37°C, for 0-hour, 1-hour, 4-hour, 6-hour, 8-hour, 24-hour, 48-hour and 72-hour time intervals. At each time

interval, a 100µl reading of each respective sample, were analysed using the POLARstar Omega plate reader (BMG Labtec, Germany), at a wavelength ranging from 250nm- 1000nm.

3.3 Biological Characterization of MPA-capped CdTe/ZnS QDs

Biological characterization took place in the Biotechnology and Medical Bioscience department, of the University of the Western Cape.

Table 3.2 - Materials and Reagents for Biological Assays

Item	Supplier
15ml and 50ml Conical Tubes	Biosmart
2ml Cryovial tubes	Biosmart
2ml Eppendorf Tubes	Biosmart
Cell proliferation agent WST-1	Sigma-Aldrich
Dimethyl sulfoxide	Sigma-Aldrich
Dulbecco's Modified Eagles Medium (DMEM)	Thermofischer-Scientific
Fetal Bovine Serum (FBS)	Thermofischer-Scientific
Fluoroshield with DAPI	Sigma-Aldrich
Folded Capillary Zeta cell and Polystyrene cuvettes	Micron-Scientific
Fx Cycle PI/RNase Staining solution	Thermofischer-Scientific
Paraformaldehyde	Sigma-Aldrich
Penicillin streptomycin	Lonza-Biowhittaker
Pipette tips- yellow 200µl and blue 1000µl	Lasec
Phosphate buffered saline (PBS)	Lonza-Biowhittaker
Sterile Flat bottom 6, 24 and 96 well plates	Whitehead Scientific
Tissue culture dishes 60mm and 100mm	Whitehead Scientific
Triton-X100	Sigma-Aldrich
Trypan Blue	Whitehead Scientific
Trypsin- Versene (EDTA)	Lonza-Biowhittaker

3.3.1 Tissue Culture

3.3.1.1 Tissue Culture- Cell Harvesting

Two cell lines were used to carry out the biological component of the study, that being NB SH-SY5Y cells and GB U87 cells. Cells were fostered in DMEM supplemented with 10% FBS and 1% penicillin/streptomycin. The NB SH-SY5Y cells were donated from the radiobiology department of Stellenbosch University, Tygerberg hospital campus. GB U87 cells, were kindly donated by Professor S. Prince's laboratory, of the University of Cape Town.

3.3.1.2 Thawing of cells

The cryovials containing the frozen cells were collected from the -80°C freezer and thawed at room temperature. The contents were transferred to a 15ml conical tube, with the addition of 4ml supplemented DMEM medium, followed by centrifugation at 700g for 5 minutes. The supernatant was removed and discarded, and the pellet resuspended in 2ml supplemented DMEM. The cell suspension was then transferred to a 100mm X 20mm cell culture dish, with the addition of 8ml supplemented DMEM. The cells were placed in a water jacketed Celculture model CCL- 17013-8 CO_2 incubator (Esco, Singapore), at 37°C and 5% CO_2 until a 70-90% confluency was reached.

3.3.1.3 Trypsinization

Upon reaching the desired confluency, cells underwent trypsinization with 1X Trypsin after discarding the medium and washing with 2ml 1X PBS. Thereafter, the 1X PBS was removed and 2ml of trypsin was added and placed in the incubator for 3-5 minutes. Once cells were detached from the cell culture dish, confirmed by viewing under the CKX31SF inverted microscope (Olympus, Japan), supplemented DMEM was added to neutralize the trypsin.

3.3.1.4 Cell Seeding and Trypan Blue

After trypsinization, 10µl of trypan blue was added to 10µl cell suspension in a 2ml Eppendorf tube and mixed properly by resuspension. Thereafter, 10µl of cell suspension was placed on a haemocytometer for a cell count under the CKX31SF inverted microscope (Olympus, Japan).

Trypan blue facilitates visualization of cell morphology in that it exclusively stains non-viable cells with an uptake of its' blue dye, in contrast to viable cells appearing opaque in colour which do not take up the dye (Uliasz and Hewitt, 2000). The average of the four quadrants were calculated and multiplied by the dilution factor of 2, which yielded cells in Mio/ml and further multiplied by 10 000, to yield the total cell count (Only viable cells, were calculated here; thus, viable cells/4, X2, x10000). In order to seed for the corresponding assays, the required number of cells were divided by the calculated viable total cell count (VTCC), which yielded the volume of cell suspension required in the desired volume of supplemented DMEM (eg: Required 4000 cells X number of wells = A/ VTCC).

3.3.1.5 Cryopreservation of cells

To proceed with the cryopreservation of cells, the trypsinization process was carried out as mentioned above. Once dislodged and neutralized with 4ml supplemented DMEM, the contents were transferred to a 15ml conical tube to be centrifuged at 700g for 5 minutes. The supernatant was removed and discarded, and the pellet resuspended in 4ml of the corresponding cryofreezing medium, specific to each cell line. In the case of the NB SH-SY5Y cell line, cryofreezing medium consisted of 10% dimethyl sulfoxide in 90% FBS. The GB U87 cell line required a cryofreezing medium of 10% dimethyl sulfoxide made up in supplemented 90% DMEM. The combined cell suspension in their corresponding cryofreezing medium, were transferred into cryovials to a volume of 2ml each and stored in the -80°C freezer.

3.3.2 Immunocytochemistry for Fluorescence Confocal Microscopy

The intent was to seek the uptake and localization of the MPA-capped CdTe/ZnS QDs, in both the SH-SY5Y and U87 cell lines. The immunocytochemistry methodology herein has been adopted from Swartz, (2013), with minimal modifications.

3.3.2.1 Cell Harvesting

Preparation required that of both autoclaved coverslips and tweezers for handling of the sterile coverslips. Cells were harvested accordingly as previously described and seeded on to sterile coverslips placed in a 6 well culture plate, at a density of 3 X 10^5. The 6 well culture plates were placed in the water jacketed Celculture CO_2 incubator (Esco, Singapore), at 37°C and 5% CO_2 for

24 hours, until its desired confluency of 60-70% was reached. Samples were seeded in duplicates for each analysis.

3.3.2.2 Fixation and Permeabilization

Following the exposure time, the medium was extracted from each well. The cells were washed twice with 1X PBS and thereafter, the 1X PBS removed before adding 1ml of 4% Formaldehyde apiece and incubated at room temperature for 20 minutes covered with foil. The 1X PBS was discarded and 1ml of 0.1% Triton X100 was then added to each well for a 5-minute incubation at room temperature, covered in foil to allow for permeabilization of the cell membrane. Lastly, the 0.1% Triton X100 was removed and a final two washes with 1X PBS were achieved.

3.3.2.3 Fixed Cell Staining

To fix the cells for staining, 1X PBS was extracted and exposed the cells to the MPA-capped CdTe/ZnS QD solution at room temperature, at a comparatively low and high concentration of 50µg/ml and 250µg/ml for 1- hour and 4-hour time frames respectively, covered with foil, which protected it from the light. In this way we could compare concentration and time intensities. Following incubation, the cells were washed thrice with 1X PBS and dried by blotting the edges of the cover slips on paper towel. Fluoroshield (4,6-diamidino-2-phenylindole) (DAPI) mounting media was placed dropwise onto the labelled microscope slides and dried coverslips were carefully placed with the cells facing down, onto the mounting media. The images were then captured using the Fluorescent LSM 780 Confocal Microscope (Carl Zeiss, Germany), at 100 X magnification, under oil immersion.

Confocal microscopy utilizes a pinhole which is placed at the conjugated image plane to the focal plane, allowing in-focus light to pass at the focal point whilst blocking out-of-focus light and therefore produces very high contrast images (Webb, 1996). The confocal process is illustrated in figure 3.2 below.

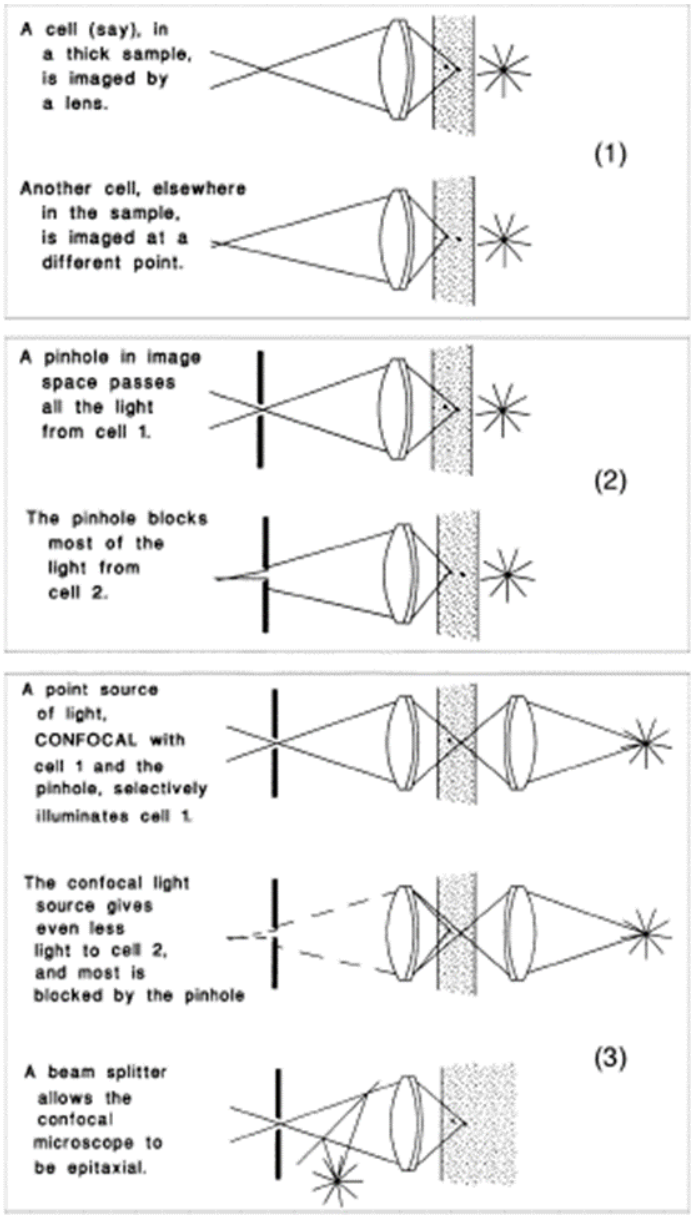

Figure: 3.2 Confocal Process- a simple view of the progression of widefield images to confocal microscope. (Webb, 1996)

3.3.3 Cell proliferation WST-1 Assay

The cell proliferation (4-[3-(4-iodophenyl)-2-(4-nitrophenyl)-2H-5-tetrazolio]-1,3-benzene disulfonate) (WST-1) kit allows for the spectrophotometric quantification (between 0.5 hours- 4 hours) of cell proliferation and viability in cell populations. It is a tetrazolium salt, that gets cleaved down to a water-soluble formazan by reacting with the mitochondrial succinate-tetrazolium reductase, based on the glycolytic production of NAD(P)H in viable cells (Ngamwongsatit *et al*.,

2008). The production of soluble formazan dye thus correlates to a number of metabolically active cells. For this assay, cells were tallied using the trypan blue assay as previously described in 3.3.1.4 and seeded into 96 well culture plates at a volume of 100µl/well, in triplicates. The number of cells required was 4000 cells/well for U87 cells and 5000 cells/well for SH-SY5Y cells. The cells were then incubated for 24 hours in a water jacketed Celculture model CCL-17013-8 CO_2 incubator (Esco, Singapore), at 37°C and 5% CO_2, and then treated with four concentrations which correlates to those in literature of the MPA-capped CdTe/ZnS QD solution namely; 5µg/ml, 10µg/ml, 15µg/ml and 20µg/ml respectively. The cells were further incubated for 24-hour, 48-hour and 72-hour time intervals respectively. At the end of each incubation period, 10µl of WST-1 cell proliferation agent, was added to each well and incubated for 3 hours in the water jacketed Celculture model CCL-17013-8 CO_2 incubator (Esco, Singapore), at 37°C and 5% CO_2 before absorbance readings were done with the POLARstar Omega plate reader (BMG Labtec, Germany), at 450nm and 620nm. All readings were taken in triplicate over three independent analysis n=3.

3.3.4 Cell Morphology

Morphology of the cells was monitored and captured using the Primovert inverted microscope (Zeiss, Germany). Cells were harvested and tallied via the trypan blue assay and seeded at 3000 cells/well in a 24-well culture plate and thereafter incubated in a water jacketed Celculture model CCL-17013-8 CO_2 incubator (Esco, Singapore), at 37°C and 5% CO_2, for 24 hours until a 70-90% confluency was attained. The cells were then treated with 4 concentrations of MPA-capped CdTe/ZnS QDs namely; 5µg/ml, 10µg/ml, 15µg/ml and 20µg/ml respectively and further incubated for 24-hour and 48-hour time frames, (72-hour time frame was later omitted due to cell dislodgement). for observation under the Primovert inverted microscope (Zeiss, Germany), objective magnification 40X. All readings were taken in triplicate over three independent analysis n=3.

3.3.5 Cell Cycle PI/ RNase FACS Analysis

The Fx Cycle PI/RNase staining solution allows for the analysis of DNA content using a flow cytometer. It enables the study of cell populations categorized amongst the three major cell cycles: G_0/G_1 phase, S phase and the G_2/M phase, in addition to DNA ploidy analysis (Nunez, 2001;

Mader, 2004). The propidium iodide (PI) intercalates into the DNA helical structure to measure the cellular DNA content, which is directly proportional to the fluorescent signals (Brown and Witwerr, 2000). The fluidic and optic components of the flow cytometer are shown in figure 3.3 below.

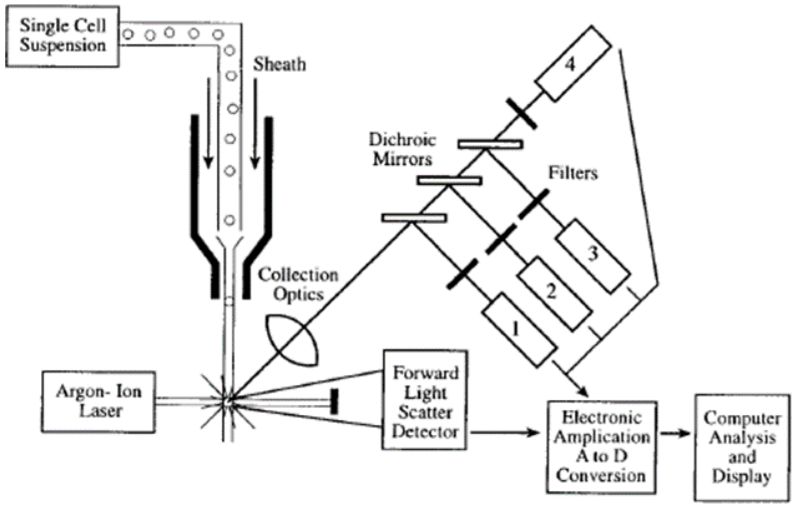

Figure: 3.3 Schematic of flow cytometer. A single cell suspension is hydrodynamically focused with sheath fluid to intersect an argon-ion laser. Signals are collected by a forward angle light scatter detector, a side scatter detector (1), and multiple fluorescence emission detectors (2-4). The signals are amplified and converted to digital form for analysis and display on a computer screen. (Brown and Witwerr, 2000).

3.3.5.1 Cell Harvest and Fixation

The cells were harvested and counted via trypan blue assay as previously described in 3.3.1.4 before seeding at 3 x 10^5 cells in 60mm x 15mm cell culture dishes and incubated for 24 hours in the water jacketed Celculture CO_2 incubator (Esco, Singapore), at 37°C and 5% CO_2. The cells were then treated with the MPA-capped CdTe/ZnS QD solution at a concentration of 20µg/ml and placed in the water jacketed Celculture CO_2 incubator (Esco, Singapore) 37°C and 5% CO_2 for a 24-hour and 48-hour time frame (72-hour time frame was omitted due to cell dislodgement). Following incubation periods, cells underwent trypsinization and once neutralized, the cell suspension was transferred to a 15ml conical tube for centrifugation at 700g for 5 minutes. The supernatant was removed and discarded, and pellet resuspended in 2ml 1X PBS. The cells were then topped up with 70% cold ethanol, to a final volume of 10ml and stored for at least 30 minutes or at the most stored for two weeks at -20°C. Samples were prepared in triplicate over two independent analysis, n=2.

3.3.5.2 FACS Analysis

Before commencing of fluorescence-activated cell sorting (FACS) analysis, the conical tubes were centrifuged at 700g for 5 minutes, and the ethanol fixative removed by decanting and pellet obtained resuspended in 1 ml of 1X PBS. Thereafter, the cell suspension was transferred to a 2ml Eppendorf and centrifuged at 700g for 5 minutes. Once again, the supernatant was removed, and washed by resuspending in 1ml of 1X PBS to obtain a very tiny pellet. The last step included the addition of 500µl PI/RNase staining solution. Once triturated, the Eppendorf's were covered with foil, shielded from the light and incubated at room temperature for 15-30 minutes. The samples were analysed using the C6 flow cytometer (BD Accuri, USA), prepared in triplicate and run over two independent analysis, n=2.

3.4 Statistics

Statistical analysis was achieved using Graphpad Prism. Data presented as the mean ± standard error mean (SEM); n=3 and n=2 where indicated. One-way ANOVA analysis was used for statistical comparisons and statistical significance levels were indicated by probability: $p < 0.05$ *, $p < 0.01$ * and $p < 0.001$ ***.

CHAPTER 4

RESULTS

4.1 Synthesis of MPA-Capped CdTe/ZnS QDs

The MPA-Capped CdTe core, coated with a ZnS shell, was successfully synthesized as described in section 3.1 of the Materials and Methods chapter, yielding relatively monodispersed and highly luminescent QD samples. Figure 4.1 below, shows the clear, bright yellow MPA-Capped CdTe/ZnS QD solution, obtained from an originally murky solution, after centrifugation.

Figure: 4.1 Displays a clear bright yellow solution of the synthesized MPA-Capped CdTe/ZnS QDs.

4.2 Physical Characterization of MPA-capped CdTe/ZnS QDs

4.2.1 Zeta Size, Poly Dispersity Index and Zeta Potential

4.2.1.1 Zeta Size and Poly Dispersity Index

ζ size and PdI were measured by DLS, the most popular technique for sizing nanoparticles and was performed using both stock (unfiltered) and filtered MPA-Capped CdTe/ZnS QD samples. The h_d size distributions obtained were based on the speed of Brownian motion and the equivalent sphere principle (upon assumption that all particles are spherical molecules). Based on the cumulant analysis, PdI indicates the type of dispersity and stability of the molecules. The h_d sizes and PdI of both unfiltered and filtered MPA-capped CdTe/ZnS QD solutions, are shown in figure 4.2. The PdI values were comparable for both the filtered and unfiltered samples; however, the h_d sizes for both solutions were significantly different. Data obtained was based on the intensity-weighted mean of 11 runs each over three independent analyses.

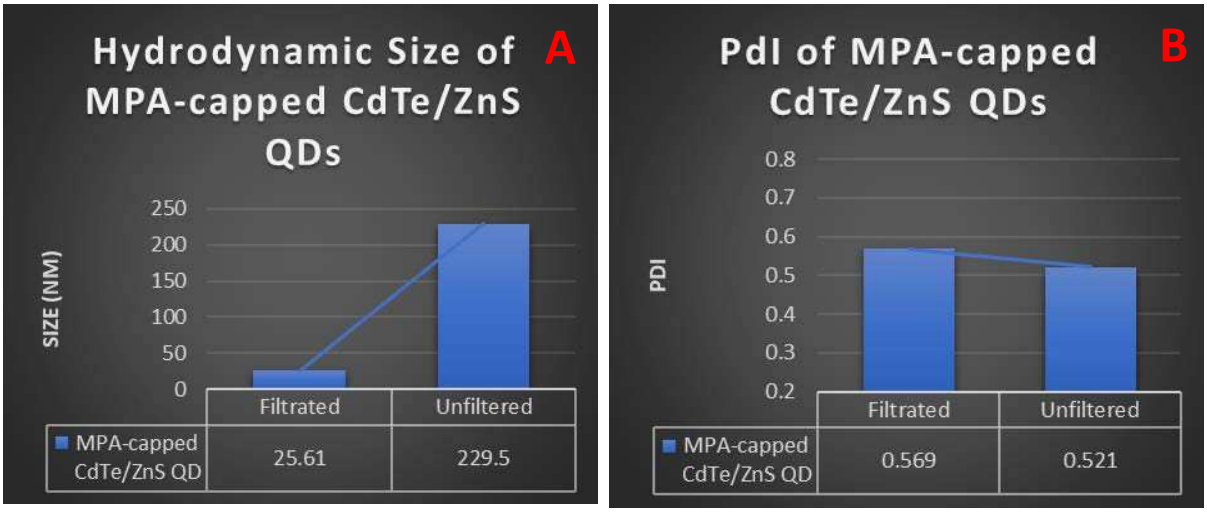

Figure: 4.2 H_d Size and PdI of MPA-capped CdTe/ZnS QDs. A) shows an intensity-weighted mean in size distribution of 229.5 nm in the unfiltered MPA-capped CdTe/ZnS QD solution and 25.61 nm in the filtered solution. B) shows an intensity-weighted mean PdI of 0.521 unfiltered sample and 0.569 PdI for filtered sample, thus starting to shift from a monodispersed solution toward polydispersity.

4.2.1.2 Zeta (ζ) - Potential

ζ-potential is a vital parameter for nanoparticles in suspension, and determines the electric potential at the slipping lane, and closely correlates to suspension stability and particle surface morphology. A large ζ- potential, be it positive or negative, has the tendency for molecules to repel each other and not allow them to flocculate, therefore a ζ- potential at +30 mV or -30 mV, renders high stability. The ζ- potential values obtained in this study yielded high stability in the unfiltered

solution, with a noticeable decrease in stability in the filtered MPA-capped CdTe/ZnS QD solution, as shown in figure 4.3. Similarly, data obtained in this study was based on the intensity-weighted mean of 11 runs each over three independent analyses.

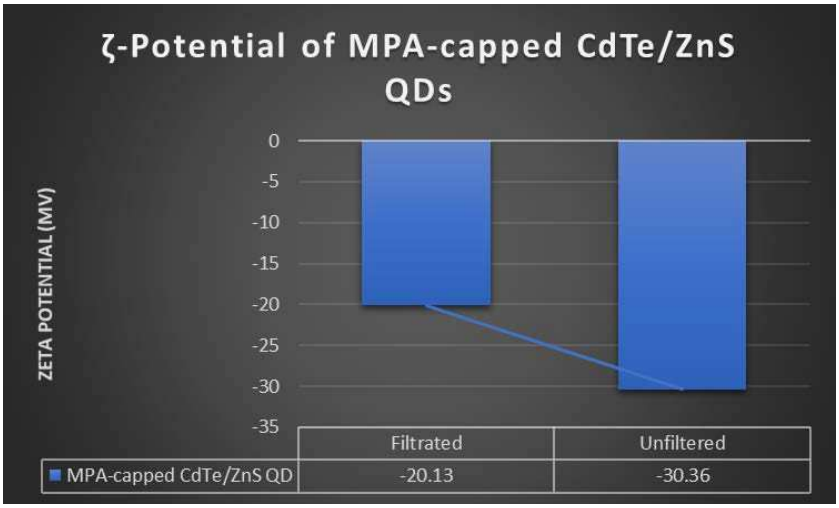

Figure: 4.3 Zeta (ζ)-Potential of anionic MPA-capped CdTe/ZnS QDs. Filtered CdTe/ZnS QDs, yielded a strong ζ-potential with an intensity-weighted mean of -30.36 mV, in contrast to a less stable ζ- potential shown in the filtered sample, at -20.13 mV.

4.2.2 Photoluminescence (PL)

The photoluminescent intensity obtained in this study by the MPA-Capped CdTe/ZnS QDs, resulted in an emission peak at 670 nm as seen in figure 4.4.1 below, which confirms its placement within the CdTe-QD emission range. Data obtained was based on three independent analyses. The excitation peak at 480 nm of the MPA-capped CdTe/ZnS QDs, seen in figure 4.4.2, is purely inserted for UV-VIS spectroscopy correlation purposes.

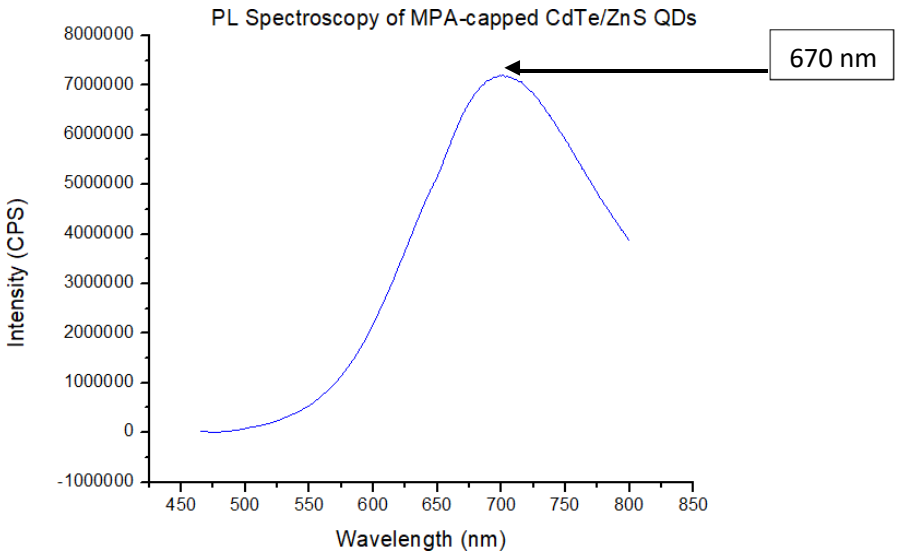

Figure: 4 4.1 PL Spectra of MPA-Capped CdTe/ZnS QDs yielding an emission peak at λ 670 nm.

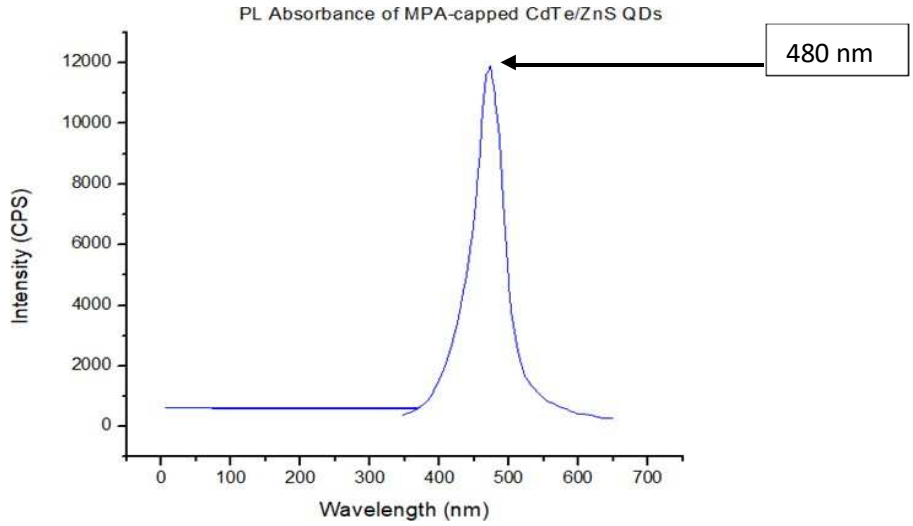

Figure: 4.4.2 PL Absorbance of MPA-Capped CdTe/ZnS QDs yielding an excitation peak at λ 480 nm.

4.2.3 UV-Vis Spectroscopy

The UV-Vis absorbance measurements were obtained from diluted MPA-Capped CdTe/ZnS QD concentrations. The absorbance wavelengths illustrated in figure 4.5, are representative at a concentration of 10 µg/ml, measured at λ 300-500 nm, which illustrates the best peak and correlates with the PL absorbance excitation peak at 480 nm yielded prior in PL analysis via the Nanolog^{TM} Spectro fluorometer (Horiba Jobin Yvon, Japan).

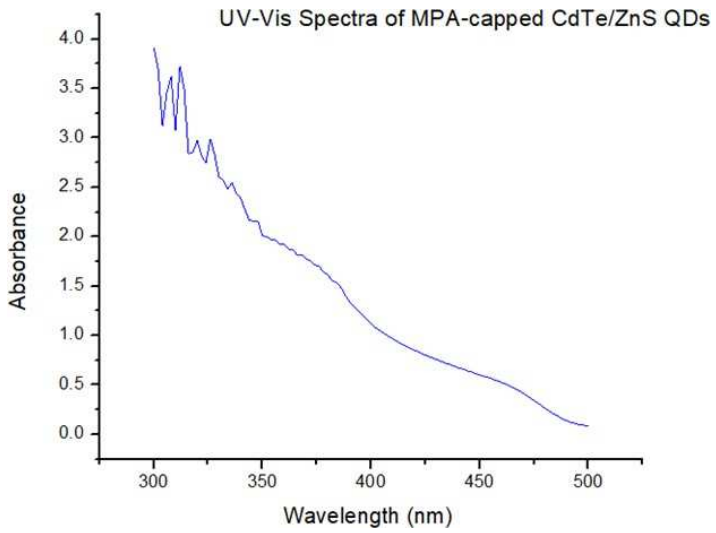

Figure: 4.5 UV-Vis Spectroscopy. Absorbance reading of MPA-Capped CdTe/ZnS QDs at 10 µg/ml.

4.2.4 HR-TEM

4.2.4.1 HR-TEM- Micrograph

HR-TEM analysis produced micrographs which are representative of the size distribution and morphology of the MPA-capped CdTe/ZnS QDs. The micrograph in figure 4.6 shows spherical-like MPA-capped CdTe/ZnS QDs, which are fairly uniform and monodispersed. Built-in size analysis software of the TEM, enabled measurement of the QDs, and revealed HD sizes of 3.66 nm, 3.965 nm and 5.909 nm (at a HD size average 4.511 nm). QD samples were submitted in triplicate, over three independent analysis, n=3.

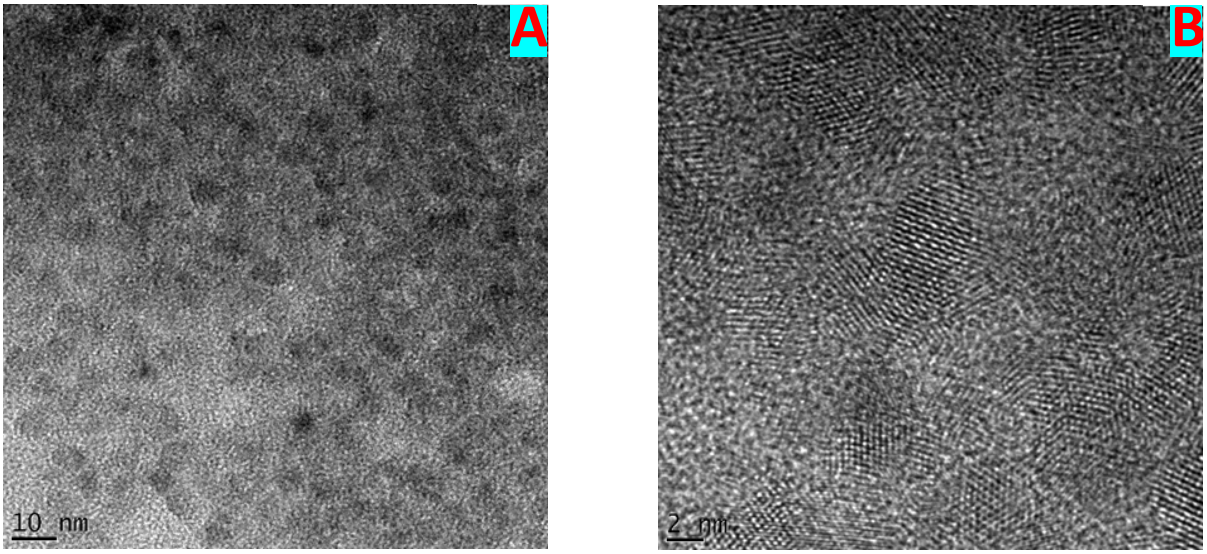

Figure: 4 6 HR-TEM Micrographs of MPA-capped CdTe/ZnS QDs, showing lattice planes in micrograph B. HD size measurements of MPA-capped CdTe/ZnS QDs, were found between 3.66 nm up to 5.909 nm. Morphology reveals a spherical-like shape and were relatively uniform and monodispersed. Scale Bar = 10 nm in micrograph A) Scale Bar = 2 nm in micrograph B).

4.2.4.2 HR-TEM- EDX Spectroscopy

EDX Spectroscopy allowed for localized chemical analysis of the MPA-capped CdTe/ZnS QDs, thus determining its composition. Qualitative analysis allows for the determination of elements present through identification of the peaks/lines present in the spectrum.

Only two of the four known elements are presented by the EDX spectrum in figure 4.7, namely, Cd and S, whilst Zn and Te remained as trace elements, in very small quantitative percentages in contrast to the observed elements. These trace elements weighted over just 1% each, quantitatively, with a 1:2 ratio represented by Cd:S.

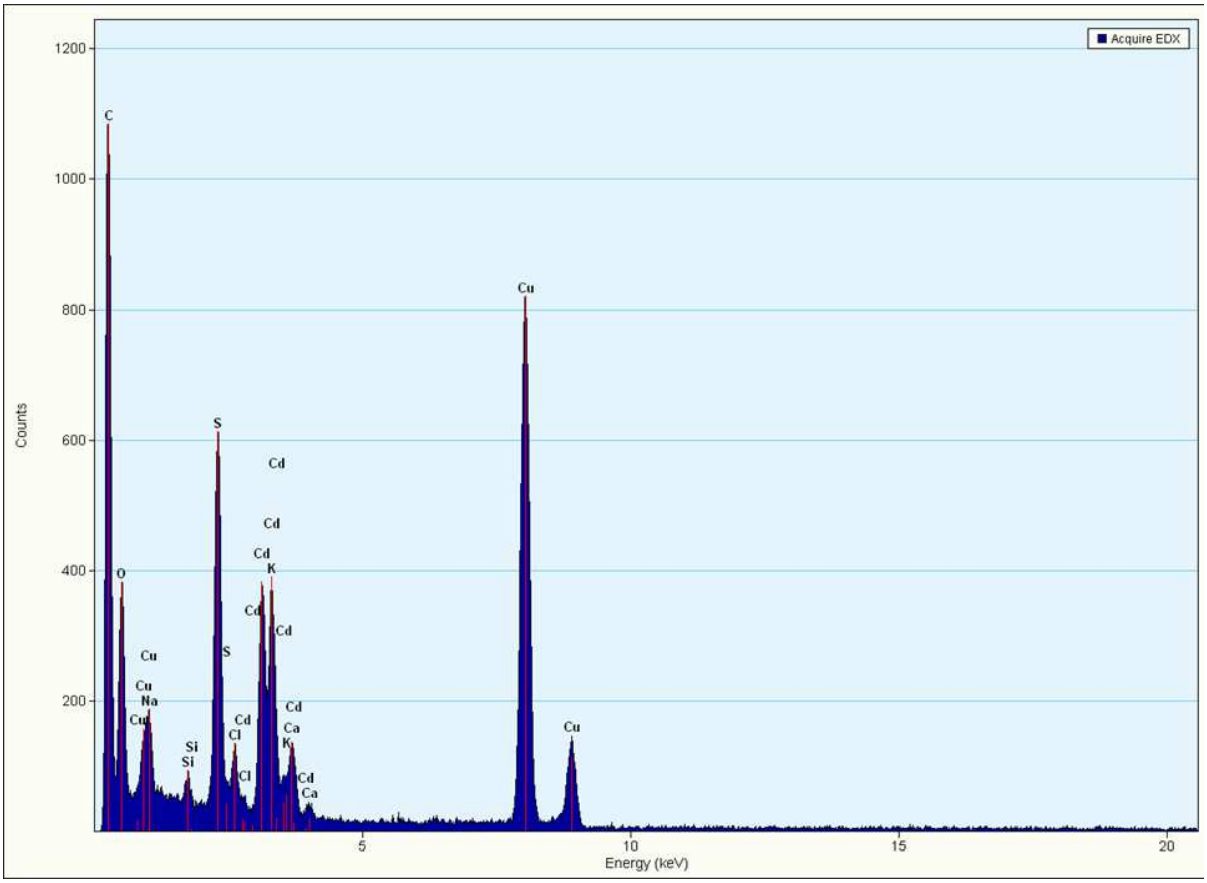

Figure: 4.7 EDX spectrum of MPA-capped CdTe/ZnS QDs Cadmium (Cd) and Sulphur (S) are identifiable, while Tellurium (Te) and Zinc (Zn) reflect as trace elements. These trace elements weighted just over 1% each quantitatively, with a 1:2 ratio represented by Cd: S.

4.2.5 Stability

QDs are subjected to complex biological environments which may affect their colloidal and optical stability, given the manipulations in both *in vivo* and *in vitro* experiments. It is therefore imperative to ensure robust aqueous colloidal stability of the QD for long term exposure. UV-Vis spectrophotometry enabled the measurement of MPA-capped CdTe/ZnS QD stability, within various milieu.

The absorbance readings reported in this study, were recorded at a wavelength range of 300- 650 nm, using the POLARstar Omega plate reader (BMG Labtech, Germany), over 72 hours, for the various sample milieu shown in figure 4.8.A and 4.8.B. Each milieu falls slightly short in wavelength behind the MPA-capped CdTe/ZnS QDs, rejoining at the plateau, with both supplemented and non-supplemented media, creating a noticeable increase in absorbance denoted by the second peak.

Incubation at 25 °C and 37 °C, showed no noticeable changes. Each milieu remains the same, except at 48 hours, supplemented media at 37 °C, peaking at a higher absorbance and FBS, begins to lag at a lower wavelength before rejoining at the plateau. Similarly, at 72 hours, BSA at 37°C, begins to lag slightly with time. Data from 1- 8 hour time frames are shown together in figure 4.8.B, as no noticeable differences were shown for the 0-24 hour time frame. The bright yellow MPA-capped CdTe/ZnS QD solution, however, retained its clarity and viscosity throughout the experiment from 0 Hours up to 72 Hours, with no signs of agglomeration.

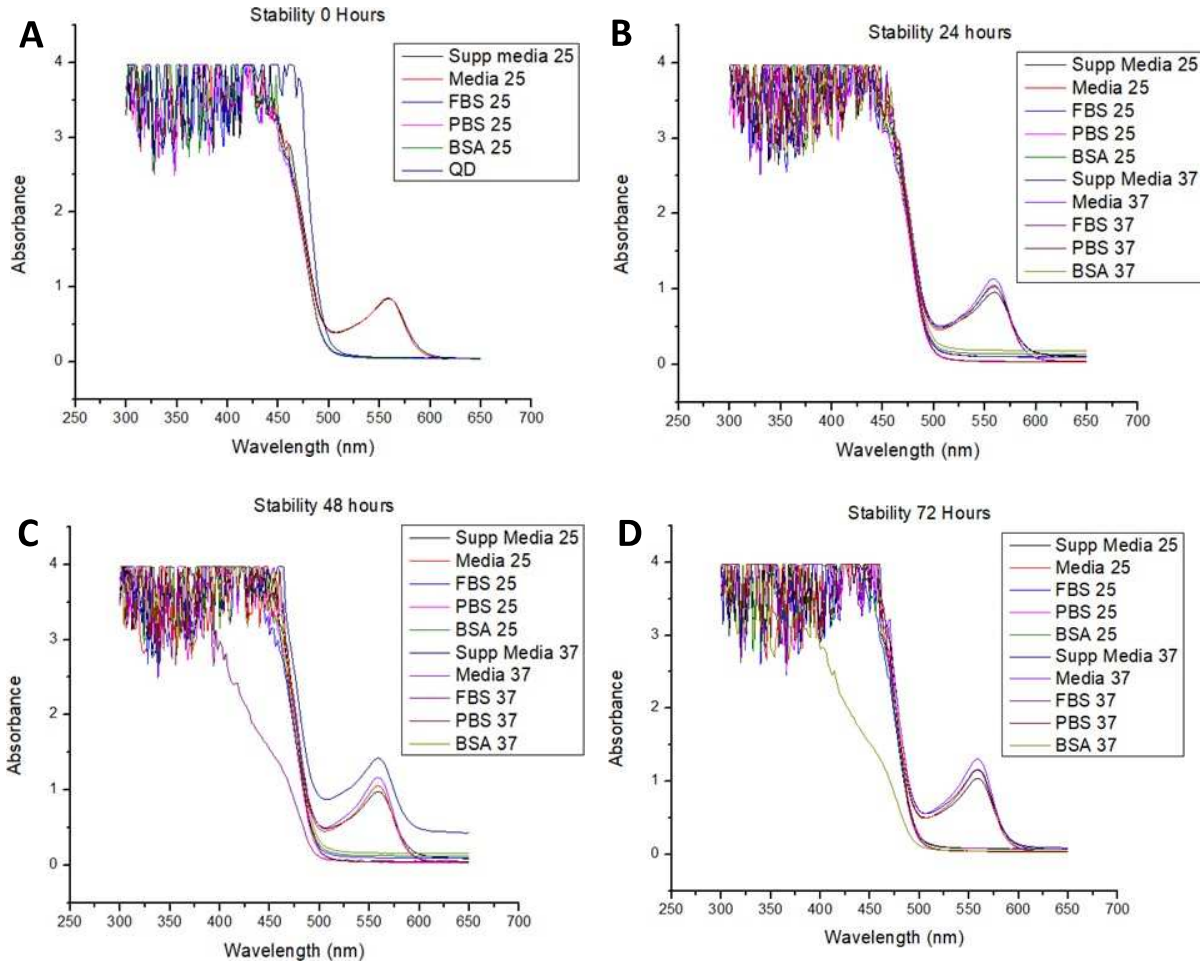

Figure: 4.8.A Stability assay. Absorbance readings measured at four time-frames namely; (A) 0 Hours (B) 24 Hours, (C) 48 Hours and (D) 72 Hours.

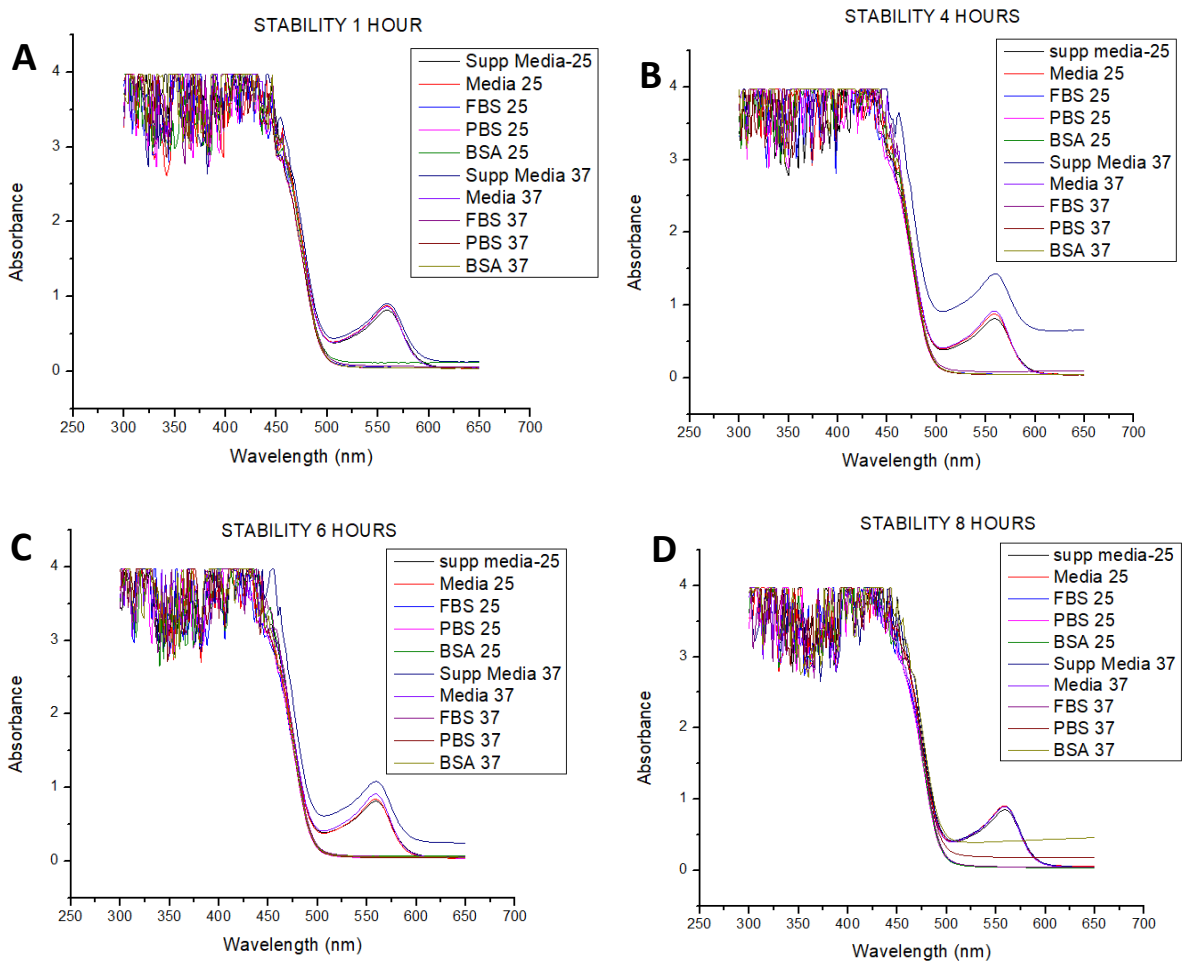

Figure: 4.8.B Stability assay. Absorbance readings measured at four time-frames namely (A) 1 Hour, (B) 4 Hours, (C) 6 Hours and (D) 8 Hours. No noticeable differences were shown to report within the initial 1-8-hour time-frames. Each milieu remains the same, with supplemented media at 37°C, peaking at a higher absorbance in B and C.

4.3 Biological Characterization

4.3.1 Fluorescence Confocal Microscopy

The confirmed uptake of MPA-capped CdTe/ZnS QDs exposed in SH-SY5Y and U87 cells were investigated utilizing fluorescence confocal microscopy. The resultant PL emission peak at 670 nm shown in figure 4.4.1, was expected in the red emission spectra. As aforementioned, images were then taken using the fluorescent LSM 780 Confocal Microscope (Carl Zeiss, Germany), at 100 X magnification, under oil immersion. The results provided are at two-time frames, 1-hour and 4-hour MPA-capped CdTe/ZnS QD exposure, and at two concentrations of 50 µg/ml and 250 µg/ml respectively, with the addition of an untreated/control for comparative purposes.

The untreated/control cell lines, depicted by square A, display only the blue DAPI stained nuclei, imaging the blue nuclei of cells top left, with no evidence of cells shown in the top right pane (red filter), thus the overlay in the bottom right pane only has the blue nuclei visible. Alternatively, illuminated MPA-capped CdTe/ZnS QDs, displayed in the treated cell lines with concentration-dependent intensities depicted by squares B-E, are shown in the split image, which reveals blue DAPI stained cell nuclei and when exposed to the red filter, the MPA-capped CdTe/ZnS QDs are illuminated, as revealed in the overlay images by bright red/pink spots, situated in the nuclei of the cell, as shown in figures 4.9.1 and 4.9.2. Therefore, the overlay image seen in the bottom left block of each treated sample square, shows distinct evidence of the uptake of the MPA-capped CdTe/ZnS QDs within the nuclei. Cytoplasmic staining may or may not seem evident in the small image provided, however, clear observations were made when obtaining images on the fluorescent LSM 780 Confocal Microscope (Carl Zeiss, Germany), showing illuminated MPA-capped CdTe/ZnS QDs in the nuclei area, with no nuclear membrane blebbing.

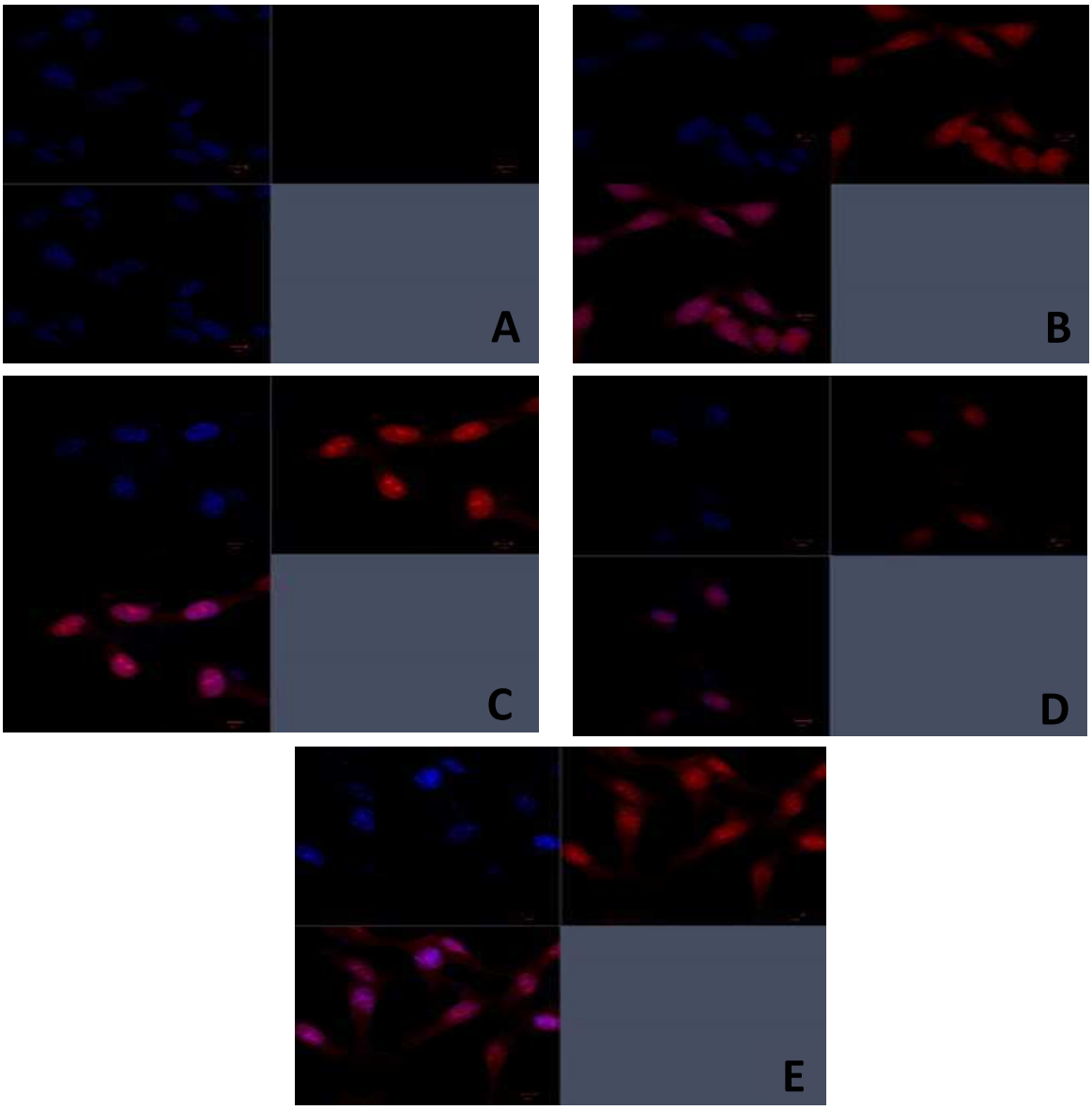

Figure: 4.9.1 Fluorescence Confocal Microscopy. SH-SY5Y Cells treated with MPA-capped CdTe/ZnS QDs, stained wtih DAPI mounting medium Untreated/Control SH-SY5Y cells. B) 50 µg/ml MPA-capped CdTe/ZnS QD treated cells at 1-hour. C) 50 µg/ml MPA-capped CdTe/ZnS QD treated cells at 1-hour. D) 250 µg/ml MPA-capped CdTe/ZnS QD treated cells at 1-hour. E) 250 µg/ml MPA-capped CdTe/ZnS QD treated cells at 4-hours. Scale Bar 5 µm.

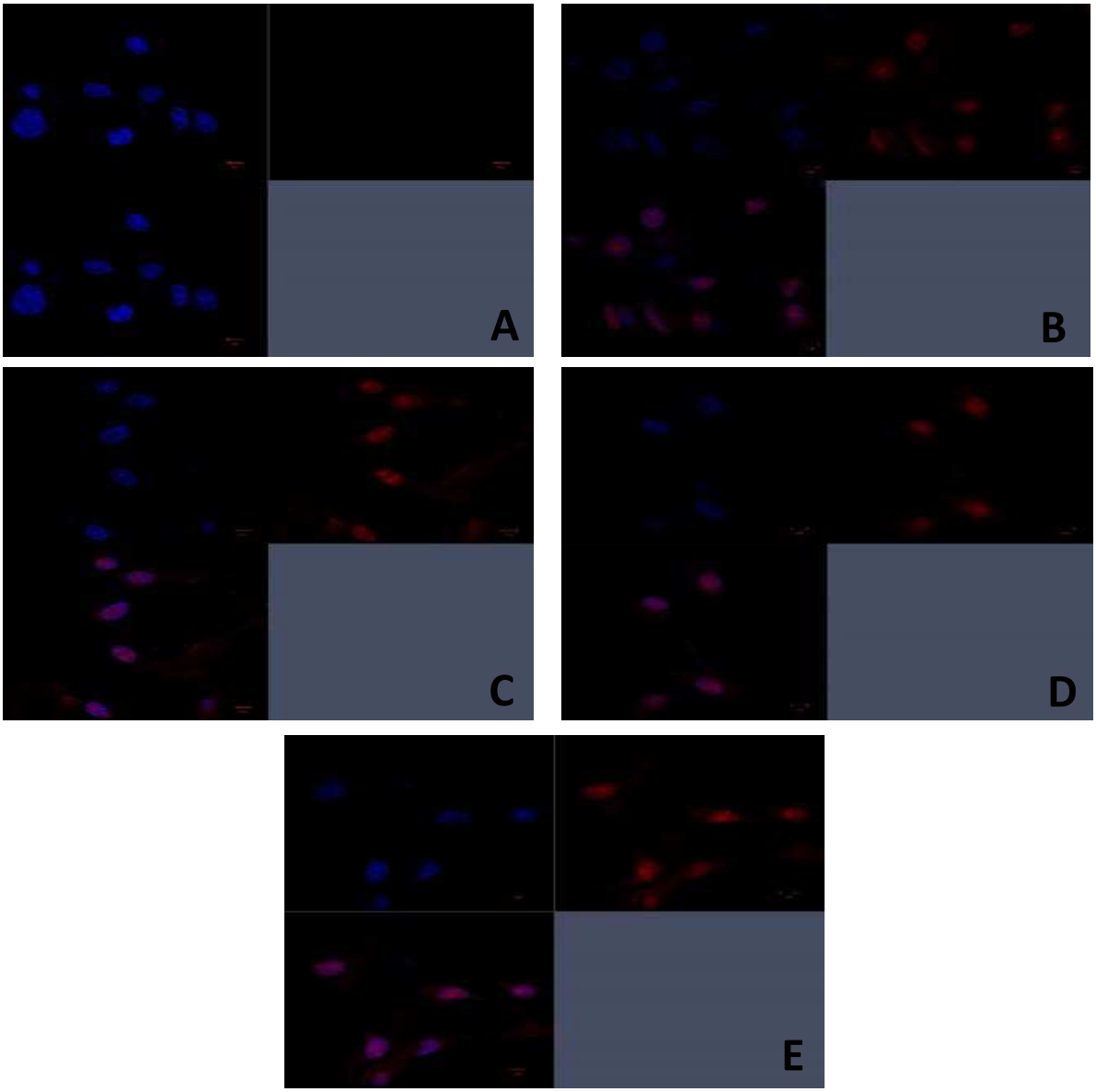

Figure: 4.9.2 Fluorescence Confocal Microscopy. U87 Cells treated with MPA-capped CdTe/ZnS QDs, stained wtih with DAPI mounting medium Untreated/Control U87 cells. B) 50 µg/ml MPA-capped CdTe/ ZnS QD treated cells at 1-hour. C) 50 µg/ml MPA-capped CdTe/ZnS QD treated cells at 4-hours. D) 250 µg/ml MPA-capped CdTe/ZnS QD treated cells at 1-hour. E) 250 µg/ml MPA-capped CdTe/ZnS QD treated cells at 4-hours. Scale Bar 5 µm.

4.3.1 WST-1 Colorimetric cell viability assay

The colorimetric cell proliferation agent WST-1, was used for the viability assay based on the metabolic activity of cells. Standardized tests viz the cell viability assay and intracellular ROS assays, are typically applied for the investigation of *in vitro* QD cytotoxicity. Treatment with the

MPA-capped CdTe/ZnS QDs, was carried out over three time intervals (24-hour, 48-hour and 72-hour) and at four respective concentrations (5 μg/ml, 10 μg/ml, 15 μg/ml and 20 μg/ml). Exposure of the MPA-capped CdTe/ZnS QDs, resulted in an increase in cell viability observed in the NB SH-SY5Y cell line, whereas a decrease in cell viability, was observed in the GB U87 cell line, as shown in figures 4.10.1 and 4.10.2 respectively. Although two disparate effects are reported here, both of the cell lines surge in effect at 72 hours, whereby: SH-SY5Y cells still shows an increase in cell viability at the 72 hour time frame but to a lesser degree and similarly, the U87 cells still showing a decreased cell viability at 72 hours to a lesser degree than 48 hours, however, still a decrease in comparison to the control. Thus, the MPA-capped Cd/Te/ZnS QDs, causing a decrease in cell viability, which is not concomitant with the increase in concentration.

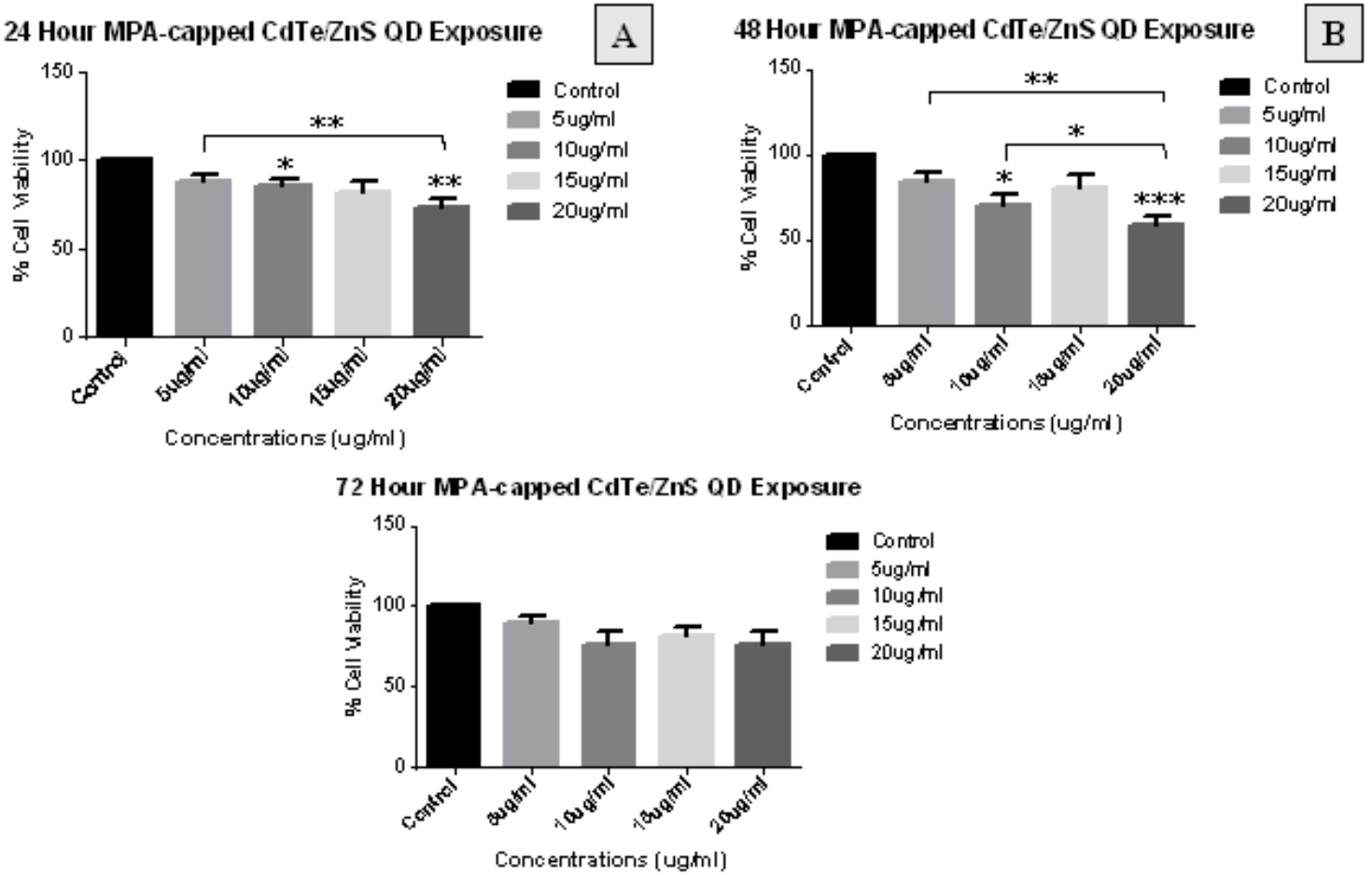

Figure: 4.10.1 WST-1 Colorimetric Cell Viability Assay in U87 cells. MPA-Capped CdTe/ZnS QDs caused a decrease in cell viability however, the decrease is not concomitant with the increase in concentration. Exposure Time A) 24 Hours B) 48 Hours C) 72 Hours. Data represented is in triplicate over 3 independent analyses, with error bars representative of calculated SEM values (Mean ± SEM; n=3). Statistical significance when compared with the control as well as inter-treatment differences (in A and B) are denoted with an asterisk where $p < 0.05$ * $p < 0.01$ ** $p < 0.001$ ***.

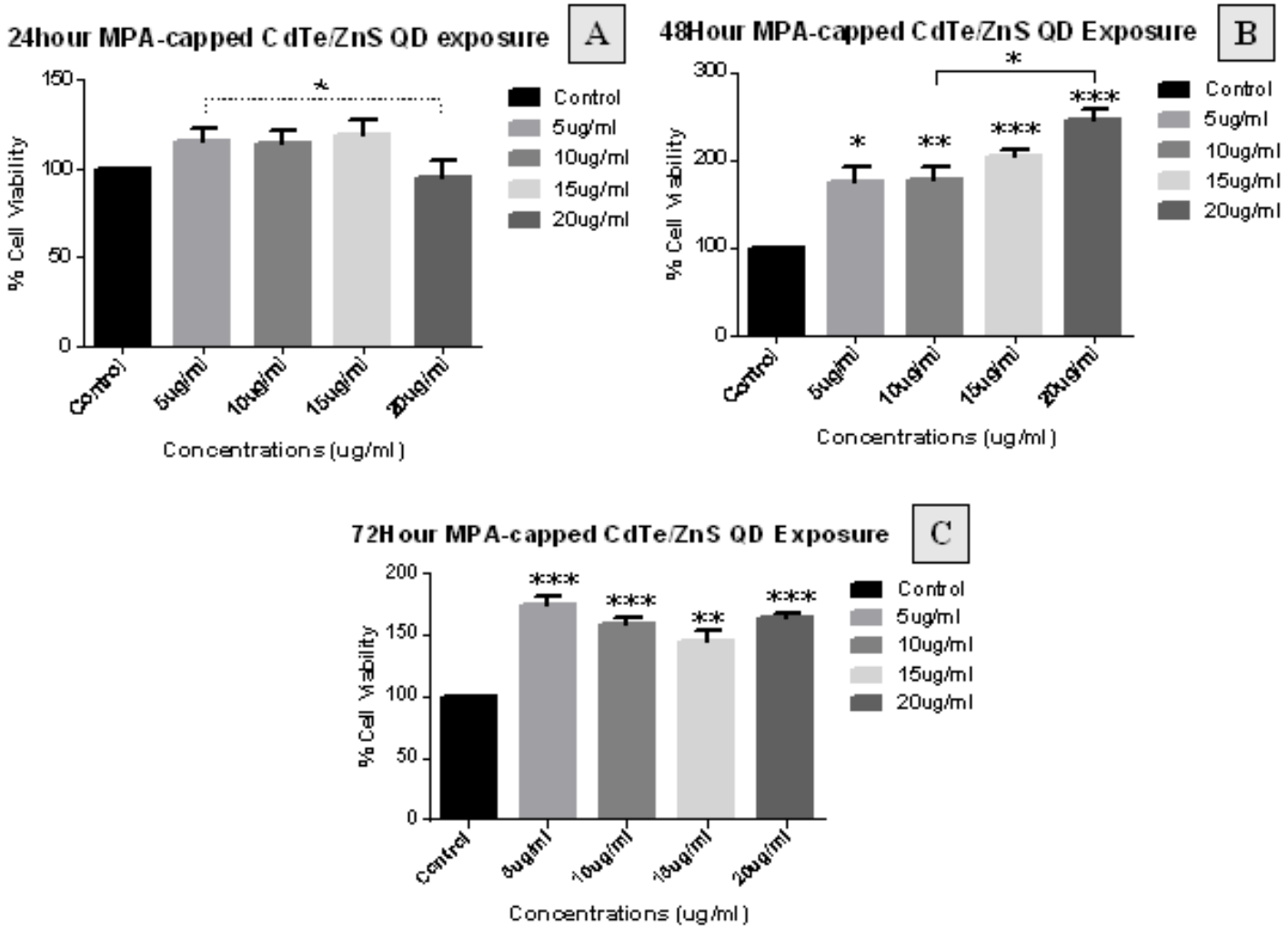

Figure: 4.10.2 WST-1 Colorimetric Cell Viability Assay in SH-SY5Y cells. MPA-Capped CdTe/ZnS QDs caused an increase in cell viability. A) 24 Hours B) 48 Hours C) 72 Hours. Data represented in triplicate over 3 independent analysis, with error bars representative of calculated SEM values (Mean ± SEM; n=3). Statistical significance when compared with the control as well as inter-treatment differences (in A and B) are denoted by asterisks, where $p < 0.05$ * $p < 0.01$ ** $p < 0.001$ ***.

4.3.2 Cell Morphology

Following exposure of both cell lines to the MPA-capped CdTe/ZnS QDs, photomicrographs were taken using the Primovert inverted microscope (Carl Zeiss, Germany), objective magnification 40X, to track any morphological changes. The images obtained, reveal a change in morphology of U87 and SH-SY5Y cells exposed to the MPA-capped CdTe/ZnS QDs. In both cell lines used for this study, the cells became rounded with grape-like clusters forming compared to the untreated control, as shown in figure 4.11.1 up until 4.11.3. Furthermore, the rounded cell morphology was more predominant in the U87 cell line which eventually dislodged from the cell culture plate at 48 hours.

Exposure Time 0 Hours	Untreated	5µg/ml	10 µg/ml	15 µg/ml	20 µg/ml
U87	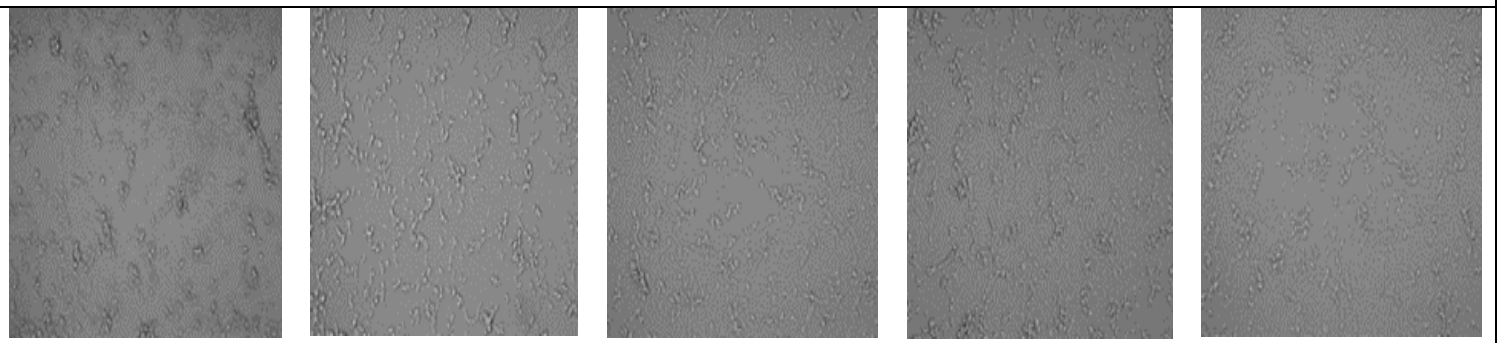				
SH-SY5Y	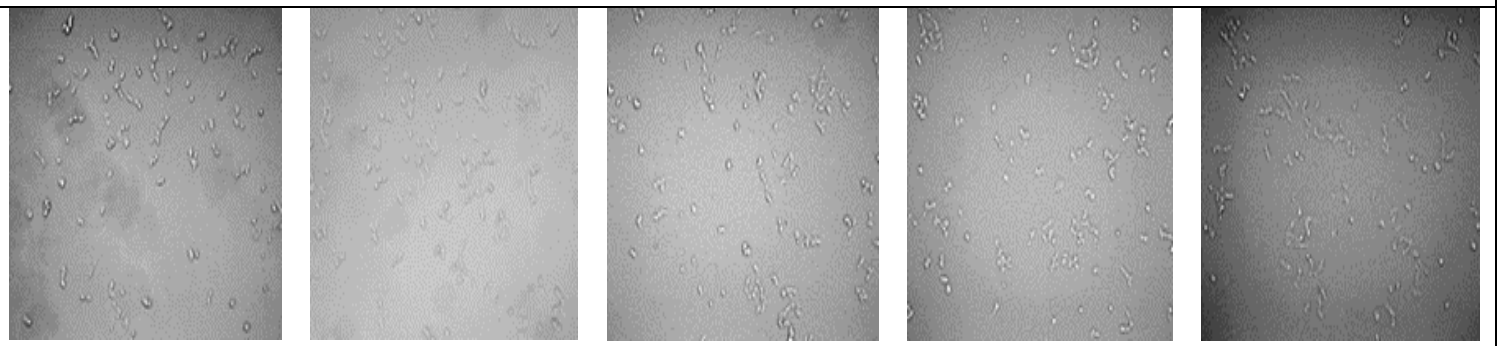				

Figure 4.11.1 Cell Morphology at 0 Hours. MPA-capped CdTe/ZnS QD exposure in U87 and SH-SY5Y cells, in comparison to untreated cells. No morphological changes noted. Objective magnification 40x.

Exposure Time 24 Hours	Untreated	5µg/ml	10 µg/ml	15 µg/ml	20 µg/ml
U87	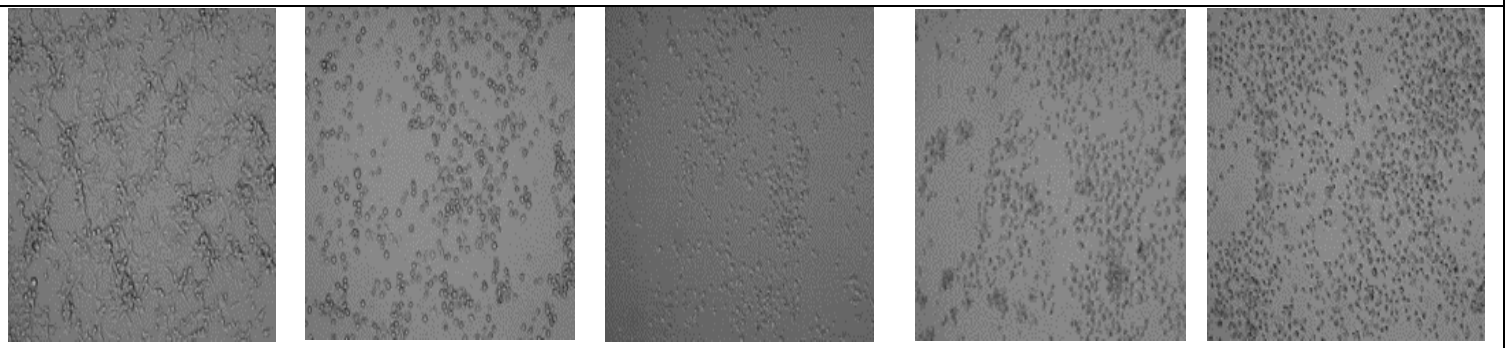				
SH-SY5Y	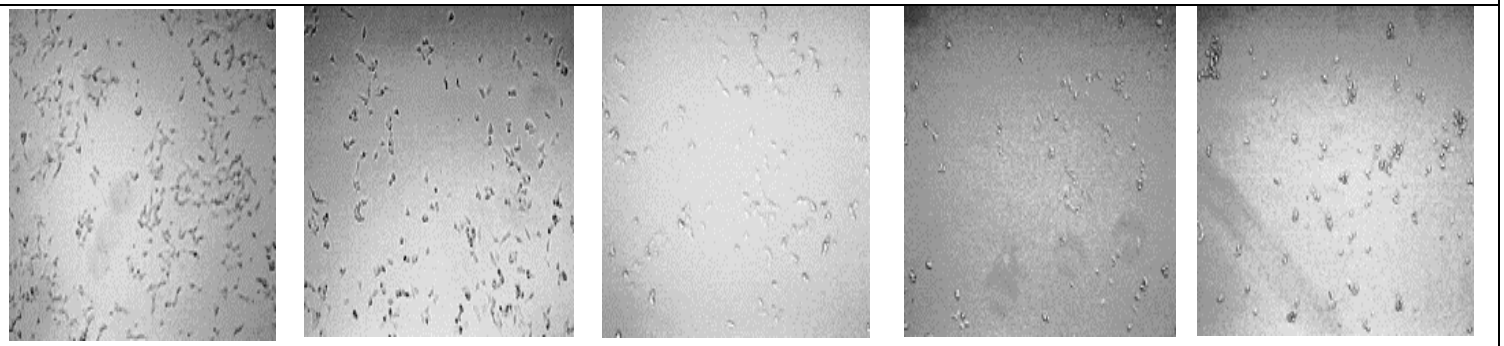				

Figure 4.11.2 Cell Morphology at 24 Hours. Slight morphological changes observed by cell rounding in MPA-capped CdTe/ZnS QD exposed U87 and SH-SY5Y cells, in comparison to untreated cells. Objective magnification 40x.

Exposure Time 48 Hours	Untreated	5µg/ml	10 µg/ml	15 µg/ml	20 µg/ml
U87	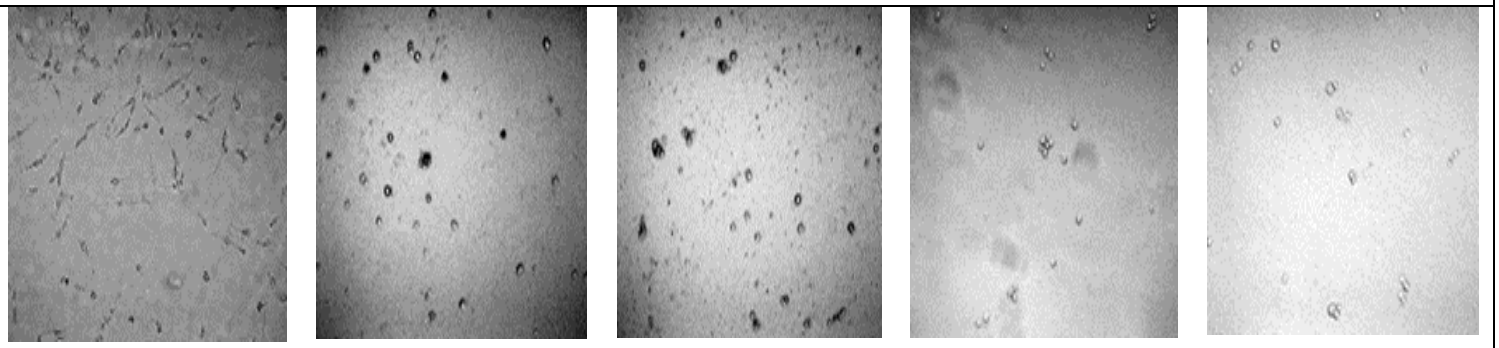				
SH-SY5Y	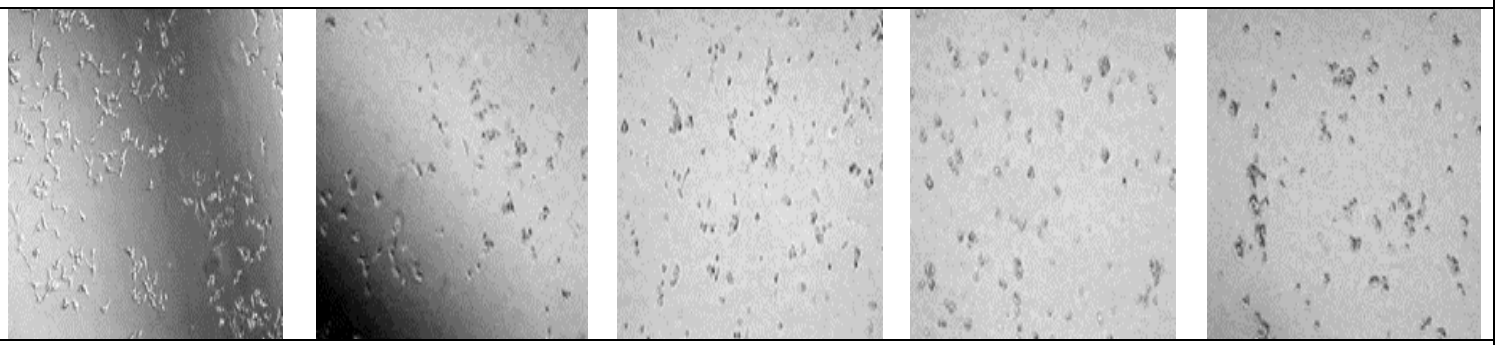				

Figure 4.11.3 Cell Morphology at 48 Hours. Cell rounding more prominent with grape-like features forming on the MPA-capped CdTe/ZnS QD exposed cells, in comparison to untreated cells. Objective magnification 40x.

4.3.3 Cell Cycle Analysis- FxCycle PI/RNase staining solution

Cell cycle analysis was carried out using the FxCycle PI/RNase staining solution, on the C6 flow cytometer (BD Accuri, USA). Cell count percentages are displayed in a frequency histogram as distributed in the three major stages of the cell cycle where; G_0/G_1 phase (red), S phase (blue) and the G_2/M phase (green).

The histograms displayed in figures 4.12.1 and 4.12.2 are representative of 20 µg/ml MPA- capped CdTe/ZnS QD exposure in U87 and SH-SY5Y cells repectively, in comparison to the untreated cells at 24 and 48 hours. Corresponding distribution percentages of the cell populations are tabulated below the figures. Together, the histograms and distribution percentages, indicate that the majority of the cell populations are locked in the G_0/G_1 phase, in both cell lines, which does not reveal significant variances in the cell cycle distributions of the two neuronal cancerous cell lines. The cell populations are however, considerably higher in G_2/M phase opposed to the S phase displayed by NB SH-SY5Y cells. Data shown are based on two independent analyses.

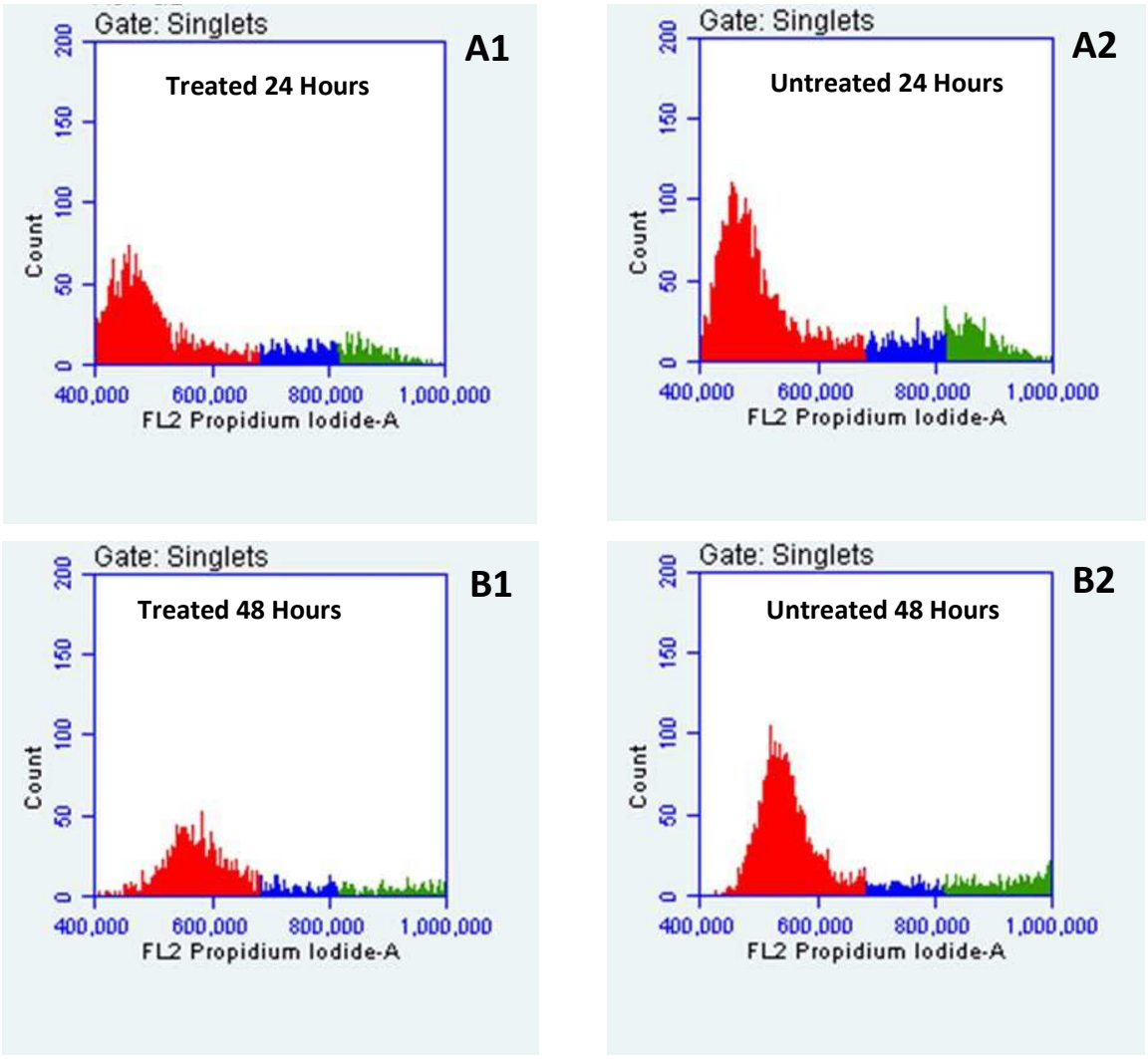

Figure: 4.12.1 Histograms of Cell Cycle Analysis of U87 cells either untreated or exposed to 20µg/ml MPA-capped CdTe/ZnS QDs. A1) Treated, 24 hours exposure. A2) Untreated, 24 hours exposure. B1) Treated, 48 hours exposure. B2) Untreated, 48 hours exposure.

Table 4.1 - Corresponding distribution percentages of the cell populations in U87 cells

	G_0/G_1 phase	S phase	G_2/M phase
A1	66.1%	15.2%	12%
A2	63.7%	15.7%	8.8%
B1	58.2%	11.1%	11.7%
B2	61%	7.5%	12.1%

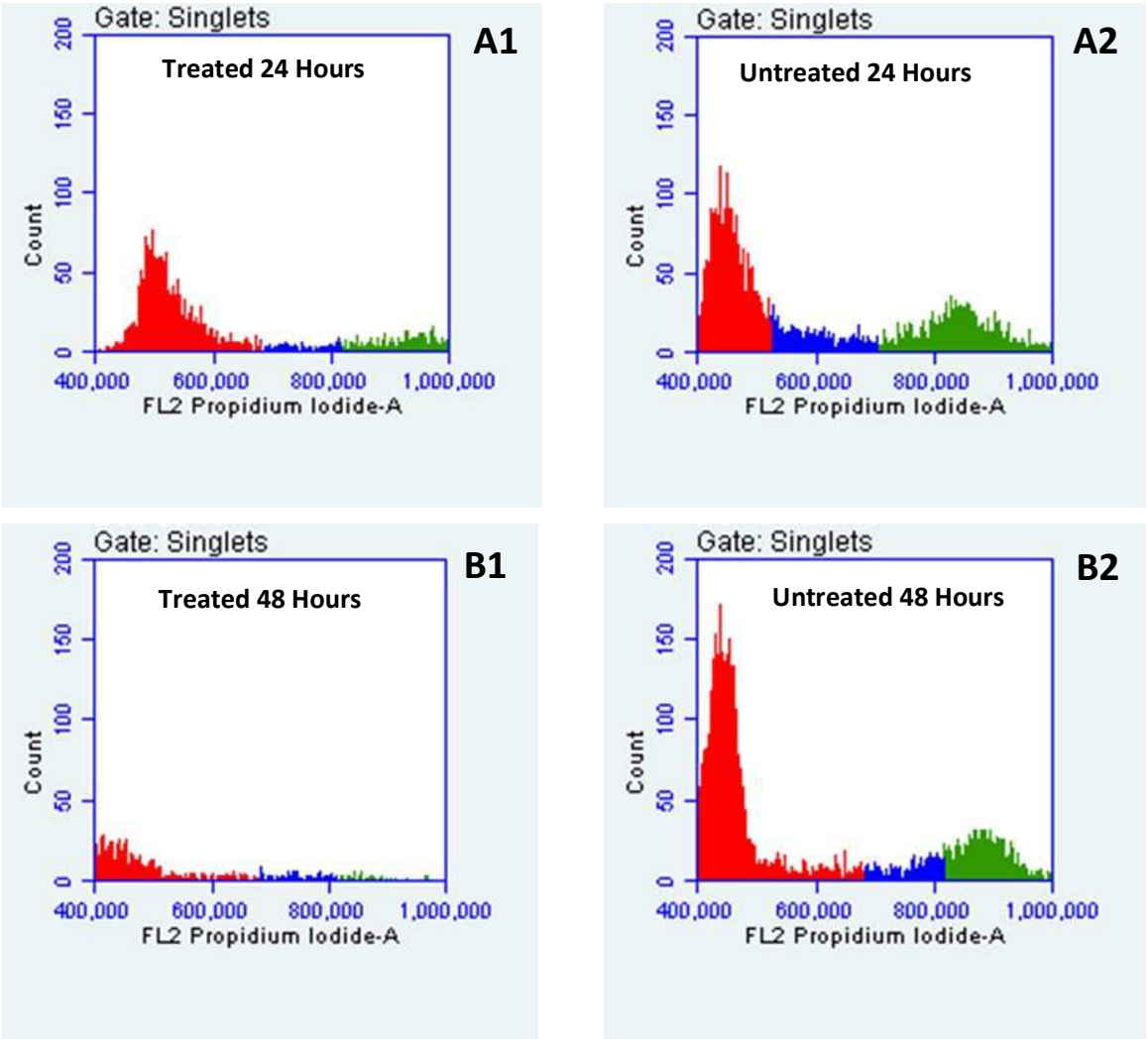

Figure: 4.12.2 Histograms of Cell Cycle Analysis of SH-SY5Y cells either untreated or exposed to 20µg/ml MPA-capped CdTe/ZnS QDs. A1) Treated, 24 hours exposure. A2) Untreated, 24 hours exposure. B1). Treated, 48 hours exposure. B2) Untreated, 48 hours exposure.

Table 4.2 - Corresponding distribution percentages of the cell populations in SH-SY5Y cells

	G_0/G_1 phase	S phase	G_2/M phase
A1	68.2%	6.5%	15.3%
A2	45.5%	14.6%	26.8%
B1	52.8%	10.9%	6.1%
B2	48.2%	7.5%	14.5%

CHAPTER 5

DISCUSSION

5.1 Synthesis of MPA-Capped CdTe/ZnS QDs

QDs display inimitable optical and electronic properties, owing to their quantum confinement properties which dictate their behaviour in biological applications. Hence, there is need to ensure concise and controlled synthesis taking into consideration the particle size, additional particle size covering such as capping agents which add to the bulk of the nanoparticle, colloidal stability, surface charge, etc. (Nho *et al*., 2010; Smith and Nie, 2010; Liu *et al*., 2015).

In this study, the MPA-capped CdTe core, coated with a ZnS shell was successfully synthesized as described in section 3.1 of the Materials sand Methods chapter, yielding relatively monodispersed and highly luminescent QDs (Yan *et al*., 2010; Chomoucka *et al*., 2013). The growth of the CdTe nanocrystal core was established by injecting the NaHTe complex into the Cd/MPA precursor, and a final addition of the ZnS precursor solution which comprised zinc acetate and thiourea, served as the shell. The MPA stabilizer possesses thiol and carboxylic acid groups and the thiol region binds strongly to the ZnS shell allowing for the aqueous dispersibility of QDs (Liu *et al*., 2015). In an uncoated or weakly stabilized CdTe core, this would result in the production of ROS *in vitro*, and thus lead to cell death (Choi *et al*., 2007). As mentioned, the ZnS shell passivates the surface and enhances PL by counteracting the quenching effect of traps/defects at the core's surface. When compared to CdSe, ZnS is less prone to oxidation and thus renders chemical stability for the QD and decreases oxidative photo stability (Smith *et al*., 2008; Smith and Nie, 2010).

5.2 Physical Characterization of MPA-capped CdTe/ZnS QDs

5.2.1 Zeta Size, Poly Dispersity Index and Zeta Potential

5.2.1.1 Zeta Size and Poly Dispersity Index

To reiterate, ζ size and PdI, were measured by DLS, yielding h_d size distributions based on the speed of Brownian motion and the equivalent sphere principle.

The unfiltered MPA-Capped CdTe/ZnS QDs from the stock solution yielded an intensity weighted mean of 229.5 nm with a size distribution range of 177-266 nm however, filtration thereof decreased the intensity weighted mean in size to 25.61, with a size distribution range of 25-30nm, which more similarly correlates to the CdTe QDs reported by Rocha *et al*., (2014) at 14.79 ± 1.70 nm using DLS analysis**.** We however, believe that the formulated QD composition was jeopardized and altered during the filtration process, as the filtered MPA-capped CdTe/ZnS QDs negatively affected physical characterization mainly the non-detection of QDs in the EDX spectroscopy elemental analysis. Therefore, only using the unfiltered QDs throughout this study, which were clarified by centrifugation subsequent to the synthesis thereof.

The presence of a few aggregates would affect the interpretation of the data, due to such parameters as "pH of the suspension medium, viscosity, temperature, concentration and particle sedimentation" (Gaumet *et al*., 2008). Furthermore, the resultant apparent size and size distribution may not be the true h_d size measurement (Xhu, 2008). DLS probes a collective diffusion coefficient (Dc), opposed to a single-diffusion from individual particles, and therefore when the "apparent particle size" is computed with the Stokes-Einstein equation it could increase/decrease with concentration, which is not necessarily the true h_d size (Xhu, 2008). Despite the considerations and sensitivity surrounding the conceivable limitations, we have not disregarded the technique but continued to use it as a viable means of measurement. Studies by Gaumet *et al*., (2008) have suggested that size measurement be done via two characterization techniques as single characterization is not satisfactory, however, one of the techniques should be a microscopic method. Due to the possible limitations and unreliability of analysing mixed size particles, the true h_d size measurement was therefore dependent on the characterization by TEM analysis. TEM analysis carried out in this study, yielded h_d size distributions between 3.66-5.909 nm in diameter, at an average of 4.511 nm, which is consistent with those anionic red emitting CdTe QD sizes reported by Lovric *et al*., (2005) revealing a diameter of 5.7 nm ± 0.1. Furthermore, orange spheroid CdTe QD particles, have been yielded in a study by Rocha *et al*., (2014) at an average size of 6.09 ± 1.48 nm, which collectively yield similar hd sizes in the orange to red emitting range.

PdI indicates the type of dispersity and stability of the molecules. Values between 0.1-0.3 are indicative of a narrow symmetric distribution and thus render stability. PdI values above 0.5, indicate a shift towards a broader distribution of molecules and could suggest agglomeration. However, a value greater than 1 would not be suitable for DLS and could infer polydispersity or mixed populations (Gaumet *et al*., 2007), which is a possible limitation in this technique, thus requiring a second microscopic characterization technique. The unfiltered MPA-Capped CdTe/ ZnS QDs in this study gave an average PdI value of 0.521, while the filtered samples yielded an intensity-weighted mean PdI value of 0.569, shown in figure 4.2 (B). These median PdI values are congruent with even higher PdI values of 0.69 reported by Rocha *et al*., (2014) which were measured over longer time-frames and reflected a more polydisperse system, comprising both small and large particles in suspension. The median PdI values presented in this study thus reflects a monodispersed solution which shifts toward polydispersity, possibly indicating agglomeration. In contrast, another study reports the synthesis of CdTe QDs embedded in gelatin, producing a narrow size distribution PdI of 0.01 at an average h_d size of 150 nm accounted for by the additional gelatin layer (Wang *et al*., 2008). The median PdI values reported in this study, along with the polydispersity reported by Rocha *et al*., (2014) can be further corroborated by the works of He *et al*., (2008) who found that the direct growth of the ZnS shell upon the CdTe core, creates strain which is subsequent to a large lattice mismatch, thus resulting in mixed size populations and furthermore, lowered PLQY.

5.2.1.2 Zeta (ζ) - Potential

In this study, the unfiltered MPA-capped CdTe/ZnS QDs yielded a strong and stable ζ- potential at an average of -30.36 mV which infers potential instability thereof (which would be deduced from the PdI values in figure 4.2.B), rendering anionic QDs. The filtered sample yielded anionic MPA-capped CdTe/ZnS QDs with a ζ- potential of -20.13 mV, data shown in figure 4.3. Lovric *et al*., (2005) alike, report a ζ- potential of good strength at -41.75 mV rendering high stability, possibly owing to its MPA stabilizer, and furthermore owing to the additional ZnS shell contained in this study. Another study reported parameters such as pH and salinity affecting the ζ- potential values and h_d size of CdTe QDs, when measured in both Milli-Q and sea water, which yielded a ζ- potential value of -42.64 ± 0.55 mV in Milli-Q water, once again consistent with that reported in this study (Rocha *et al*., 2014).

Although ζ- potential measurements consider both the particle and the environment to yield an accurate and high-resolution result, such would still not account for the accurate ζ- potential. It is noteworthy that only the unfiltered MPA-capped CdTe/ZnS QD solution was utilized throughout this study, due to the negative effects of filtration on both the ζ- potential measurements and other physical characterization techniques done.

5.2.2 Photoluminescence (PL)

CdTe-QDs have an emission spectrum range of 500-750 nm (Smith *et al*., 2008). The corresponding emission colour thereof would range between a green-yellow to red emitting QD, on the electromagnetic spectrum. The photoluminescent intensity generated by the MPA-Capped CdTe/ZnS QDs in this study, resulted in an emission peak of 670 nm as seen in figure 4.4.1, which affirms its placement within the CdTe-QD emission range. In the progressive CdTe-QD emission range, PL emissions reported by Wang *et al*., (2008) synthesized green CdTe QDs yielding an emission peak at 542 nm, and by Roche *et al*., (2014) yielding orange emitting CdTe QDs at an emission of 590 ± 5nm. Furthermore, progressing to Lovric *et al*., (2005) who synthesized anionic red emitting CdTe QDs at 632nm, which all fall within the CdTe-QD emission range, and even more so the orange to red emitting CdTe QDs correlating to the anionic red emitting MPA- capped CdTe/ZnS QDs, reported in this study.

Li *et al*., (2010) synthesized carbon-QDs (CQDs) and showed that the PL properties were size-dependent. Small CQDs (1.2nm centre), resulting in a UV light emission of 350 nm, medium CQDs (1.5-3 nm centre) resulting in a visible light emission of 400-700 nm and large CQDs (3.8 nm centre) resulting in the near-infrared emission around 800 nm. Nho *et al*., (2010) suggested that it is imperative to ensure controlled size, morphology and surface-ligands for the applications of QDs, as these may lead to substantial changes in their optical characteristics. Kim *et al*., (2015), synthesized cysteine-capped CdTe QDs, at three different pH values, to demonstrate the effects of pH on the maximum emission wavelength of QDs. Their data revealed diminution in emission intensity in its entirety at a pH < 4 or > 11, and strongest emission intensity was evident at pH 8. Therefore, the pH value is a crucial aspect in the aqueous media synthesis of QDs as it is an attributable control in both emission wavelength and the PLQY.

Although depletion in emission intensity was observed above pH 11 in the study of Kim and co-workers (kim *et al*, 2017), the synthesis route employed in this current study for MPA-capped CdTe/ZnS QDs utilized pH values of 11.5-11.7, yielding highly luminescent QDs.

5.2.3 UV-Vis Spectroscopy

Diluted MPA-Capped CdTe/ZnS QD concentrations were employed to carry out UV-Vis absorbance measurements. The absorbance wavelength illustrated in figure 4.5, is representative at a concentration of 10 μg/ml, measured at λ 300-500 nm, which correlates with the PL absorbance/excitation peak of 480 nm, yielded prior in PL analysis via the Nanolog^{TM} Horiba Jobin Yvon, Spectro fluorometer. Similarly, both Roche *et al*., (2014) and He *et al*., (2008) illustrates the UV-Vis absorption peaks of CdTe QDs, which alike are consistent with the excitation peak of 480 nm yielded in this study. UV-Vis spectroscopy was further employed to investigate the stability of the MPA-capped CdTe/ZnS QDs in various milieus and is further elaborated on in section 5.2.5.

5.2.4 HR-TEM

5.2.4.1 HR-TEM- Micrograph

An attractive feature of QDs is their size tuneable emissions owing to their novel optical properties, and when correlated with particle size, largely depends on the internal structure of the QD. However, the large surface-to-volume ratio may affect the optical properties and by decreasing the size from its bulk state, a resultant blue shift in the optical transition occurs (Smith and Nie, 2010; Vasudevan *et al*., 2015). Moreover, oxidizing agents may etch away at the QD surface, in addition to surface modifications creating traps/defects at the QD surface which may quench the fluorescence, thus the need for shell passivation via colloidal (core) shell QD synthesis to improve the PLQY and sustain quantum confinement, as implemented by the MPA-capped CdTe/ZnS QDs in this study, for biological application (Smith and Nie, 2010).

The HR-TEM micrographs produced in this study are representative of the size distribution and morphology of the MPA-capped CdTe/ZnS QDs. Thus, the micrographs obtained showed spherical like MPA-capped CdTe/ZnS QDs, which were fairly uniform and monodispersed, furthermore, revealing an average h_d diameter size measurements of ±4.511 nm. Micrograph B, at

a scale bar of 2 nm, shows the evident lattice planes which spans the QD particle. These micrographs are structurally alike with those reported by Swartz (2013), whom synthesized spherical green fluorescent CdSe/ZnS QDs. Additionally, He *et al*., (2008), synthesized various CdTe QDs, with HR-TEM micrographs displaying the CdTe core alone, along with the complete core-shell CdSe/ZnS QD, consistent with the evident lattice planes which extends the entire QD, therefore, absent of inimical effects exerted by the shell upon the crystalline form of the core, and furthermore, report similar QD sizes ranging between 2.6 nm (core only) up to 4.5nm (shell included), which ultimately creates a red shift in QD emission due to the bulk of shell growth upon the core. Moreover, the works of Duan *et al*., (2009) is synonymous with the representative micrographs in this study, in that their TEM analysis of MPA-capped CdTe QDs, yielded spherical, monodispersed QDs, with well-resolved lattice planes accounting for its highly crystalline structure and lastly, reported HDs averaging 3 nm. In this study, the relatively monodispersed MPA-capped CdTe/ZnS QDs can be correlated with the median PdI value of 0.521, which indicated a near monodispersed shift towards polydispersity, retrieved in the zeta size distribution analysis. Although size distribution data retrieved from the zeta size measurements based on the speed of Brownian motion via DLS yielded QD sizes between 177-229 nm in the unfiltered sample, the true size validation was affirmed microscopically via HR-TEM analysis. DLS is not disregarded as a technique, however, the possible limitations surrounding this technique especially with polydisperse cell populations, has been highly considered.

5.2.4.2 HR-TEM- EDX Spectroscopy

Localized chemical analysis of the MPA-capped CdTe/ZnS QDs was carried out by EDX Spectroscopy, in order to determine the composition thereof. Qualitative analysis allowed for the determination of elements present through identification of the peaks/lines present in the spectrum, which get matched with those in literature/standards. Only two of the four elements were presented by the EDX spectrum, namely, Cd and S, whilst Zn and Te remained as trace elements in very small quantitative percentages in contrast to the observed elements.

Swartz (2013) produced an EDS spectrum which revealed small quantitative percentages of Zn and S however, were able to achieve detection of all four elements pertaining to their CdSe/ZnS QD. Likewise, an EDX analysis by Al-Ali *et al*., (2015), showed positive detection of each sample composition of their CdSe/ZnS QDs synthesized with various surface functionalization's.

Differing the QD formulation itself, would not have an effect on the observed elemental compositions, however, varying the QD constituents, definitely affects the QDs functional role. Not only does the MPA act as a stabilizer, the ZnS shell offers a passivating role while enhancing PL. ZnS, is also less prone to oxidation, renders chemical stability and decreases oxidative photostability when compared to CdSe. Additionally, an uncoated or weakly stabilized CdTe core is subsequent to ROS production and inevitable cell death.

Collectively, various elements could possess marked differences in their properties, compared to the individual constituent elements and thus EDX Spectroscopy relying heavily on the standards for peak identification, furthermore, energy-dispersive variants may find it hard to distinguish between emissions when the energies are in close proximity, or find difficulty in identifying the marked characteristic peaks yielded by trace elements resulting from contextual noise, which could possibly account for the results observed in this study (Barron, 2013).

Quantitative analysis allowed for the determination of MPA-capped CdTe/ZnS QD stoichiometry, however, this does not necessarily correlate with the empirical formula as all the elements were not always visible, as per the resultant EDX spectroscopy presented.

5.2.5 Stability

Given the complex biological environments which may affect QD colloidal and optical stability and their manipulations in both *in vivo* and *in vitro* experiments, it is imperative to ensure robust aqueous colloidal stability of the QD for long term exposure (Liu *et al*., 2015). MPA-capped CdTe/ZnS QD stability was measured within various milieu using UV-Vis spectrophotometry. Given QDs promising applications and various advantages over organic fluorophores due to their distinctive properties, the tendency to aggregate or lose luminescence is still a vital factor to be considered in an intracellular environment, under both isotonic and acidic conditions with a pH < 5 (Hoshino *et al*., 2004).

However, in this study, the bright yellow MPA-capped CdTe/ZnS QD solution retained its clarity and viscosity throughout the experiment, with no signs of agglomeration, from 0 Hours up to 72 Hours. Rocha *et al*., (2014) investigated the turbidity of CdTe QDs in order to assess the change in sedimentation rates and deduced that consequential formation of larger aggregates result in

lowered turbidity and increased sedimentation rates. Although the various milieu remained fairly constant without any marked increase/decrease over the investigated time frames, Lovric *et al*., (2005), reported increased fluorescence in a more acidic media, with the maximal fluorescence intensity value at 5.5 pH, whereby any value lesser or greater than 5.5 pH, resulted in a decrease in fluorescence intensity. Furthermore, Liu *et al*., (2015), investigated QD stability in three biological buffers namely, ddH_20, non-supplemented and supplemented DMEM (to simulate an environment where QDs interact in the bloodstream with the possibility of protein absorption and inevitable agglomeration thereof), at both room temperature and 37°C, over 72 hours at 1-hour time intervals. PL peaks were monitored to evaluate the colloidal stability of four QD formulations and revealed a decrease thereof in the DMEM in comparison to the distilled water, suggesting that accountable factors such a pH, ions and oxygen, overall contribute to defects at the QD surface and subsequent decrease/quenching of PL. Additionally, fluorescence stability of CdTe QDs embedded in Gelatin, synthesized by Wang et al., (2008), were reported to be stable for at least 15 days in milieus such as PBS (pH 7.4) and water. We are therefore aware of the potential factors which affect the stability of MPA-capped CdTe/ZnS QDs, as reported in literature, and these particles are known to be highly stable to withstand the various experimental milieus.

5.2.6 Summary for Physical Characterization

In summary, data deduced from the physical characterization techniques, yielded anionic red emitting MPA-capped CdTe/ZnS QDs, with an affirmed emission of 670nm within therespective CdTe QD spectra range. The size distribution was near monodispersed, revealing size measurements between 3.66nm up to 5.909nm, with a strong ζ-potential, robust stability, and no agglomeration, as possibly suggested by its median PdI values. The objective of synthesizing and characterizing relatively monodispersed and highly luminescent MPA-capped CdTe/ZnS QDs, was therefore satisfactorily met and allowed for further biological evaluation of the biological activity of these nanoparticles.

5.3 Biological Characterization

5.3.1 Fluorescence Confocal Microscopy

The purpose of fluorescence confocal microscopy was to investigate the uptake and an indicative

localization of the MPA-capped CdTe/ZnS QDs, expected in the red emission spectra. The results revealed highly luminated MPA-capped CdTe/ZnS QD uptake in the nuclei of both cell lines.

Lovric *et al*., (2005), investigated the subcellular localization and cytotoxicity of CdTe-QDs and reported that QD size has significant effect on these two factors. Green QDs were synthesized with an emission of λ 530nm, in addition to longer wavelength red emitting QDs of λ 630nm, whereby, the green emitting QDs were taken up into the nuclei in contrast to the red emitting QDs being present in the cytoplasm, which furthermore, caused chromatin condensation, nuclear membrane blebbing and a rounded cell morphology at higher concentrations of the CdTe-QD suggestive of cytotoxicity. Literature has described that the induction of ROS and organelle damage may be accounted for by the subcellular distribution and internalization of QDs, therefore, Choi *et al*., (2007), investigated the lipid peroxidation thereof via spectrophotometric and confocal analysis, observing a significant shift toward oxidation and moreover, when combined with BODIPY-C_{11} dye and Mitotracker Deep Red 633, discovering lipid peroxidation exuded by the mitochondrial membranes. Their study however, entailed the synthesis of both cysteamine-capped CdTe-QDs in addition to NAC modified cysteamine-capped CdTe-QDs, with the latter causing mitigation of the lipid peroxidation effects, as earlier mentioned.

In the aforementioned study by Choi *et al*., (2007), cell death was reported in surface functionalized cysteamine-capped CdTe-QDs exposed in SH-SY5Y cells and further validated by FACS analysis, which displayed both apoptotic and necrotic cell death, alongside mitochondrial and lysosomal swelling, and perinuclear localization of the organelles. Furthermore, the FACS analysis of their study revealed the upregulation of FAS expression, suggestive of QD-mediated oxidative stress induced cytotoxicity. In another study, confocal analysis revealed that increased fluorescent intensities were concentration-dependent of the QDs655-Tf in the U87 cell line, which coincides with the concentration-dependent intensities shown in this study, moreover, their work revealed a QDs655-Tf labelling efficiency of 99.8% showing successful targeting of U87 cells, without significant cytotoxicity (Yukawa *et al*., 2013).

Whilst MPA-capped CdTe/ZnS QD uptake and localization is reported within the nuclei of both cell lines in this study, no evident nuclear membrane blebbing was seen, as confirmed by clear observations using images from the fluorescent LSM 780 Confocal Microscope (Carl Zeiss, Germany). Despite the relatively small image provided in Figure 4.91 and 4.9.2, rounded cell morphology with grape-like clusters was observed in both cell lines but more prominent in the U87

cell line which had lower cell viability. However, since the morphological changes are evident in both cell lines, it thus cannot be directly correlated with nanotoxicity. The uptake and nuclear localization, along with the observed morphological features, are evident in both cell lines, regardless of the disparate cell viability effects.

5.3.2 WST-1 Colorimetric cell viability assay

The WST 1 colorimetric cell proliferation agent was employed for cell viability which monitored the metabolic activity of cells. Treatment with the MPA-capped CdTe/ZnS QDs was cell line-specific as there was an increase in cell viability in the NB SH-SY5Y cell line, and a decline in cell viability in the GB U87 cell line. Given the disparate effect, both cell lines are most impacted at 48 hours, while 72 hours shows a lesser but prominent effect. The noticeable effect of a decline in cell viability caused by Cd QDs exposure is well documented in many different cell lines including HEK293 cells, SH-SY5Y and U87 cells in literature (Su *et al*., 2010; Steponkiene *et al*., 2011; Kim *et al*., 2012). Studies on the cytotoxic effects of QDs on CNS cancers are relatively few in literature and QD cytotoxicity appears to generally depend on a number of factors, including surface functionalization (e.g. a ZnS shell, PEG-coating, etc), duration of exposure, dosage, etc. In one study, CdTe QDs were reported to induce dose- and time- dependent apoptotic effects in NG108-15 murine neuroblastoma and human hepatocellular carcinoma cells (Jan *et al*. 2008), which conforms to the findings from this study. The MPA- capped CdTe/ZnS QD toxicity exerted upon the U87 cell line in this study, is synonymous with the reports of Kim *et al*., (2012) in which CdSe/ZnS QDs were exposed to neural cell lines as well as Steponkiene *et al*., (2011) in which MPA-capped CdTe QDs were exposed to four cancer cell lines including a GB cell line, resulting in a decrease in a cell viability.

Unlike the concentration-dependent increase in viability observed in the SH-SY5Y cells in this study especially following 48-hour exposure, Choi *et al*., (2007), observed a significant reduction in SH-SY5Y cell viability following exposure to cysteamine-capped CdTe-QDs via the MTT assay, which was corroborated with FACS data analysis. Liu *et al*., (2015) reported dissimilar cellular uptake of the QDs, showing differences in the cytotoxicity and tends to support the hypothesis that each type of QD formulation will react differently in the same cell type, potentially accounting for the incongruous increase in cell viability observed in this study compared to the decreased viability reported by Choi *et al*., (2007) in their study with CdTe-QD void of a ZnS shell. Similarly,

Havrdova *et al*., (2016) exposed three different cQDs with altered surface functionalizations to the same mouse fibroblast NIH/3T3 cell line and observed a decrease in cell viability in all treatments except the pristine-formulated cQDs which showed an initial marked increase in cell viability, which later decreased with increasing concentration. Given the consequential QD formulation effect, along with surface modifications, a study by Lovric *et al*., (2005), showed significant toxicity effects at high concentrations of CdTe-QDs exposed in PC12 cells for upwards of 24 hours, with enhanced toxicity displayed in smaller green-emitting CdTe-QDs, in contrast to the red emitting CdTe-QDs.

However, when PC12 cells were treated with both conjugated and non-conjugated BSA in anionic CdTe QDs, protective effects were reported with pronounced protection in the conjugated form. Additionally, studies on conjugated and non-conjugated NAC CdTe-QDs have shown mitigated toxicity effects in the presence of free NAC and to a lesser extent in the conjugated form (Lovric *et al*, 2005; Choi *et al*, 2007). Thus, the physicochemical properties of various surface-modified ZnS-coated CdSe QDs characterized by ζ- potential, fluorescence intensities and HD, will allow for accurate determination and reporting of cytotoxic dependency on surface-covering molecules (Hoshino *et al*., 2004).

More recent studies revealed that no single factor is responsible for the cytotoxic effects of QDs in biological environments, but rather a combination of constituent elements in the particle formulations majorly core composition, particle surface charge, surface coating, HD of the QDs and the concentration ingested by cells (Su *et al*., 2010; Liu *et al*., 2015). A study by Liu *et al.,* (2013) reported alleviation of CdTe/ZnS (core-shell) cytotoxicity opposed to the naked CdTe formulations and showed that positively-charged QDs possess higher toxicities than negatively-charged ones, supporting our findings on the anionic MPA-capped CdTe/ZnS QDs synthesized in this study. These reports ultimately correlate with the disparate effects observed in this study with the U87 and SH-SY5Y cell lines, and possibly account for the cytotoxic effects observed by Choi and co-workers in SH-SY5Y cells exposed to cationic cysteamine- capped CdTe-QDs opposed to the increase in viability shown in this study by a different formulated anionic MPA-capped CdTe/ZnS QDs.

5.3.3 Cell Morphology

Morphological changes were observed using the Primovert inverted microscope (Carl Zeiss, Germany), which revealed variation in the morphology of cells exposed to the MPA-capped CdTe/ZnS QDs. The cell morphology converted to a rounded cell shape with grape-like clusters forming on the cells and was evident in both cell lines in comparison to the untreated control. The noticeable rounding of cells was more predominant in the U87 cell line which eventually lifted from the cell culture plate at 48 hours. The pronounced rounding and dislodging of cells in the U87 cell line, possibly correlates with the decreased metabolic activity, evident in the WST-1 colorimetric cell viability assay, whereby U87 cells, resulted in a decline in percentage cell viability, which was most pronounced at 48 hours, with a lesser but prominent decline at 72 hours. However, the marked cell rounding and dislodgment of the GB U87 cells, cannot be directly correlated with cytotoxicity and concomitant cell death, since similar morphological changes were observed in the NB SH-SY5Y cells. Additionally, no single attributing factor may account for the cytotoxicity exerted by QDs in biological environments.

The observed decline in U87 cell viability is congruent with previous findings in literature and seems to be a cytotoxic trend in numerous cell lines as mentioned in the section 5.3.1. On the other hand, surface modification and change in QD formulation yielding such products as QDs655-Tf, Pegylated CdSe/ZnS QDs and Aptamer-labelled QDs, resulted in little to no significant cytotoxicity in U87 cells as reported in literature, with optimal biocompatibility exhibited in the aptamer labelled QD (Yukawa *et al*., 2013; Tang *et al*., 2017).

Earlier studies have described morphological changes such as chromatin condensation, nuclear membrane blebbing and rounded SH-SY5Y morphology exerted by red-emitting CdTe-QDs (Lovric *et al*., 2005). In another report, CdTe QDs caused cell wall breakage and cytoplasm blebbing in exposed yeast *(Saccharomyces cerevisiae)* cells (Han *et al*., 2012). Additionally, studies have shown that Cd^{2+} exposure alone caused cell shrinkage and rounding, but when encompassed in the formulated QD, resulted in mitigation of cytotoxicity with no obvious morphological changes, while the application of the ZnS shell offered protective reduction in toxicity (Peng *et al*., 2013; Tang *et al*., 2017). These reports along with the data retrieved in this study tend to suggest that the effects of QD are dependent on the QD formulation and the degree of receptor expression on cells in the case of the targeted QD study. The morphological changes observed in this study were cell line-specific, time and concentration-dependent.

5.3.4 Cell Cycle Analysis- FxCycle PI/RNase staining solution

The FxCycle PI/RNase staining solution was employed for cell cycle analysis utilizing the C6 flow cytometer (BD Accuri, USA). Cell cycle distributions are displayed in a frequency histogram as population percentages amongst the three major stages of the cell cycle: G_0/G_1 phase – a singular pair of chromosomes, doubling of cell organelles, S phase - DNA synthesis/replication with fluctuating amounts of DNA and the G_2/M phase - (two phases with undistinguishable identical DNA content) entail the completion of DNA replication possessing two sets of paired chromosomes, to the onset of mitosis - a cell division process comprised of mitosis and cytokinesis into a resultant 2 daughter cell division (Nunez, 2001; Mader, 2004).

The histograms and their corresponding distribution percentages of the cell populations are representative of 20 µg/ml MPA-capped CdTe/ZnS QD exposure in U87 and SH-SY5Y cells in comparison to the untreated cells at 24 and 48 hours (while the 72-hour time frame, was omitted due to cell dislodgement as previously mentioned). In the U87 cell line, the highest percentage of cell count occupancy for both the treated and untreated cells was found in the G_0/G_1 phase with amounts from 58% and above proposing its arrest in the G_0/G_1 phase, where cell growth has occurred in G_1 or the latter inhibition of growth or apoptotic death in G_0, in contrast to the S phase and G_2/M phase, which represented fairly low and similar cell counts between the two (Hsieh *et al*., 2006). Similarly, the histograms and corresponding distribution percentages of SH-SY5Y cells, also revealed a high percentage of cell count occupancy in the G_0/G_1 phase displayed in both untreated and MPA-capped CdTe/ZnS QD treated cell lines, however, an increased G_2/M phase cell count was observed here taking into consideration the corresponding distribution percentages, compared to the U87 cells, thus revealing a higher population passing the cell cycle check point into the S and G_2/M phases, which furthermore correlates with the observed increase in cell viability of MPA-capped CdTe/ZnS QDs exposed in SH-SY5Y cells, yielded in the WST-1 colorimetric cell viability assay. Literature has stated, that the absence of a ZnS shell in both cationic and anionic QDs has led to "multipolar spindles, misaligned chromosomes, and G2/M checkpoint failures" (Liu *et al*., 2013).

Similarly, Hsieh *et al*., (2006) have utilized CdSe/ZnS QDs to tag human bone marrow mesenchymal stem cells (hBMSCs), revealing no substantial variances in the viability of cells, nor the cell cycle distributions thereof, as the CdSe/ZnS QD exposed and control samples showed similar cell cycle populations distributed amongst the G_0/G_1, S and G_2/M phases, with the highest

percentages found in the G_0/G_1 phase followed by the G_2/M phase. These cell cycle distribution percentages are synonymous with those reported in this study. To further support our findings, a comparable study by Al-Ali *et al*., (2015), reported no significant changes in the cell cycle dynamics of various CdSe/ZnS QD formulations exposed to THP-1 cells and that of the control treatment. Once again, the highest cell count occupancy was found in the G_0/G_1 phase followed by the G_2/M phase, as reported in this study. However, although Al-Ali and co-workers report no variation in cell cycle dynamics, they discovered that the QDs were able to induce an acute inflammatory response and alterations to transcriptional gene activity. Furthermore, a cytotoxic and cell cycle study by Havrdova *et al.,* (2016) report that surface charge plays a key factor in the significant toxicities observed by CQDs, synthesized with various surface functionalizations exposed to the mouse fibroblast (NIH/3T3) cell line. This tends to suggest that the addition of polymers could account for G_0/G_1 cell arrest, and variable factors such as cell morphology, toxicity, along with CQD location and entry to the nucleus, all differed with the various QD surface functionalizations in the same cell line.

5.3.5 Summary of Biological Characterization

Successful synthesis of MPA-capped CdTe/ZnS QDs allowed for the biological evaluation of the QDs in SH-SY5Y and U87 cell lines. The biological characterization techniques employed included confocal fluorescence microscopy, a cell viability assay, cell morphology evaluation and cell cycle analysis. Data obtained showed a cell line-specific viability effect as there was an increase in SH-SY5Y viability and a decrease in U87 viability. The cell rounding morphology and the formation of grape-like clusters appeared to be more pronounced in the observed decline in GB U87 cell viability but cannot be directly correlated with nanotoxicity considering that similar morphological changes were also seen in the SH-SY5Y cell line. When viewed under confocal fluorescence microscopy, no evidence of membrane blebbing or chromatin condensation was seen as reported by previous studies, possibly due to the protective ZnS shell and MPA stabilizer effects. Furthermore, confocal fluorescence microscopy allowed for the evaluation of the localization and uptake of the MPA-capped CdTe/ZnS QDs, which showed a distinct nuclear localization and concentration-dependent emission intensities.

Cell cycle evaluation showed no significant variances in the cell cycle distribution among both cell lines, as the majority of cells were arrested in the G_0/G_1 phase, either in the growth phase or

retracted in apoptotic death. The second highest cell population was reported in the G_2/M phase by SH-SY5Y cells, with the G_2/M phase lagging slightly behind the S phase in U87 cells, displaying no marked differences among the treated and control cell lines. The observed increase in SH-SY5Y cell viability, could be associated with the higher populations of these cells observed in the G_2/M phase, opposed to the lowered populations and decline in U87 viability at this phase.

5.4 Limitations of study

As the emphasis of this research was the practical implementation of the taught component of the MSc Nanoscience programme in the form of synthesis of nanoparticles leading to a mini- thesis, only a limited number of experiments were required for the preliminary evaluation of the biological effects of the synthesized MPA-capped CdTe/ZnS QD nanoparticles. Thus, time constraint imposed the following limitations to the current study:

1. Pure Cd was not exposed to cells for comparative toxicity studies
2. Photoluminescent quantum yield (PLQY) measurements of QDs in various milieus could have served as an extended stability study
3. The lack of a non-cancerous cell line as control to determine the safety of QDs to normal (non-cancerous) cells
4. Absence of experiments demonstrating the effects of a known cancer treatment drug as pharmacological control to determine the relative efficacy of QDs.
5. Lack of biological evaluation of cell morphology and cell cycle analysis at a 72- hour exposure time frame, due to cell dislodgement.
6. Possible negative impact of the filtration stage of the QD formulation process

5.5 Conclusion and Future Recommendations

The aim of the study was to synthesize highly luminescent MPA-capped CdTe/ZnS QDs and to evaluate the biological activity of these NPs using two neuronal cancer cell lines namely, U87 and SH-SY5Y cells. The synthesis of these QDs was satisfactorily achieved, producing anionic, fairly monodispersed and highly luminescent red-emitting MPA-capped CdTe/ZnS QDs, which were also highly stable.

When exposed to the cell lines, considerable uptake and localization was observed in the nuclei of

cells, with noticeable morphological changes in cell shape, void of membrane blebbing. The most significant variety of observations seen were in the biological characterization, as cell viability increased in SH-SY5Y neuroblastoma cells but decreased in U87 glioblastoma cells. The decrease in cell viability seems to be a common trend in the reviewed literature as various cell lines were reported to show lower viability and higher toxicity when exposed to especially positively charged CdTe QDs.

Great emphasis is placed on the methodology for QD formulation, surface functionalization and charge, which dictate the effects exerted on cell lines to which these NPs are exposed. Thus, active targeting of cell lines and omission of non-specific binding could circumvent the possible associated toxicities, non-targeted delivery and other shortfalls observed in this study. To address these shortfalls, it is therefore imperative to further functionalize the surfaces of the MPA-capped CdTe/ZnS QDs while maintaining their integral small size, as many studies have conjugated aptamers/ligands for specific targeting to the overly expressed receptors on the cancer cell lines and shown magnificent uptake of the modified QD in contrast to the standard QD.

Once an efficient surface functionalization is established and the biocompatibility of the QDs is evaluated both *in vitro* and *in vivo*, the limitations associated with research involving treatment with QDs could be addressed. Although QDs are promising for use in nanomedicine due to their diverse applications, extensive *in vivo* research needs to be carried out on the pharmacokinetics of QDs and potential cytotoxic or genotoxic effects.

Future studies could explore the following aspects that will help elucidate the potential use of QDs as anti-cancer agents:

1. Surface functionalization of QDs for targeted delivery
2. Inclusion of an additional cell viability assay such as trypan blue exclusion assay to confirm observed cell viability studies with WST-1.
3. Investigation of possible inflammatory and oxidative stress responses following QD treatment
4. Investigation of the migration/invasion parameters which may have accounted for the observed morphological changes.

5. Investigation of apoptotic changes in the dislodged cell populations using standard assays as well as cell cycle analysis.

REFERENCES

1. Ahmed, N., Bhurgri, Y., Sadiq, S and Shakoor, K.A. (2007) "Pediatric brain tumours in karachi". *Asian Pacific Journal of Cancer Prevention*. 8: 399-404.

2. Al-Ali, A., Singh, N., Manshian, B., Wilkinson, T., Wills, J., Jenkinsa, G.J.S. and Doak, S.H. (2015) "Quantum dot induced cellular perturbations involving varying toxicity pathways". *Toxicology Research*. 4: 623-633.

3. Alexis, F., Rhee, J-W., Richie, J.P., Radovic-Moreno, A.F., Langer, R. and Farokhzad, O.C. (2008) "New frontiers in nanotechnology for cancer treatment". *Seminars and Original Investigations*. 26: 74-85.

4. Alibolandi, M., Abnous, K., Ramezani, M., Hosseinkhani, H. and Hadizadeh, F. (2014) "Synthesis of AS1411-aptamer-conjugated CdTe quantum dots with high fluorescence strength for probe labeling tumour Cells". *Journal of Fluoresc*ence 24:1519–1529.

5. Aliosmanoglu, A and Basaran, I. (2012) "Nanotechnology in Cancer Treatment". *Nanomedicine and Biotherapeutic Medicine*. 2: (4).

6. Alvarez-Barrientos, A., Arroya, J., Canton, R., Nombela, C. and Sanchez-Perez, M. (2000) "Applications of Flow Cytometry to Clinical Microbiology". *American Society for Microbiology*. 13 (2) 167-195.

7. Alvarez, J.I., Cayrol, R. and Prat, A. (2011) "Disruption of the central nervous system barriers in multiple sclerosis". *Biochemica et Biophysica Acta* 1812: 252-264.

8. Ashkenazi, R., Gentry, S.N. and Jackson, T.L. (2008) "Pathways to Tumorigenesis-Modelling Mutation Acquisition in Stem Cells and Their Progeny". *Neoplasia*. 10: 1170-1182.

9. Bakalova, R., Zhelev, Z., Kokuryo, D., Spasov, L., Aoki, I. and Saga, T. (2011) "Chemical nature and structure of organic coating of quantum dots is crucial for their application in imaging diagnostics". *International Journal of Nanomedicine*. 6: 1719-1732.

10. Balani, S., Nguyen, L.V. and Eaves, C.J. (2017) "Modeling the process of human tumorigenesis". *Nature Communications* 1-10.

11. Barron, A.R. (2013) "Physical Methods in Chemistry and Nano Science". Houston, Texas. Rice University. [Online] Available: http: cnx.org/content/col10699/1.16/

12. Begley, D.J. (1996) "The Blood-brain Barrier: Principles for Targeting Peptides and Drugs to the Central Nervous System". *Journal of Pharmacy and Pharmacology*. 48: 136-146.

13. Bentzen, E.L., Tomlinson, I.D., Mason, J., Gresch, P., Warnement, M.R., Wright, D., Sanders-Bush, E., Blakely, R., and Rosenthal, S.J. (2006) "Surface Modification to Reduce Nonspecific Binding of Quantum Dots in Live Cell Assays". *Bioconjugate Chemistry*. 16: 1488-1494.

14. Brem, S.S., Bierman, P.J., Brem, H., Butowski, N., Chamberlain, M.C, Chiocca, E.A, DeAngelis, L.M., Fenstermaker, R.A., Friedman, A., Gilbert, M.R., Hesser, D., Junck, L., Linette, G.P, Loeffler, J.S, Maor, M.H., Michael, M., Moots, P.L., Morrison, T., Mrugala, M., Nabors, L.B., Newton, H.B, Portnow, J., Raizer, J.J., Recht, L., Shrieve, D.C., Sills, A.K., Jr, Vrionis, F.D. and Wen, P.Y. (2008) "Clinical Practice Guidelines in Oncology". *Journal of the National Comprehensive Cancer Network*. 9 (4) 352-400.

15. Bruchez, M. Jr., Moronne, M., Gin, P., Weiss, S. and Alivisatos, A.P. (1998) "Semiconductor nanocrystals as fluorescent biological labels". *Science*. 281 (5385): 2013-2016.

16. Califiano, A. and Alvarez, M.J. (2017) "Recurrent architecture of tumour initiation,

progression and drug sensitivity". *Nature Reviws Cancer.* 17 (2) 116-130.

17. Cao, Y. (2017) "Tumorigenesis as a process of gradual loss of original cell identity and gain of properties of neural precursor/progenitor cells". *Cell Bioscience* 7 (61) 1-14.

18. Carlson, K., Jortner, B.S. and Ehrich, M. (2000) "Organophosphorus Compound-Induced Apoptosis in SH-SY5Y Human Neuroblastoma Cells". *Toxicology and Applied Pharmacology*. 168: 102-113.

19. Carmeliet, P. and Jain, R.K. (2000) "Angiogenesis in cancer and other diseases". *Nature*. 407: 249-257.

20. Castro-Obregon, S. (2010) "The discovery of lysosomes and autophagy". *Nature Education*. 3(9)49-52.

21. Chaffer, C.L. and Weinberg, R.A. (2015) "How does multistep tumourigenesis really proceed". *Cancer Discovery*. 5 (1) 22-24.

22. Chamoucka, J., Drbohlavov, J., Majzlikova, P., Prasek, J., Pekarek, J., Hrdy, R. and Hubalek, J. (2013) "Conjugation bovine serum albumin with CdTe quantum dots''. *Nanocon*. 16 (18) 1-6.

23. Chan, W.C.W., Maxwell, D.J., Gao, X., Bailey, R.E., Han, M. and Nie, S. (2002) "Luminescent quantum dots for multiplexed biological detection". *Current Opinion in Biotechnology*. 13: 40-46.

24. Chan, W.C.W. and Nie, S. (1998) "Quantum dot bioconjugated for ultrasensitive nonisotopic detection". *Science*. 281 (5385): 2016-2018.

25. Choi, A.O., Cho, S.J., Desbarats, J., Lovric, J. and Maysinger, D. (2007a) "Quantum dot-induced cell death involves Fas upregulation and lipid peroxidation in human neuroblastoma cells". *Journal of Nanobiotechnology* 5:1.

26. Choi, H.S., Liu, W., Misra, P., Tanaka, E., Zimmer, J.P., Ipe, B.I., Bawendi, M.G. and

Frangioni, J.V. (2007b) “Renal clearance of nanoparticles”. *Natural Biotechnology*. 25 (10): 1165-1170.

27. Cipolla, M.J. (2009) “*The Cerebral Circulation*”. Morgan and Claypool Lifesciences. “*Chapter 6: Barriers of the CNS*”. San Rafael, California. [Online] Available: https://www.ncbi.nlm.nih.gov/books/NBK53084/

28. Clapp, A.R., Goldman, E.R. and Mattoussi, H. (2006) “Capping of CdSe-ZnS quantum dots with DHLA and subsequent conjugation with proteins”. *Nature Protocols*. 1 (3): 1258-1267.

29. Clogston, J.D. and Patri, A.K. (2011) “Characterization of nanoparticles intended for drug delivery”. *Zeta Potential Measurement*. 63-70.

30. Conter, H.J., Gopalakrishnan, V., Ravi, V., Ater, J.L., Patel, S. and Araujo, D.M. (2014) “Adult versus pediatric neuroblastoma: The M.D. Anderson cancer centre experience”. *Sarcoma*. Article ID 375151: 1-6.

31. Davis, M.E. (2016) “Glioblastoma: overview of disease and treatment”. *Clinical Journal Oncology Nursing.* 20 (5): S2-8.

32. Donado, F., Moctezuma, R.E., López-Flores, L., Medina-Noyola, M. and Arauz-Lara, J.L. (2017) “Brownian motion in nonequilibrium systems and the Ornstein-Uhlenbeck stochastic process”. *Scientific Reports* 7: 12614.

33. Duan, J., Song, L. and Zhan, J. (2009) “One-pot synthesis of highly luminescent CdTe quantum dots by microwave irradiation reduction and their Hg_{2+}-sensitive properties”. *Nano Research*. 2: 61-68.

34. Dumba, M., Jawad, N and McHugh, K. (2014) “Neuroblastoma and nephroblastoma: an overview and comparison”. *Cancer Imaging*. 14 (Suppl 1) O15: 1-2.

35. Faria, A., Meireles, M., Fernandes, I., Santos-Buelga, C., Gonzalez-Manzano, S., Duenas, M., de Freitas, V. and Mateus, N. (2014) “Flavonoid metabolites transport across a human

BBB model". *Food Chemistry*. 149: 190-196.

36. Fink, S.L. and Cookson, B.T. (2005) "Apoptosis, pyroptosis and necrosis: mechanistic description of dead and dying eukaryotic cells". *Infection and Immunity*. 73 (4) 1907- 1916.

37. Galli, R., Binda, E., Orfanelli, U., Cipelleti, B., Gritti, A., De Vitas, S., Fiocco, R., Foroni, C., Dimeco, F. and Vescovil, A. (2004) "Isolation and characterization of tumorigenic, stem-like neural precursors from human glioblastoma". *Cancer Research*. 64:7011- 7021.

38. Galuzzi, L. and Vitale, I. (2018) "Molecular mechanisms of cell death: recommendations of the nomenclature committee on cell death 2018". *Cell Death and Differentiation*. 25: 486-541.

39. Ganong, W.F. (2000) "Circumventricular organs: definition and role in the regulation of endocrine and autonomic function". *Clinical and Experimental Pharmacology and Physiology*. 27: 5-6, 422-427.

40. Gaumet, M., Vargus, A., Gurny, R. and Delie, F. (2007) "Nanoparticles for drug delivery: The need for precision in reporting particle size parameters". *European Journal of Pharmaceutics and Biopharmaceutics* 69: 1-9.

41. Ghobrial, I.M., Witzig, T.E. and Adjei, A.A. (2005) "Targeting apoptosis pathways in cancer therapy". *A Cancer Journal for Clinicians*. 55: 178-194.

42. Gilany, K., Elzen, R.V., Mous, K., Coen, E., Van Dongen, W., Vandamme, S., Gevaert, K., Timmerman, E., Vandekerckhove, J., Dewilde, S., Van Ostade, X. and Moens, L. (2008) "The proteome of the human neuroblastoma cell line SH-SY5Y: an enlarged proteome". *Bochemica et Biophysica Acta* 1784: 983-985.

43. Gomez-Santos, C., Ferrer, I., Santidria, A.F., Barrachina, M., Gil, J. and Ambrosio, S. (2003) "Dopamine induces autophagic cell death and_-synuclein increase in human neuroblastoma SH-SY5Y Cells". *Journal of Neuroscience Research*. 73: 341-350.

44. Green, D.R. (1998) "Apoptotic pathways: minireview the roads to ruin". *Cell*. 94:695- 698.

45. Guillery, R.W. (2005) “Observations of synaptic structures: origins of the neuron doctrine and its current status”. *Philosophical Transactions of the Royal Society B*. 360: 1281-1307.

46. Haley, B. and Frenkel, E. (2008) “Nanoparticles for drug delivery in cancer treatment”. Urologic Oncology: *Seminars and Original Investigations*. 26: 57-64.

47. Han, X., Lai, L., Tian, F., Jiang, F-L., Xiao, Q., Li, Y., Yu, Q., Li, D., Wang, J., Zhang, Q., Zhu, B., Li, R. and Liu, Y. (2012) “Toxicity of CdTe quantum Dots on Yeast *Saccharomyces Cerevisiae”. Epub* 10;8 (17)*:* 2680-2689.

48. Han, J., Jun, Y., Kim, S.H., Hoang, H.H., Jung, Y., Kim, S., Kim, J., Austin, R.H., Lee, S. and Park, S. (2016) “Rapid emergence and mechanisms of resistance by U87 glioblastoma cells to doxorubicin in an in vitro tumour microfluidic ecology”. *Proceedings of the national academy of sciences of the united states of America*. 50:14283-14288.

49. Hanson, L.R. and Frey, W.H. (2008) “Intranasal delivery bypasses the blood-brain barrier to target therapeutic agents to the central nervous system and treat neurodegenerative disease”. *BMC Neuroscience*. 9 (Suppl 3): S5.

50. Havrdova, M., Hola, K., Skopalik, J., Tomankova, K., Petr, M., Cepe, K., Polakova, K., Tucek, J., Bourlinos, A.B. and Zboril, R. (2016) “Toxicity of carbon dots e Effect of surface functionalization on the cell viability, reactive oxygen species generation and cell cycle”. *Carbon* 99: 238-248.

51. He, Y., Lu, H-T., Sai, L-M., Su, Y-Y, Hu, M., Fan, C-H., Huang, W. and Wang, L-H. (2008) “Microwave synthesis of water-dispersed CdTe/CdS/ZnS core-shell-shell quantum dots with excellent photostability and biocompatibility”. *Advanced Materials*

20: 3416-3421.

52. He, Q., Liu, J., Xiaopeng, L., Li, W., Liu, Z., Ding, Z. and Tuo, D. (2018) “Towards improvements for penetrating the blood-brain-barrier- recent progress from a material and pharmaceutical perspective”. *Cells*. 7 (24) 1-21.

53. Heiman, D. (2004) “Photoluminescence spectroscopy”. *Physics U600, Adv Lab I-Physics*

of Waves and Optics. Northern University.

54. Heine, P., Ehrlicher, A. and Käs, J. (2015). "Neuronal and metastatic cancer cells: Unlike brothers". *Biochemica et Biophysica Acta* 1853: 3126-3131.

55. Hines, M.A. and Guyot-Sionnest, P. (1996) "Synthesis and characterization of strongly luminescing ZnS-capped CdSe nanocrystals". *The Journal of Physical Chemistry*. 100 (2): 468-471.

56. Hirose, Y., Berger, M.S. and Pieper, R.O. (2001) "p53 Effects both the duration of G_2/M arrest and the fate of temozolomide-treated human glioblastoma cells". *Cancer Research*. 61:1957-1963.

57. Hongmei, Z. and Ntuli, T.M. 2012, *Apoptosis and medicine Chapter 1: Extrinsic and Intrinsic Apoptosis Signal Pathway Review,* InTech Publishers [Online] Available: Apoptosis and Medicine

58. Hoshino, A., Fujioka, K., Oku, T., Suga, M., Sasaki, Y.F., Ohta, T., Yasuhara, M., Suzuki, K. and Yamamoto, K. (2004) "Physicochemical properties and cellular toxicity of nanocrystal quantum dots depend on their surface modification". *Nano Letters* 4,11: 2163-2169.

59. Hsieh, S-C., Wang, F-F., Lina, C-S., Chena, Y-J., Hung S-C. and Wang, Y-J. (2006)"The inhibition of osteogenesis with human bone marrow mesenchymal stem cells by CdSe/ZnS quantum dot labels". *Biomaterials* 27: 1656–1664.

60. Jan, E., Byrne S.J., Cuddihy, M., Davies, A.M., Volkov, Y., Gunko, Y.K., Kotov, N.A. (2008) "High-content screening as a universal tool for fingerprinting of cytotoxicity of nanoparticles". *American Chemical Society Nano.* 2: 928–938

54. Jiang, Y., Marinescu, V.D., Xie, Y., Jarvius, M., Maturi, N.P., Haglund, C., Olofsson, S., Lindberg, N., Olofsson, T., Leijonmarck, C., Hesselager, G., Alafuzoff, I., Frykna, M., Larsson, R., Nelander, S. and Urhbom, L. (2017) "Glioblastoma cell malignancy and drug sensitivity are affected by the cell of origin". *Cell Reports*. 18: 977-990.

55. Juzenas, P., Chen, W., Sun, Y., Coelho, M.A.N., Generalov, R., Generalova, N. and Christensen, I.L. (2008) "Quantum dots and nanoparticles for photodynamic and radiation therapies of cancer". *Advanced Drug Delivery Reviews* 60: 1600-1614.

56. Kim, B.M. (2017) "The implications of several forms of programmed necrosis for cancer therapy". *Journal of cancer science and therapy*. 9 (9) 630-635.

57. Kim, T-H., El-Said, W.A. and Choi, J.W. (2012) "Highly sensitive electrochemical detection of potential cytotoxicity of CdSe/ZnS quantum dots using neural cell chip". *Biosensors and Bioelectronics.* 32: 266– 272.

58. Kim, J., Hui, B.T., Sakthivel, K., Choi, H.J., Joo, W.H., Shin, S.K., Lee, M.J. and Y-I. Lee. (2015) "Highly fluorescent CdTe quantum dots with reduced cytotoxicity-A robust biomarker". *Sensing and Bio-Sensing Research.* 3: 46-52.

59. Kipligat, A., Onani, M.O., Meyer, M., Akenga, T.A. and Dejene, F.B. (2016). "Synthesis and characterization of luminescence magnetic composite". *Physica B*. 480: 147-155.

60. Kipnis, J and Filiano, A.J. (2017) "Neuroimmunology in 2017: The central nervous system: privileged by immune connections ". *Nature Reviews*. 18: 2.

61. Kirchner, A., Liedlm, T., Kudera, S., Pelegrino, T., Mun oz Havier, A., Gaub, H.E., Stolzle, S., Fertig, N. and Parak, W.J. (2005) "Cytotoxicity of colloidal CdSe and CdSe/ZnS nanoparticles". *Nano Letters*. 5 (2) 331-338.

62. Kovalevich, J. and Langford, D. (2013) "Considerations for the use of SH-SY5Y neuroblastoma cells in neurobiology". *Methods in Molecular Biology*. 1078: 9-21.

63. Li, H., He, X., Kang, Z., Huang, H., Liu, Y., Liu, J., Lian, S., Tsang, C.H.A., Yang, X. and Lee, S.T. (2010) "Water-soluble fluorescent carbon quantum dots and photocatalyst design". *Angewandte Chemie International Edition*. 49: 4430-4434.

64. Liu, J., Hu, R., Liu, J., Zhang, B., Wang, Y., Liu, X., Law, W-C., Liu, L., Ye, L. and Yong, K-

T. (2015) “Cytotoxicity assessment of functionalized CdSe, CdTe and InP quantum dots in two human cancer cell models”. *Materials Science and Engineering* C57: 222-231.

65. Liu, Y., Wang, P., Wang, Y., Zhu, Z., Lao, F., Liu, X., Cong, W., Chen, C., Gao, Y. and Liu, Y. (2013) “The influence on cell cycle and cell civision by various cadmium- containing quantum dots”. *Special Issue: National Centre for Nanoscience and Technology of China.* Volume 9, Issue 14: 2440-2451.

66. Lovric, J., Bazzi, H.S., Cuie, Y., Fortin, G.R.A., Winnik, F.M. and Maysinger, D. (2005) “Differences in subcellular distribution and toxicity of green and red emitting CdTe quantum dots”. *Molecular Medicine.* 83: 377-385.

67. Lu Peng, L., He, M., Chen, B., Wu, O., Zhang, Z., Pang, D., Zhu, Y. and Hu, B. (2013) “Cellular uptake, elimination and toxicity of CdSe/ZnS quantum dots in HepG2 cells”. *Biomaterials* 34: 9545-9558.

68. Mader, S.S. (2004) “Biology, Eighth Edition”. McGraw-Hill (ed). “The cell cycle and cellular production”. *New York*: 148-166.

69. Martini, F.H. (2006) “*Fundamentals of Anatomy and Physiology- Seventh Edition*”. Pearson Education. San Francisco. “Chapter 12: Neural Tissue”. 379-420.

70. Mattoussi, H., Palui, G. and Na, H.B. (2011) “Luminescent quantum dots as platforms for probing in vitro and in vivo biological processes”. *Advanced Drug Delivery Reviews* 64: 139-166.

71. McCorry, L.K. (2007) “Physiology of the autonomic nervous system”. *American Journal of Pharmaceutical Education*. 71 (4) Article 78: 1-11.

72. Medintz, I.L., Mattoussi, H. and Clapp, A.R. (2008) “Potential clinical applications of quantum dots”. *International Journal of Nanomedicine*. 3 (2): 151-167.

73. Meyers, C.A. (2008) “How chemotherapy damages the central nervous system”. *Journal of Biology*. 7 (11) 1-3.

74. Mizushima, N. (2007) “Autophagy: process and function”. *Genes and Development*. 21: 2861-2873.

75. Moghimi, S.M., Hunter, A.C. and Murray, J.C. (2005) “Nanomedicine: current status and future prospects”. *The Federation for American Societies and Experimental Biology journal*. 3: 311-330.

76. Murray, A.B., Noms, D.J. and Bawendi, M.G. (1993) “Synthesis and characterization of nearly monodisperse CdE (E= S, Se, Te) semiconductor nanocrystallites”. *Journal of the American Chemical Society*. 115: 8706-8715.

77. Ngamwongsatit, P., Banada, P.P., Panbagred, W. and Bhunia, A.K. (2008) “WST-1-based cell cytotoxicity assay as a substitute for MTT-based assay for rapid detection of toxigenic *Bacillus* species using CHO cell line”. *Journal of Microbiological Methods* 73: 211-215.

78. Nho, M., Kim, T., Lee, H., Kim, C-K. Joo, S-W. and Lee, K. (2010) “Fluorescence quenching caused by aggregation of water-soluble CdSe quantum dots”. *Colloids and Surfaces A: Physicochemical Engineering Aspects* 359: 39-44.

79. Nunez, R. (2001) “DNA measurement and cell cycle analysis by flow cytometry”. *Current Issues in Molecular Biology*. 3 (3) 67-70.

80. Oh, S-J., Yang, J-I., Kim, O., Ahn, E-J., Kang, W.D., Lee, J-H., Moon, K-S., Lee, K-H. and Cho, D. (2017) “Human U87 glioblastoma cells with stemness features display enhanced sensitivity to natural killer cell cytotoxicity through altered expression of NKG2D ligand”. *Cancer Cell International*. 17-22.

81. Ohgaki, H. (2009) “Epidemiology of brain tumors in: Verma M. (eds) cancer epidemiology”. *Methods in Molecular Biology, volume 472*. Humana Press. [Online] Available: https://doi.org/10.1007/978-1-60327-492-0_14

82. Onoshima, D., Yukawa, H. and Baba, Y. (2015) “Multifunctional quantum dots-based cancer diagnostics and stem cell therapeutics for regenerative medicine”. *Advanced Drug Delivery*

Reviews 95: 2–14.

83. OpenStax, Biology. (2015) "The neuron- external structure and classification". OpenStax CNX. [Online]Available: https://cnx.org/contents/GFy_h8cu@9.87:c9j4p0aj@3/Neurons-and-Glial-Cells

84. Orrenius, S., Nicotera, P. and Zhivotovsky, B. (2011) "Cell death mechanisms and their implications in toxicology". *Toxicological sciences*. 119 (1) 3-19.

85. Ostrom, Q.T., Bauchet, L., Davis, F.G, Deltour, I., Fisher, J.L., Langer, C.E., Pekmezci, M., Schwartzbaum, J.A., Turner, M.C., Walsh, K.M., Wrensch, M.R. and Barnholtz-Sloan, J.S. (2014) "The epidemiology of glioma in adults: a "state of the science" review". *Neuro-Oncology*. 16 (17) 896-913.

86. Pachter, J.S., De Vries, H.E. and Fabry, Z. (2003) "The blood-brain barrier and its role in immune privilege in the central nervous system". *Journal of Neuropathology and Experimental Neurology*. 62 (6) 593-604.

87. Peng, L., He, M., Chen, B., Wu, O., Zhang, Z., Pang, D., Zhu, Y. and Hu, B. (2013) "Cellular uptake, elimination and toxicity of CdSe/ZnS quantum dots in HepG2 cells". *Biomaterials*. 34: 9545-9558.

88. Pierotti, M.A., Sozzi, G. and Croce, C.M. 2003*, Oncogenes in the initiation and progression of neoplasia, Holland-frei cancer medicine*, 6th edition. Bookshelf ID: NBK14021

89. Resch-Genger, U., Rabolle, M., Cavaliere-Jaricot, S., Nitscke, R. and Nann, T. (2008) "Quantum dots versus organic dyes as fluorescent labels". *Nature Methods* 5:9 763-775.

90. Rickert, C.H. and Paulus, W. (2001) "Epidemiology of central nervous system tumours in childhood and adolescence based on the new WHO classification". *Child's Nervous System*. 17: 503-511.

91. Rocha, T.L., Gomes, T., Cardosa, Letendre, J., Pinheiro, J.P., Sousa, V.S., Texeira, M.R. and

Bebianno, M.J. (2014) “Immunocytotoxicity, cytogenotoxicity and genotoxicity of cadmium-based quantum, dots in the marine mussel Mytilus galloprovinicialis”. *Marine Environmental Research* 101: 29-37.

92. Rosenthal, S.J., Chang, J.C., Kovtun, O., McBride, J.R. and Tomlinson, I.D. (2010) “Biocompatible quantum dots for biological applications”. *Chemical Biology* 28: 18 (1) 10-24.

93. Rzigalinski, B.A. and Strobl, J.S. (2009) “Cadmium- containing nanoparticles: Perspectives on pharmacology and toxicology in quantum dots”. *Toxicology and Applied Pharmacology* 238: 280–288.

94. Saharan, V and Pal, A. (2016) “Chitosan based nanomaterials in plant growth and protection”. Chapter 2: Synthesis of chitosan-based nanoparticles *Springerbriefs in plant science.* 17-19. [Online] Available: Doi: 10.1007/978-81-322-3601-6_2

95. Shipley, M.M., Mangold, C.A. and Szpara, M.L. (2017) “Differentiation of the SH-SY5Y human neuroblastoma cell line”. *Journal of Visualized Experiments*. 108 (53193): 1-19.

96. Siemann, D.W. (2011) “The unique characteristics of tumor vasculature and preclinical evidence for its selective disruption by tumor-vascular disrupting agents”. *Cancer Treatment Revolution* 37 (1) 63-74.

97. Singh, OP. and Nehru, R.M. (2008) “Nanotechnology and cancer treatment”. *Asian Journal of Experimental Science*. 22 (2) 45-50.

98. Smith, A.M., Duan, H., Rhyner, M.N., Ruan, G. and Nie, S. (2006) “A systematic examination of surface coatings on the optical and chemical properties of semiconductor quantum dots”. *Physical Chemistry Chemical Physi*cs 8: 3895-3903.

99. Smith, A.M., Duan, H., Mohs, A.M. and Nie, S. (2008) “Bioconjugated quantum dots for in vivo molecular and cellular imaging”. *Advanced Drug Delivery Reviews* 60: 1226– 1240.

100. Smith, A.M. and Nie, S. (2010) “Semiconductor nanocrystals: structure, properties, and band

gap engineering". *American Chemical Society* 43 (2) 190-200.

101. Steponkiene, S., Kavaliauskiene, S., Purviniene, R., Rotomskis, R and Juzenas, P. (2011) "Quantum dots affect expression of CD133 surface antigen in melanoma cells". *International Journal of Nanomedicine* 6: 2437–2444.

102. Su, Y., Hub, M., Fan, C., He, Y., Li, Q., Li, W., Wang, L-H., Shen, P. and Huang, Q. (2010) "The cytotoxicity of CdTe quantum dots and the relative contributions from released cadmium ions and nanoparticle properties". *Biomaterials* 31: 4829-4834.

103. Swartz, L.T. (2013) "Discriminative eradication of cancer cells using quantum dots functionalized with peptide-directed delivery of a pro-apoptotic peptide". Unpublished MSc mini-thesis. Belville: University of the Western Cape.

104. Tait, S.W.G., Ichim, G. and Green, D.R. (2014) Die another way- non-apoptotic mechanisms of cell death". Journal of Cell Science. 127: 2135-2144.

105. Tan, M. and Yu, D. (2013) "Molecular Mechanisms of ErbB2-Mediated Breast Cancer Chemoresistance". *In: Madame Curie Bioscience Database (Internet). Austin (TX): Landes. Bioscience; 2000-2013*.
[Online] Available: https://www.ncbi.nlm.nih.gov/books/NBK6194/

106. Tang, J., Huang, N., Zhang, X., Zhou, T., Tan, Y., Pi, J., Pi, L., Cheng, S., Zheng, H., and Cheng, Y. (2017) "Aptamer-conjugated PEGylated quantum dots targeting epidermal growth factor receptor variant III for fluorescence imaging of glioma". *International Journal of Nanomedicine.* 12: 3899–3911.

107. Tarafdar, J and Adhikari, T. (2015) "Soil science: an introduction". Chapter 27: Nanotechnology in soil science. 775-807.

108. Tlsty, T.D. and Coussens, L.M. (2006) "Tumor stroma and regulation of cancer development". *The Annual Review of Pathology: Mechanisms of Disease*. 1: 119-150.

109. Torchilin, V.P. (2010) “Passive and active drug targeting: Drug delivery to tumors as an example”. In: M. Schäfer-Korting (eds) drug delivery. Handbook of experimental pharmacology. Volume 197. Springer, Berlin. Heidelberg. [Online] Available: https://doi.org/10.1007/978-3-642-00477-3_1

110. Tsujimoto, Y. (1997) “Apoptosis and necrosis: Intracellular ATP level as a determinant for cell death modes”. *Cell Death and Differentiation*. 4: 429-434.

111. Uliasz, T.F. and Hewitt, S.J. (2000) “A microtiter trypan blue absorbance assay for the quantitative determination of excitotoxic neuronal injury in cell culture”. *Journal of Neuroscience Methods* 100: 157-163.

112. Vakatesh, H. and Monje, M. (2017) “Neuronal activity in ontogeny and oncology”. *Trends in Cancer*. 3 (2) 89-112.

113. Vasudevan, D., Gaddam, R.R., Trinchi, A. and Cole, I. (2015) “Core-shell quantum dots: Properties and applications”. *Journal of Alloys and Compounds* 636: 395-404.

114. Wakaskar, R.R. (2017) “Passive and active targeting in tumor microenvironment”. *International Journal of Drug Development and Research*. 9 (2): 37-41.

115. Wang, Z.L. (2000) “Transmission electron microscopy of shape-controlled nanocrystals and their assemblies”. *Journal of Physics and Chemistry* 104:6 1153-1175.

116. Wang, Y., Chen, H., Ye, C. and Hu, Y. (2008) “Synthesis and characterization of CdTe quantum dots embedded gelatin nanoparticles via a two-step desolvation method”. *Materials letters* 62: 3382-3384.

117. Wang, Y. and Chen, L. (2011) “Quantum dots, lighting up the research and development of nanomedicine”. *Nanomedicine: Nanotechnology, Biology and Medicine*. 7: 385-402.

118. Weinstein, J.L., Katzenstein, H.M. and Cohn, S.L. (2003) “Advances in the diagnosis and treatment of neuroblastoma”. *The Oncologist*. 8: 278-292.

119. Wollman, D.A., Irwin, K.D., Hilton, G.C., Dulcie, L.L., Newbury, D.E. and Martinis, J.M. (1997) "High-resolution, energy dispersive microcalorimeter spectrometer for X-Ray microanalysis". *Journal of Microscopy* 188:3 196-223.

120. Wyllie, A., Donahue, V., Fischer, M.S.B., Hill, D., Keesey, J. and Manzow, S. (2003) "Roche molecular biochemicals apoptosis and cell proliferation". *2nd revised edition*. 1-142. [Online] Available: http://diyhpl.us/~bryan/irc/protocol-online/protocol-cache/21552_Apoptosis.pdf

121. Xie, Y., Bergstrom, T., Jiang, Y., Johansson, P., Marinescu, V.D., Lindberg, N., Segerman, A., Wicher, G., Niklasson, M., Baskaran, S., Sreedharan, S., Everlien, I., Kastemar, M., Hermansson, A., Elfinah, L., Libard, S., Holland, E.C., Hesselager, G., Alafuzoff, I., Westermark, B., Nelander, S., Forsberg-Nilsson, K. and Uhrbom, L. (2015) "The human glioblastoma cell culture resource: Validated cell models representing all molecular subtypes". *EBioMedicine*. 2: 1351-1363.

122. Xing, Y., Chaudry, Q., Shen, C., Kong, K.Y., Zhau, H.E., Chung, L.W., Petros, J.A., O'Regans, R.M., Yezhelyev, M.V., Simons, J.W., Wang, M.D. and Nie, S. (2007) "Bioconjugated quantum dots for multiplexed and quantitative immunohistochemistry". *Nature Protocols*. 2 (5): 1152-1165.

123. Xu, R. (2008). "Progress in nanoparticles characterization: Sizing and zeta potential measurement". *Particuolgy* 6: 112-115.

124. Yang, P., Zhang, A., Sun, H., Liu, F., Jiang, Q. and Cheng, X. (2010) "Highly luminescent quantum dots functionalized and their conjugation with IgG". *Journal of Colloid and Interface Science*. 345: 222-227.

125. Youdim, K.A., Shukitt-Hale, B. and Joseph, J.A. (2004) "Flavanoids and the brain: interactions at the blood–brain barrier and their physiological effects on the central nervous system". *Free Radical Biology and Medicine*. 37 (11) 1683-1693.

126. Yu, D. and Hung, M-C. (2009) "*Breast cancer chemosensitivity*". *Advances in*

experimental medicine and biology. 608: 119-122.

127. Yukawa, H., Tsukamoto, R., Kano, A., Okamoto, Y., Tokeshi, M., Ishikawa, T., Mizuno, M. and Baba, Y. (2013) "Quantum dots conjugated with transferrin for brain tumour cell imaging". *Cell Science and Therapy* 4:3 150. doi:10.4172/2157-7013.1000150.

128. Yukawa, H., Watanabe, M., Kaii, N., Okamoto, Y., Tokeshi, M., Miyamoto, Y., Noguchi, H., Baba, Y. and Hayashi, S. (2012) "Monitoring transplanted adipose tissue-derived stem cells combined with heparin in the live by fluorescence imaging using quantum dots". *Biomaterials*. 33 (77): 2177-2186.